UNIVERSITY OF CALIFORNIA,
IRVINE

Reactive Oxygen Species Formation From Ambient Particles and Their Roles In Chemical Aging

DISSERTATION

submitted in partial satisfaction of the requirements
for the degree of

DOCTOR OF PHILOSOPHY

in Chemistry

by

Brian Chi Hyun Hwang

Dissertation Committee:
Associate Professor Manabu Shiraiwa, Chair
Professor James N. Smith
Professor Sergey Nizkorodov

2021

Dedication

To my friends and family.

“It’s hard to beat a person who never gives up”

-George Herman Ruth

Table of Contents

List of Abbreviations

- **α** = surface accommodation coefficient of gaseous species. Probability of a gaseous species sticking at the surface upon collision.
- **AA:** Ascorbic acid
- **AIOMFAC: A**erosol **I**norganic-**O**rganic **M**ixtures **F**unctional **G**roups **A**ctivity **C**oefficients. Thermodynamic model used to predict how much of chemical of interest are present in each phase for film mixtures.
- **B_0**: Magnetic Field
- **BaP**: Benzo[a]pyrene
- **BMPO:** 5-*tert*-Butoxycarbonyl-5-methyl-1-pyrroline-N-oxide
- **BMPO-R**: Carbon-centered organic radical BMPO adduct
- **BMPO-OR**: Oxygen-centered organic radical BMPO adduct
- **BMPO-OH**: Hydroxyl radical BMPO adduct
- **BMPO-OOH**: Superoxide anion radical trapped by BMPO. BMPO adduct.
- **CW-EPR: C**ontinuous **w**ave **e**lectron **p**aramagnetic **s**pectrometer
- **DART-MS**: **D**irect **A**nalysis in **R**eal **T**ime **M**ass **S**pectrometry
- **dB**: Decibel. Relative unit for measuring microwave power
- **DMPO**: 3,4-dihydro-2,3-dimethyl-2H-pyrrole 1-oxide
- **DTT**: Dithiothreitol
- **DTT_m:** Mass normalized (in this dissertation: normalized to $PM_{2.5}$ mass) DTT activity or intrinsic DTT activity
- **DTT_v:** Volume normalized DTT activity or Ambient DTT activity
- **D:** Diffusion coefficient of a molecule in the bulk
- **D_p:** diameter of a particle

- **E_a:** activation energy
- **EC:** Elemental carbon.
- **EDTA:** Ethylenediaminetetraacetate
- **EPFR:** Environmentally Persistent Free Radical
- **$EPFR_m$**: Mass normalized (in this dissertation: normalized to $PM_{2.5}$ mass) EPFR concentration.
- **$EPFR_v$:** Volume normalized EPFR concentration or Ambient EPFR concentration
- **EPR:** Electron paramagnetic resonance spectrometer
- **Fig**: Figure
- **f_s :** mole fraction of the product formed**.**
- **g:** g-value. EPR characteristic parameter that can be obtained from taking the ratio of microwave frequency absorbed by the sample over the magnetic field that the signal was observed.
- **G:** Gauss. Unit to measure magnetic field strength
- **GHz**: Gigahertz. Unit to measure current
- **ΔH:** Peak-to-peak distance or EPR linewidth. The distance between two peaks measured from an EPR signal in Gauss.
- **HiVol:** High Volume Sampler with a with a $PM_{2.5}$ impactor
- **HULIS:** HUmic-LIke Substances
- **I-5, I-710:** Interstate 5 and 710. Highway locations that the particle samples were collected in this dissertation at Anaheim and Long Beach, respectively.
- **I_n:** Nuclear spin
- **k**: Boltzmann Constant
- **k_{BR}**: bulk rate coefficient
- **kHz:** Kilohertz

- $K_{sol,cc}$: Henry's Law Coefficient
- **k_{SLR} :** surface rate ceofficient
- **MOUDI:** Micro-Orifice Uniform Deposit Impactor. Cascade impactor.
- **N_l :** Number of lines observed in EPR.
- **OH·:** Hydroxyl radical
- **$O_2^{\cdot-}$:** Superoxide anion radical
- **OP:** Oxidative potential
- **OR·:** Oxygen-centered organic radical. Unpaired electron resides mainly on the oxygen atom of the molecule.
- **PAHs:** Polycyclic aromatic hydrocarbons
- **PhO·:** Phenoxy radical
- **PM:** Particulate matter
- **r:** Radius of the particle
- **R·:** Carbon-centered organic radical. Unpaired electron resides mainly on the carbon atom of the molecule.
- **RH:** relative humidity
- **ROI:** Reactive oxygen intermediate. Chemisorbed oxygen atom bound to delocalized electron on an aromatic surface.
- **ROS:** Reactive oxygen species.
- **SOA:** Secondary Organic Aerosol
- **τ_d:** Desorption lifetime of a gaseous molecule. The time duration of a molecule that sticks at the surface.
- **τ_{cd}**: e folding time of equilibration
- **TEMPOL:** 4-hydroxy-2,2,6,6-tetramethylpiperidin-1-oxyl
- **ν:** dynamic viscosity

List of Tables

List of Figures

Acknowledgements

I am truly grateful for the people I've met and experience I have been through to get to where I am at today. At the bottom of my heart, I am forever in a debt of gratitude and hope to return the favor in the future.

I would especially like to thank my advisor, Professor Manabu Shiraiwa for the patience and support during the entirety of my program. In your lab, I was able to gain experience in field campaign, laboratory measurements, and modeling. I am truly thankful to you for entrusting me with the project that included the brightest minds in the atmospheric field: Professor Jonathan Abbatt and Professor Andreas Zuend. Additionally, it was my dream to work with my undergraduate school, UC Riverside, and I thank you for making this dream into a reality.

I would also like to thank my advancement and defense committee members: Professor Donald Blake, Professor Finlayson-Pitts, Professor Jim Smith, Professor Douglas Tobias, Professor Sergey Nizkorodov, and Professor Jasper Vrugt. Professor Donald Blake, I enjoyed the conversations I had with you at the hallway. Your stories of persistence in the chemistry field (organic chemistry and advancement) still inspire me to never give up. Professor Finlayson-Pitts, thank you for allowing me to sit in your class and get experience in laboratory technique. I want to sincerely thank Professor Jim Smith for all the useful information on analytical techniques and clarification on kinetic and instrument concepts over the past five years. I still look over your class notes and the Atmospheric Measurement textbook.

My group members: Mohammed, Wing-Sy, Randy, Vy, Ying, Jinlai, Kasey, Sukriti, and especially Pascale and Ting, thank you all for your support and help throughout graduate school. Pascale and Ting, both of you are great mentors and I truly appreciate all of your advice, guidance, and availability. I also truly appreciate the big faith you had in my driving skills, Ting. I got my

first car when my father retired as a taxi driver which was one week prior to the highway project. I told you that I only drove on the highway once in my life, but you still put your faith in me and stayed calm in the passenger seat as I drove the U-Haul van. Thanks to you, I finally have the confidence to take the highway and I became a better driver. Randy and Vy, you have been a tremendous help in my projects, and I hope the best for your professional careers.

I learned how to properly use a tool and troubleshoot an instrument from Cyril McCormick, Mark Steinborn, Jim Dao, Charles Hanson, and Donald Mannikko. Thank you all for your patience and help.

I would also like to thank UC Riverside, Desert Research Institute, and South Coast Air Quality Management members who supported me during the highway project. I will never forget the kindness that the UC Riverside team showed me at the sampling site.

I was extremely fortunate to make great and supportive friends in graduate school: Brian Nguyen, Jeffrey Tsai, Simon Luo, Vivian Chen, Josh Rhee, Tyler Heiss, and Sunny Sun. I still miss our karaoke nights and hope to continue to carry on this tradition after the pandemic. Also, thank you all for encouraging me and listening to all my struggles in graduate school. Thank you, Brian, for reaching out to me when I was struggling in the candidacy exam. You are a great friend and I will forever cherish our time together.

I would not have attended graduate school without the support from Professor Jack Eichler, Professor Vincent Lavallo, Professor Thomas Morton, and Professor Yadong Yin from UC Riverside. Professor Jack Eichler, thank you for taking me as an undergraduate researcher and always supporting through my toughest moments.

My church family and childhood friends are like my extended family. Thank you for looking out for me when I was in trouble and giving me advice in life. As a first-generation

immigrant, my parents were always busy and did not have much time to spend with me while I was growing up. I did not have a mentor in life until I met Brian and Sam teachers. Thank you both for being my mentors. Words cannot describe the kindness you have shown me throughout my life.

I would also like to thank National Science Foundation, Health Effects Institute, and Japan Automobile Research Institute for funding my graduate studies. I received permissions for all the figures in this dissertation from Taylor & Francis, Springer Nature, Royal Society of Chemistry, Elsevier, John Wiley and Sons, Bruker, American Chemical Society, and Copernicus Publications. In addition, thank you to *Proceedings of the National Academy of Science* and *American Chemistry Society Earth and Space Chemistry* for allowing me to reuse my published work in this dissertation.

Lastly, and certainly not least, I love my family. Thank you appa and umma for always supporting and raising me. I truly appreciate the sacrifices you made for me and Kevin throughout our entire lives. You truly are my role models and taught me to never give up. I would also like to thank my aunt and cousin for helping our family settle in California. I cannot wait to watch my niece, Claire, grow and I hope I can be a great role model to her. In addition, I would like to thank my heavenly Father and Jesus for always watching over me and the people I care about.

Curriculum Vitae
Brian Chi Hyun Hwang

Education

University of California, Irvine (UCI) Sept. 2021
Ph.D. in Chemistry

University of California, Riverside (UCR) June 2015
B.S. in Chemistry

Research Experience

University of California, Irvine. Dept. of Chemistry. Jan. 2017 – present
Graduate Student Researcher
Principal Investigator: Prof. Manabu Shiraiwa

- **Field Studies and Laboratory Measurements**
  - Lead the UCI team in Real-World Tire and Brake-Wear Emissions project. Collected highway $PM_{2.5}$ and size-segregated particles using a $PM_{2.5}$ high-volume sampler and Micro-Orifice Uniform Deposit Impactors (MOUDI), respectively.
  - Measured radicals from collected samples and radicals formed in aqueous solution using an electron paramagnetic resonance (EPR) spectrometer. Also, measured DTT decay using UV-VIS spectrophotometer.
- **Modeling**
  - Created a code based on a kinetic model to explain the ozonolysis of polycyclic aromatic hydrocarbons (PAHs) in a chemical mixture using Matlab.
- **Safety Representative and Equipment Manager**
  - Maintained detail and accurate records of available chemicals and safety operating procedures. Repaired electronic instruments with the assistance of manufacturer technicians and wrote reports on how to fix technical issues.

University of California, Riverside. Dept. of Chem. June 2015 – Nov. 2015
Undergraduate Research Assistant
Principal Investigator: Prof. Yadong Yin

- **Synthesis and Analysis of Nanoparticles**
  - Synthesized polyvinylpyrrolidone coated iron oxide nanoparticles. Analyzed size distribution of synthesized polyvinylpyrrolidone coated iron oxide nanoparticles using dynamic light scattering technique.

University of California, Riverside. Dept. of Chem. June 2012 – June 2014
Undergraduate Research Assistant
Principal Investigator: Prof. Jack F. Eichler

- **Synthesis and Chemical Analysis**
  - Synthesized 2,9-di-*sec*-butyl-phenanthroline and Au (III) phenanthroline complex. Separated 2,9-di-*sec*-butyl-phenanthroline from the organic mixture using column chromatography and analyzed the chemical structure using ^{1}H Nuclear Magnetic Resonance (NMR) spectrometer.

Publications

- **Hwang, B**.*; Fang, T.*; Pham, R.; Wei, J.; Gronstal, S.; Lopez, B.; Frederickson, C.; Galeazzo, T.; Wang, X.; Jung, H.; Shiraiwa, M., Environmentally Persistent Free Radicals, Reactive Oxygen Species Generation, and Oxidative Potential of Highway PM2.5. *ACS Earth and Space Chemistry* 2021.

- Zhou, S.*, **Hwang, B. C. H.***, Lakey, P. S. J., Zuend, A., Abbatt, J. P. D., Shiraiwa, M.: Multiphase Reactivity of Polycyclic Aromatic Hydrocarbons is Driven by Phase Separation and Diffusion Limitations. *Proceedings of the National Academy of Sciences* **2019,** *116*, (24), 11658.

- Olsen, P. M.; Ruiz, C.; Lussier, D.; Le, B. K.; Angel, N.; Smith, M.; **Hwang, B. C. H.**; Khatib, R.; Jenkins, J.; Adams, K.; Getcher, J.; Tham, F.; Chen, Z.; Wilson, E. H.; Eichler, J. F., Synthesis, characterization, and antitumor activity of unusual pseudo five coordinate gold(III) complexes: Distinct cytotoxic mechanism or expensive ligand delivery systems? *Journal of Inorganic Biochemistry* **2014,** *141*, 121-131.

* = co-first authors

Awards

- Chemistry Graduate Dissertation Fellowship. **Feb. 2021**.

- Student Poster Award at the 38th Annual American Association for Aerosol Research Conference. **Oct. 2020**.

Presentations

- **Hwang, B.**; Fang, T.; Pham, R.; Wei, J.; Jung, H.; Shiraiwa, M., Environmentally Persistent Free Radicals and Reactive Oxygen Species Measurements in the Size-Segregated Ambient Particles Collected at the Highway and Urban Sites, *38th American Association for Aerosol Research*, **Oct. 2020** (poster).

- **Hwang, B.**; Fang, T.; Mochida, M.; Shiraiwa, M., Formation of Reactive Oxygen Species by Size-Segregated Particles Collected in Forest and Urban Environments, *37th American Association for Aerosol Research*, **Oct. 2019** (poster)**.**

- **Hwang, B.**; Fang, T.; Mochida, M.; Shiraiwa, M., Formation of Reactive Oxygen Species by Size-Segregated Particles Collected in Forest and Urban Environments, *2019 Inhaled Aerosol Dosimetry*, **Oct. 2019** (poster).

- **Hwang, B.**; Zhou S.; Lakey, P.; Abbatt J.; Shiraiwa, M., Diffusion Limitations and Shielding Effects in the Ozonolysis of Polycyclic Aromatic Hydrocarbons Embedded in Secondary Organic Aerosols, *2018 International Aerosol Conference*, **Sept. 2018** (poster).

- **Hwang, B.**; Zhou S.; Lakey, P.; Abbatt J.; Shiraiwa, M., Multiphase Reactivity of Polycyclic Aromatic Hydrocarbons Depend on Diffusion Limitation and Phase Separation, *2018 Lake Arrowhead Conference Sponsored by AirUCI*, **Sept. 2018**. (oral).

- **Hwang, B.**; Olsen, P. M.; Ruiz, C.; Lussier, D.; Le, B. K.; Angel, N.; Smith, M; Khatib, R.; Jenkins, J.; Adams, K.; Getcher, J.; Tham, F.; Chen, Z.; Wilson, E. H.; Eichler, J. F. Synthesis, Characterization, and Anticancer Activity of Gold (III) Complexes Bearing Alkyl-Subsitituted 1,10-Phenanthroline Ligands. **Nov. 2013** (poster).

Teaching Experience

University of California, Irvine. Sept. 2016 – Sept. 2017, Mar. 2018, 2019, Sept. 2020

Graduate Teaching Assistant

- Taught general and organic chemistry laboratory courses. Created PowerPoint presentations to clarify concepts. Held discussion courses in general chemistry.

California State University, Northridge Sept. 2015 – Apr. 2016

Tutor for BUILD PODER program

- BUILD PODER is a research training program for undergraduates funded by the National Institute of Health. The goal is to help underrepresented groups enter the STEM field.
- Tutored students in general and organic chemistry.

Abstract of the Dissertation

Reactive oxygen species (ROS), including hydroxyl radical (OH·), superoxide anion ($O_2^{\cdot-}$), ozone (O_3) and oxygenated organic radicals, play an important role in atmospheric and physiological processes. Polycyclic aromatic hydrocarbons (PAHs), including benzo[a]pyrene (BaP), are among the most prominent toxic compounds that can be found in indoor and outdoor environments. Their chemical lifetimes are highly determined by ROS such as ·OH and O_3, but the chemical degradation mechanism and kinetics of PAHs against these ROS remain to be elucidated.

Emerging health-related studies suggest that inhaled ambient particles serve as exogenous ROS sources. The ROS generated from the particles can potentially disturb the physiological functions in our body, which can lead to oxidative stress and adverse health effects. Application of electron magnetic resonance (EPR) spectrometer to atmospheric chemistry have provided additional information on the type of ROS that can be generated from ambient particles. Past studies report environmentally persistent free radicals (EPFRs) can be found in car exhaust and biomass burning particles. These particles containing EPFRs have been shown to generate ROS in aqueous solution, but EPFR measurements in ambient particles are still limited.

Chapters 2 and 3 focus on the EPFR measurements and the type of ROS detected from aqueous extract of fine particulate matter ($PM_{2.5}$) collected at two different highway sites and during the wildfire events using EPR spectrometer. The ·OH and carbon-centered organic radical formation have been detected in aqueous extracts of highway $PM_{2.5}$. In contrast, ·OH, $O_2^{\cdot-}$, carbon and oxygen-centered organic radicals have been found to be generated from wildfire PM_1 and PM_{10} depending on the wildfire events that occurred in Southern California. The ·OH and carbon-centered organic radical were detected in aqueous extracts of coarse particles collected from

wildfire events, which demonstrates the redox-active chemical components in wildfire PM are size-dependent. Chapter 2 discusses the correlations between the measured EPFR, ROS, and traffic-related pollutants. The chemical and EPFR measurements at the Long Beach highway (Interstate-710) show positive correlations between EPFR in highway fine PM and CO, NO_2, and elemental carbon (EC), which are pollutants typically found in exhaust emissions. The negative correlation between EPFR and O_3 was also observed at the collection sites, which suggests EPFR is most likely emitted from primary source at the highway. Positive correlation between EPFR and OH· generated from the highway fine PM was also observed at the Long Beach suggesting OH· are generated from similar source as EPFR. Lastly, the toxicity of highway particle was assessed using DTT (dithiothreitol) activity and the correlation with ROS was explored. High positive correlation between DTT activity and ROS was observed at the Anaheim highway (Interestate-5). Chapter 3 also investigates size dependent EPFR and ROS measurements. EPFR was mainly found in wildfire PM_1 and found to be approximately 10 times higher compared to the highway and urban background. $O_2^{\cdot-}$ was also found to be size-dependent and only detected in yellow-brownish extracts of wildfire samples, suggesting redox-active chemical components in brown carbon may play a role in $O_2^{\cdot-}$ formation. These findings highlight the interplay of various PM redox active chemical components and the complex relationship between ROS formation and DTT activity.

Ozone (O_3) is a major oxidant inducing chemical transformation of organic compounds in the atmosphere and organic films found in indoor environments. Chapter 4 discusses the ozonolysis of BaP in multicomponent thin films that can be found in indoor environments and in the atmosphere. Rapid degradation of BaP in thin films against O_3 was initially observed but found to decay much slower at longer exposure time in direct analysis in real-time mass spectrometry (DART-MS) kinetic experiments. Kinetic multilayer modeling revealed that the diffusivity of BaP

from bulk to the surface limits the decay of BaP, resolving long-standing unresolved observations of incomplete PAH decay upon prolonged ozone exposure. Ozonolysis of BaP decay in alpha-pinene secondary organic material (SOM) film under dry and humid conditions was also explored. The thermodynamic modeling predicted BaP is immiscible in the SOA mixtures and these results were implemented in the kinetic model. The kinetic model simulations showed that the slow decays of BaP in SOA mixtures under dry and humid conditions are also dependent on the bulk diffusivity of BaP in immiscible BaP layer upon prolonged ozone exposure. Lastly, BaP was found to be miscible in organic oils such as squalene, linoleic acid, and cooking oil based on visual inspection and thermodynamic model. However, the kinetic and thermodynamic model results show oxidation products forms a viscous crust in the organic films and hinders diffusion of BaP from the film interior to the surface. These findings demonstrate that phase separation and slow diffusion play a key role in the long-range transport of PAHs in the atmosphere and their fates in indoor environments.

Chapter 1: Introduction

1.1 Background

1.1.1 Importance of Air Pollution

Figure 1.1: Silverado Fire in Irvine CA, on 10/26/20. (Photos credited to Kelvin Cheng).[1]

The chemicals in air affect Earth's environment and public health every day. Anthropogenic activities such as driving emit significant amounts of carbon dioxide into the atmosphere, which traps the heat from escaping Earth and gradually warms up the planet.[2] The global rise in temperature then worsens drought conditions in certain parts of the world, and increases the occurrence of wildfires and other natural disasters (Figure 1.1).[3-5] A recent study estimated that indoor and outdoor air pollution are responsible for millions of deaths and premature deaths worldwide.[6-7] Air pollution is now considered to be one of the world's most formidable threats to environmental health. Thus, more research related to atmospheric chemistry is needed to better elucidate how exposure to certain chemicals in air can affect the climate and public health.[8]

1.1.2 Outdoor and Indoor Air Quality Topics

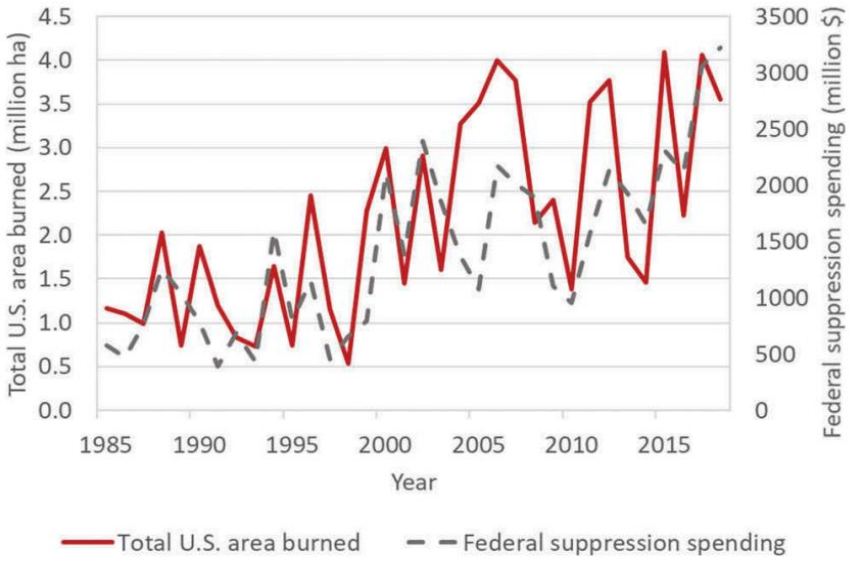

Figure 1.2: The red line displays the number of area burned by the wildfire in the United States (U.S) in units of hectare (1 ha = 10,000 m^2). The dashed grey line is the cost of spending by the federal government to suppress the wildfire in the U.S. (Adopted from Jaffe et al.)[9]

Particulate matter (PM) plays a major role in climate and is one of the top risk factors attributed to burden of disease globally.[7] The government has placed stringent regulations on PM with an aerodynamic diameter less than ($PM_{2.5}$), due to its ability to penetrate deep into our lungs, which can then contribute to cardiovascular and respiratory diseases.[10-14] $PM_{2.5}$ mass concentration is the current metric to assess the air quality.[15] In California, during the early 21th century, approximately 20% of $PM_{2.5}$ has been attributed to primary vehicle emissions.[16] In response, the federal and state government agencies implemented numerous regulations on tailpipe emission. These government regulations require all heavy-diesel trucks to use filters that remove diesel exhaust particles (DEP).[16] DEP is a well-studied pollutant that contributes to $PM_{2.5}$ and causes adverse health effects for humans.[16-18] Although $PM_{2.5}$ mass concentration and pollutants associated with DEP, such as elemental carbon (EC) and polycyclic aromatic hydrocarbons (PAHs), have reduced significantly in Southern California over the past decades, several studies

suggest $PM_{2.5}$ toxicity has not significantly changed due to the increase in contribution of non-exhaust emissions.[16, 19-21]

Non-exhaust emissions include brake/tire wear and resuspended road dust. Particle number and mass size distribution measurements show brake and tire wear can contribute to $PM_{2.5}$.[22-23] Furthermore, non-exhaust emissions are found to be abundant in metals, such as iron and copper. Exposure to non-exhaust emissions in excess amounts can be harmful.[24-26]

Currently, there are no standard regulations on non-exhaust emissions, despite the expectation of these emissions dominating in the upcoming decades as countries increasingly transition to cleaner technologies.[27] Although the role of iron and copper in PM toxicity is still being explored, the leading hypothesis involves the generation of reactive oxygen species (ROS) from iron and copper.[12, 26, 28]

In certain parts of the U.S., including California, the emission source from the wildfires is another growing concern. Figure 1.2 shows the total area burned by wildfires in the U.S. has increased since 1985, and is projected to continue increasing throughout the upcoming decade.[9] Last year, California faced its largest wildfire, and the daily average $PM_{2.5}$ concentration reached as high as ~ 150 $\mu g/m^3$ in certain California counties, which exceeded the 24-hour $PM_{2.5}$ standard (35 $\mu g/m^3$) by roughly four times.[29] Compared to other anthropogenic sources, the toxicity mechanism of wildfire $PM_{2.5}$ is not well understood. However, since wildfires are expected to occur more frequently on the West Coast of United States, the federal government is expected to increase funding for air-quality research regarding wildfire suppression.[9, 30] Certain chemicals such as copper that may generate ROS were reported to be elevated during wildfires, which indicates ROS generation from wildfire PM should also be explored.[12, 31]

Since humans spend most of their time indoors, which has considerably increased due to the recent coronavirus-related restrictions and shelter-in-place mandates, the importance of understanding the chemistry that occurs indoors has become more apparent.

Benzo[a]pyrene (BaP) is a precursor to carcinogenic and mutagenic compounds, such as benzo[a]pyrene-7,8-diol-9,10-epoxide, and can be emitted by indoor activities such as cooking and smoking.[32-36] BaP can also be transported from the outdoors, which will most likely then accumulate on indoor surfaces and dust.[33] The potential toxic products that can be formed from BaP and its ambient and indoor sources make BaP a crucial chemical compound that must be investigated.

1.2 Reactive Oxygen Species (ROS)

Reactive oxygen species (ROS) is a term used to describe oxygen containing molecules that play an important role in physiological and atmospheric processes. ROS is composed of radicals, molecules, and ions that contain an unpaired valence electron such as superoxide, hydroxyl radical, organic radicals, alkoxy radicals, phenoxy radicals, peroxyl radicals, and ozone. ROS also include non-radical species: hydrogen peroxide, organic hydroperoxide, and organic peroxides. These chemicals are also generated by cells for defense against pathogens, cell signaling, and redox regulation, and homeostasis is maintained via ROS scavenging by the antioxidants and enzymes in human body.[37]

The redox-active metals and certain organic compounds in ambient particles can generate exogenous ROS and cause an imbalance between antioxidants and ROS levels in the body. If the ROS levels exceed the antioxidants, ROS homeostasis can be disrupted and lead to adverse health effects.[28, 38] However, the chemical components in ambient particles that may be responsible for generating ROS are still not well understood.[15] This dissertation will investigate on which

chemical components from highway and wildfire PM are responsible for ROS formation in water using correlation and size distribution analyses.

1.2.1 Ambient Source of ROS: Peroxides

Isoprene and terpenes are some of the most abundant volatile organic compounds in the atmosphere and their oxidation products have been shown to generate ROS in aqueous solution.[39-41] However, their contributions to ROS formation from ambient particle are still being explored.[39, 42-43] A photooxidation product of isoprene, isoprene hydroxy hydroperoxide (ISOPOOH), has been shown to react with Fe(II) via Fenton-like reaction and generate hydroxy and alkoxy radicals in water.[44] Volatile organic compounds can also be oxidized, and their semi-volatile oxidation products can condense into secondary organic aerosol (SOA).[41] Additionally, isoprene and terpene SOA have also been shown to generate same type of ROS in water via thermal decomposition of labile organic compounds, most likely organic hydroperoxide.[40] More recently, $O_2^{\cdot-}/HO_2$ has shown to form from isoprene and certain terpene SOA in aqueous solution via unimolecular decomposition of α-hydroxyperoxyl radical.[45] These laboratory studies demonstrate biogenic SOA can be significant sources of ROS in ambient particle and further studies must be made to investigate how peroxides and peroxy radicals can contribute to ROS formation in ambient particles.

1.2.2 Ambient Source of ROS: Quinones

One of the mechanisms in PM toxicity involves DNA damage from reactions with ROS generated from redox cycling between quinone and redox-active metals.[46-47] Quinones such as naphthoquinone are found to be abundant in soot that are emitted significantly from tailpipe, wildfire, and cooking.[31, 48-49] The mean concentration of 1,2-napthoquinone in the organic extract of diesel exhaust particles was found to be 13.69 μg/g.[50] 9,10-phenanthraquinone and 9,10-

anthraquinone were found to be in a similar range. The mass loading of quinones in an urban environment can range from 0.06 – 1.1 ng m^{-3}.[51] Soot has been shown to generate ROS mainly due to the redox-active quinones that are on the surface of the particles.[52] Quinones are also present in macromolecular compounds, HUmic-LIke Substances (HULIS).[53] HULIS have been shown to catalytically generate ROS from interaction with quinones and certain alkaloids, but ROS measurements from HULIS containing compounds are still limited.[54] Laboratory measurements also suggest quinones are an essential ingredient in ROS formation from urban particles in aqueous solution.[55] However, their role in ROS formation from ambient particles still remain to be elucidated.

1.2.3 Ambient Source of ROS: Environmentally Persistent Free Radicals

Environmentally persistent free radicals (EPFRs) are free radicals that have lifetime of days to indefinite time.[56] Ambient particles containing EPFRs have been shown to generate ROS including ·OH but their role in ROS formation is still not well elucidated.[55, 57] EPFRs generated from incomplete combustion are thought to be cyclopentadienyl, phenoxyl, and semiquinone radicals[58]. Semiquinone radicals are known to generate ·OH and damage DNA.[37, 46] EPFRs can also be formed from ozonolysis of polycyclic aromatic hydrocarbons and photooxidation of naphthalene with ·OH radical.[40, 59] This adds complexity in understanding the EPFRs source in the atmosphere. Table 1.1 shows EPFRs concentrations measured from cigarette tar, exhaust particles, and biomass burning sources.[60] Further studies must be conducted to understand how EPFR can generate ROS from inhaled ambient PM and their sources.

Table 1.1 EPFR Concentrations and Their Sources

Sources	EPFR Concentration (Spins/μg)	EPFR Concentration (pmol/μg)	References
Cigarette tar	3×10^{10}	0.05	61
Diesel Exhaust Particles	~ 10^{16} - 10^{17}	~ 0.01 – 0.1	60
Gasoline Exhaust Particles	~ 10^{16}	~ 0.01	60
Woodsmoke soot	~ 10^{15}	~ 0.001	60
Wildfire Charcoal	2.46×10^{12} - 1.49×10^{13}	4.09 – 24.7	62

1.2.4 Iron and Copper

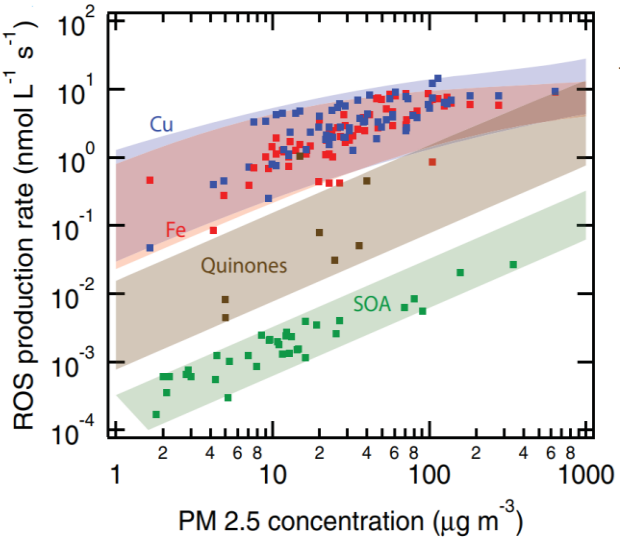

Figure 1.3: ROS production rates calculated using kinetic model individual chemical components in the $PM_{2.5}$: copper (blue), iron (red), quinones (brown), and aerosol formed from low volatility oxidized organic compounds also known as secondary organic aerosol (SOA, green). (Adopted from Lakey et al.)[28]

As mentioned above, metals such as copper and iron can react with organic compounds such as peroxides and quinones in ambient particles and generate ROS. Figure 1.3 shows ROS production rates in a simulated epithelial lining fluid (ELF) environment calculated based on $PM_{2.5}$ mass concentration measured at various geographic locations around the world.[28] The shaded color regions are the upper and lower limits of ROS production rates, which were calculated using a

kinetic model for individual chemical components that are found in $PM_{2.5}$: copper (blue), iron (red), quinones (brown), and SOA (green). The results from the kinetic model show copper and iron can generate the most ROS in ELF, which can cause adverse health effect in humans who are exposed to high $PM_{2.5}$ mass concentration for an extended period of time. Iron and copper are found to be abundant in non-exhaust emission sources.[24-26, 63] Copper and Iron can be found to be high as 234,000 and 637,000 mg/kg in break wear lining and dust, respectively.[24-25] ROS generated from non-exhaust emission sources have yet to be extensively quantified, and more research connecting ROS measurements with epidemiological studies are necessary for creating better health-related policies in the future.

1.3 Oxidative Potential

Oxidative potential (OP) is a metric that relates the particle's ability to generate ROS while depleting antioxidants, and numerous methods have been developed for OP measurements.[64-65] Acellular assays have been extensively used compared to cellular studies because they require less time and resources.[64] Also from a chemical perspective, there are fewer variables in acellular assays compared to cellular assays to study individual chemical components of the particle for ROS generation.[64] The most common acellular OP assays include electron paramagnetic resonance measurements (OP^{EPR}), dithiothreitol assay (OP^{DTT}), ascorbic acid assay (OP^{AA}), and glutathione assay (OP^{GSH}).[40, 66-68] The OP^{EPR} measures the ROS generation from the particle in the presence of antioxidants while the other mentioned acellular assays measure the depletion rate of a reducing agent (DTT) or antioxidants (AA, GSH).

For EPR measurements in OP studies, a stable organic compound is used to react with the ROS generated from the ambient particles to form more stable radicals that can be quantified, also known as the spin-trapping technique. Multiple type of ROS (i.e., $OH^{\cdot}$, $O_2^{\cdot -}$, and organic radicals)

can be detected simultaneously using EPR while other optical and electrochemical methods for ROS measurement lose specificity or only a single ROS can be quantified.[69] Although EPR is a powerful tool that can provide quantitative and qualitative ROS data, only few studies connecting EPR measurements with health endpoints are reported compared to other acellular assays.[64] Thus, linking EPR studies with other acellular OP measurements can provide a better understanding of a particle's toxicity and motivate further epidemiological studies involving EPR measurements in the atmospheric community.

Ascorbate (AA) and glutathione (GSH) have been extensively studied because they are among the most abundant antioxidants found in human lungs and can react with a wide range of radicals, including ROS.[37] There are a few studies that have explored the consumption rate of AA and GSH exposed to PM in order to better understand how individual antioxidants is involved in the redox process between PM and antioxidants.[64, 68] While high AA consumption rates were observed in these studies, low GSH consumption rates were observed for particle-toxicity study, which led to use an alternative assay to study thiol depletion, dithiothreitol (DTT).[66]

The redox-active components in ambient particle catalyze the transfer of an electron from DTT to molecular oxygen mimicking the well-known biological process: superoxide anion radical formation from the electron transport chain initiated by nicotinamide adenine dinucleotide phosphate (NADPH).[70] The success in implanting OP^{DTT} to assess PM toxicity resulted in studies that investigate which chemical components in PM are responsible for the redox cycling in this assay. The plausible candidates were copper, iron, and certain quinones that are redox-active and found to be most abundant in fine PM compared to other chemical species. The DTT oxidation by redox-active iron (Fe(II) and Fe(III)) were found to be slow, while the copper was found to most likely react with DTT directly.[71] Certain quinones such as phenanthraquinone are found to have

high DTT consumption rates and generate hydroxyl radical in the presence of iron, which suggests quinone in PM plays the major role in redox cycling observed in OP^{DTT}.[66, 72] The OP^{DTT} also showed correlations between chemicals found in tailpipe and wildfire emissions, such as benzo[g]pyrene and pyrene, which can form quinones if oxidized.[31, 52, 64]

1.4 Phase State and Miscibility

Ambient particles can exist as liquids or solids depending on their composition and ambient conditions.[73-74] Particle's phase states determine the diffusion rates within the particles that can influence the growth rate of the particles and chemical lifetime of persistent organic compounds such as PAHs.[75] Understanding how the phase state can affect particle's growth rate and multiphase reactions between oxidants and chemicals in the particle's bulk can provide models better predictions on environmental impacts of ambient particles. Shiraiwa and Seinfeld have shown that secondary organic material (SOM) mass concentration can be overestimated by one order of magnitude without accounting for the gas and bulk diffusion in a kinetic model.[76] Shiraiwa et al., also showed that the chemical half-life of reactive compounds in amorphous solid particles can be much longer compared to in semisolid or liquid particles.[77] These results highlight the importance of implementing phase states in climate and air quality models.

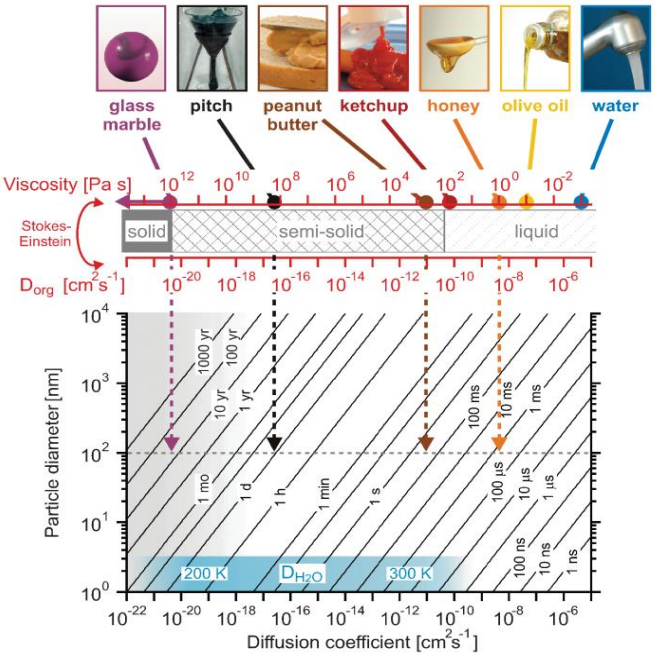

Figure 1.4: The upper scale shows the dynamic viscosity and its corresponding diffusion coefficient values of a molecule with a molecular radius of 1 nm for liquid, semi-solid, and solid. The lower panel shows the e folding time of equilibration (τ_{cd}) as a function of diffusion coefficient values. (adopted from Koop et al.)[78]

The dynamic viscosity, ν, is a physical quantity that describes the fluidity of the system and diffusion coefficient (D) of the molecule. Diffusion coefficient of a molecule can be calculated using the Stokes-Einstein equation:[77]

$$D = \frac{kT}{6\pi r\nu} \quad (\text{eq. } 1)$$

where k is the Boltzmann constant, T is the temperature, and r is the radius or thickness of the system. Figure 1.4 shows diffusion coefficient of the substance calculated by the viscosity range using eq. 1 for a particle with a radius 1 nm and gives a visual example of what type of familiar substances fall within certain viscosity ranges.[78] The system can be classified into 3 main categories based on the viscosity scale: liquid (< 10^2 Pa s), semi-solid (10^2 - 10^{12} Pa s), and solid (> 10^{12} Pa s). An amorphous system that has thicker viscosity than the solid is classified as a glass solid. Ambient particles have been shown to exist in all different phase states: liquid to an

amorphous solid. Molecular transport is highly determined by the bulk phase state of the system and figure 1.5 shows the e folding time of equilibration (τ_{cd}), defined as the time when the concentration of molecule at the particle core deviates by less than a factor of 1/e from the equilibrium value, and this value can be calculated using the equation.[77]

$$\tau_{cd} = \frac{D_p^2}{4\pi^2 D} (\text{eq. } 2)$$

The e-folding lifetime for a particle with a diameter of 100 nm (shown in dashed horizontal line) is about 1 ms if the particle is viscous as a honey (orange dashed line). However, the e-folding lifetime can last as long as a decade for a glassy solid particle (purple dashed line) which can have a significant impact in particle growth and aging. Modeling results also show particles with high viscosity plays a major role in long range transport of toxic compounds in the atmosphere.[79-82]

1.4.1: Phase Transition

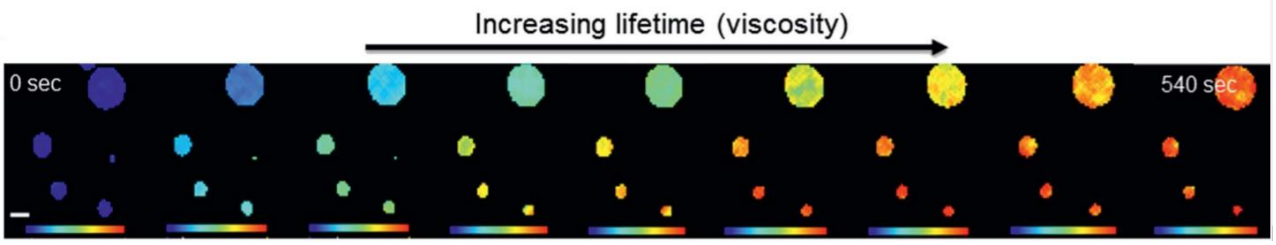

Figure 1.5: Snapshots of fluorescence results for laboratory generated particles containing oleic acid and fluorescence dye exposed to high concentration of O_3 are recorded at selected time interval: 0 s (initial) to 540 (s). The rainbow scale is the fluorescence lifetime of the dye in the particle from 1 (blue) to 4.8 ns (red) and the scale bar is 40 µm to show relative size of the particle under observation. (adopted from Hosny et al.)[83]

Ambient particles are prone to oxidation by oxidants such as OH radical and O_3, which can change the particle phase state over time. Hosny et al., investigated the phase transition of oleic acid particles upon exposure of O_3.[83] They generated oleic acid particle containing the fluorescence dye and measured the fluorescence intensity as the oleic acid gets oxidized over time. The image taken at 540 s (Figure 1.5) shows the fluorescence dye inside the organic aerosol fluoresces for

longer time (~ 4 ns) as the particle gets more viscous due to formation of high molecular weight compounds from oxidation of oleic acid against O_3.[83] A few studies, including the Figure 1.5 study, have shown viscosity increases as compounds with high molecular weight forms.[84-85] Carboxylic acid (-COOH), alcohol (C-OH), peroxides (-OOH or -C(O)-), and aldehyde (-CHO) contain functional groups that can form strong hydrogen bond with each other, which will then make particle more viscous.[84, 86] These studies indicate particle phase transition is highly dependent on the molecular weight and functional groups of oxidized compounds, which can prolong the lifetime of toxic compounds in the atmosphere. There are only a few studies that have investigated the phase transition of particles using limited number of precursors such as oleic acid and terpenes, despite indoor and outdoor environments being composed of numerous, different organic compounds.[82-83, 85, 87] Studies involving phase transition using different precursors, such as polycyclic aromatic hydrocarbons (PAHs) abundantly found on soot, are lacking. Thus, in order to study how phase transitions also plays a role in long-range transport of carcinogenic PAHs in the atmosphere, phase transition using different precursors must be further investigated.

1.4.2: Phase Separation

Atmospheric particles consist of a myriad of different organic and inorganic compounds that can have multiple interactions based on their molecular structures and polarity within the bulk. These chemical interactions often lead the particles to adopt a multiphase system in which chemicals with similar polarity or functional groups will mix while dissimilar molecules tend to separate from the mixture and form a completely different phase. Imaging techniques revealed ambient particles can have multiphase system.[74] Additionally, immiscibility of organic compounds with different polarities have also been observed adding complexity in our understanding of particle phase state. Laboratory generated polycyclic aromatic hydrocarbon (PAHs) particles with

viscous organic coating had significant amounts of PAHs remain unreacted in the particle exposed to O_3 due to slow bulk diffusivity at the coating layers.[88-89] These results further reveal phase states play an important role in long range transport of toxic compounds for multiphase systems. However, ambient particles are prone to chemical aging and oxidized organic compounds may phase separate with nonpolar parent compounds within the bulk. There are only limited number of studies available that investigate how phase transition and separation affect the lifetime of chemical species. Thus, additional work into phase transition and its effect are necessary to elucidate the mechanism that prolong the lifetime of toxic compounds in the atmosphere.

1.5 Goal and Organization of the Dissertation

The overall goal of the dissertation is to explore which chemicals may be responsible for ROS formation from highway and wildfire PM in water. Ozonolysis of PAHs in solid and liquid multicomponent films were also investigated to better understand how phase separation and transition can affect reaction mechanism and kinetics.

Chapter 2 discusses EPFR and ROS formation measurements from highway fine PM and its correlation with highway-related pollutants and DTT assay. We hypothesized that iron and copper will show a strong correlation with the formed ROS measurements, as past measurements suggest the sampling site is significantly influenced by non-exhaust emissions. Correlation analysis revealed strong correlations with EPFR and metals, while the correlation between formed ROS and metal was weak. This suggests metals may play an important role in stabilizing EPFR, and more complex chemistry may be involved in ROS generation from highway fine PM. Interestingly, correlation analysis showed strong correlations between ROS generated from the aqueous extracts of fine PM and DTT activities at one of the highways.

Chapter 3 is a preliminary work on EPFR and ROS generation measurements from size-segregated wildfire PM. Only a finite amount of studies have explored the EPFR abundance and ROS formation from wildfire PM, despite potential ROS sources from metals and aromatic compounds are abundant in wildfire emission. EPFR from wildfire PM_1 was found to be approximately ten times higher than the urban background. ·OH, $O_2^{\cdot-}$, and organic radicals were formed from aqueous extract of wildfire $PM_{<1}$. The $O_2^{\cdot-}$ was only detected in yellow aqueous extract of PM_{10} or PM_1 depending on the wildfire events.

Chapter 4 investigates the chemical kinetics between PAHs and O_3 in multicomponent organic film. Benzo[a]pyrene (BaP) was selected for this study because BaP can be emitted from wide range of sources and its oxidation products are toxic. We hypothesized BaP oxidation products will also be immiscible with BaP due to difference in polarities in a multicomponent film. The experimental and modeling results show BaP is immiscible in SOA film at dry and humid conditions, and that it forms a surface layer at the SOA film. BaP oxidation products were also found to be immiscible in indoor-related liquid organic films, and that it forms a surface layer on top of the organic film. The surface PAHs and oxidized PAHs layer at SOA and organic liquid film slows the bulk diffusivity of BaP and prolong the lifetime of these toxic chemicals, respectively.

1.6 General Methods of the Dissertation

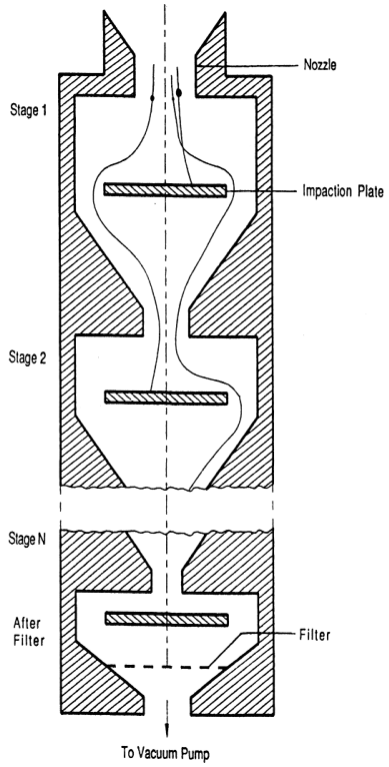

Figure 1.6: The general schematic of how cascade impactors work is shown. (adapted from Baron et al.)[90]

1.6.1 Particle Sampling

The high-volume sampler with a $PM_{2.5}$ impactor (Hi-Vol, Tisch Environmental, flow rate 1.13 m^3 min^{-1}) and Micro-Orifice Uniform Deposit Impactor (MOUDI, TSI Incoporated, Shoreview, MN, USA) were used to collect fine and size-segregated PM, respectively. These sampling devices collect particles through an airstream starting from the opening also known as nozzle (Figure 1.6). Particles may stick on the impaction plate containing a filter based on their inertia. For sampling devices with multiple impaction plates such as MOUDI, the lighter particles will pass through each N stage, and the smallest particles are expected to collect at the most bottom stage.

The collection efficiency (η) of particles at each stage for MOUDI also differs depending on particle diameter (D_p), flow velocity (V), particle density (ρ), air viscosity (μ), and physical dimensions of the nozzle (D_b) at each stage. The collection efficiency can be calculated with the equation:

$$\eta = \frac{D_p V \rho}{18 \mu D_b} \quad (\text{eq. } 3)$$

Figure 1.7: MOUDI was stored in an aluminum container for sampling during the wildfire.

The MOUDI was inserted into a 44" x 30" x 30" aluminum container for samples collected between November to December 2020 at Rowland Hall, Irvine (Figure 1.7). This container was used for sampling particles during the wildfire because the strong wind frequently occurred.

The size-segregated particles were collected using MOUDI at a flow rate of 30 L min^{-1}. The Hi-Vol l flow rate was calibrated at the sampling location under ambient conditions using five different flow rates: 1.02, 1.08, 1.13, 1.19, and 1.25 m^3 min^{-1}. Then, the flow rate was set to 1.13 m^3 min^{-1} to collect fine PM at the location because the cut-off diameter of 2.5 μm is at 1.13 m^3 min^{-1}. Figure 1.8 shows ambient particles collected at the sampling site using Hi-Vol and MOUDI.

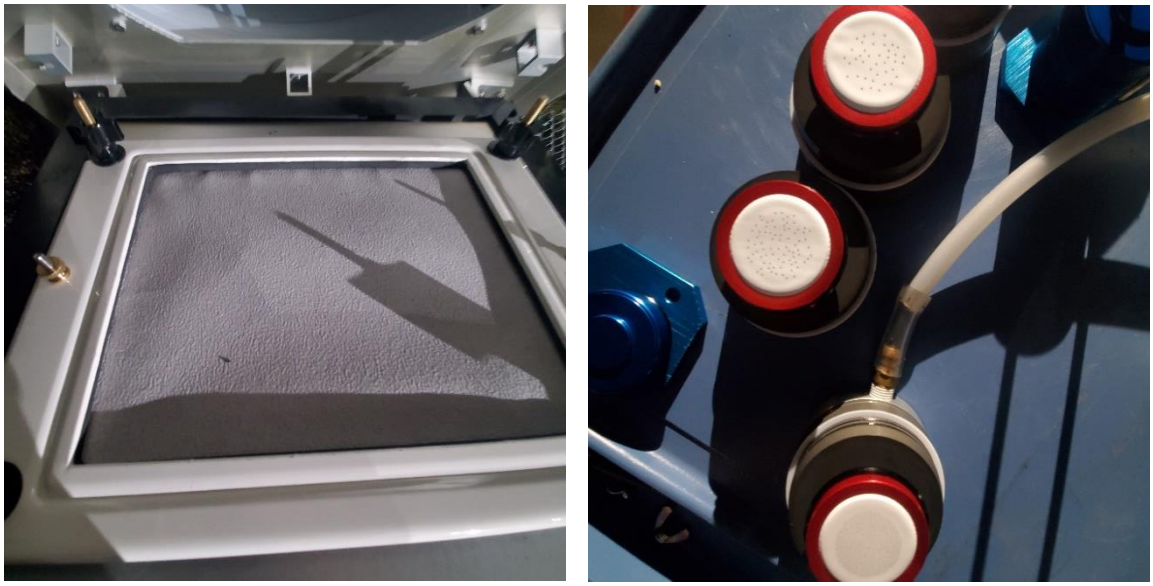

Figure 1.8: Ambient particles were collected on filters using Hi-Vol (left) and MOUDI (right) at the highway, Anaheim.

1.6.2 Filter Preparation

Prebaked 8” × 10” micro-quartz filters and Teflon filters were loaded on filter holder and impactor stages, respectively. Quartz filters were baked at 550°C for 4 to 6 hours. A Hi-Vol and MOUDI were set up at each site and fine and size-segregated particles were collected onto quartz and Teflon filters, respectively. After collection, the quartz filters were wrapped in prebaked aluminum foil and Teflon filters were stored in Petri dishes. The filters were immediately stored in a freezer (-18 °C). Portions of the quartz filters collected from the sampling sites were cut using a circular punch with a diameter of 2.54 cm, and used for measurement of EPFRs, ROS, and DTT activities. A whole Teflon filter was used for EPFR measurement. Then, the filter was cut in half for measurements of ROS and DTT activities.

1.6.3 Sampling Location

Figure 1.9 shows the sampling locations where the ambient samples were collected in Southern California: urban site (a campus building at the University of California, Irvine (UCI), 33°38'40.4"N 117°50'39.3"W, elevation 20 meters) and two highway sites in Anaheim (Interstate

5, 33°49'09.4"N 117°55'07.5"W) and Long Beach (Interstate 710, 33°51'34.0"N 118°12'01.0"W) within 20 meters from the highway roads. The Interstate 5 (I-5) is one of the busiest highways in Southern California and known as a commuter route from Orange County to the city of Los Angeles. The other highway site, Interstate 710 (I-710), is a major route that connects Long Beach and the Los Angeles city with a higher fraction of heavy-duty vehicles and known as a heavy-duty corridor.[19] Particle filter samples were collected for 4 – 12 hours daily from 1/28/2020 to 2/3/2020 at the Anaheim site, for 6 – 12 hours per day from 2/4/2020 to 2/10/2020 (except on 2/9/2020) at the Long beach site, and for 8 – 11 hours at the urban site from 2/23/2020 to 2/29/2020 (except on 2/28/2020). Samples were also collected for 2.5 - 3 days from 10/26/20 – 12/6/20 at UCI during the two wildfire events: Silverado Fire (10/26/20 – 11/7/20) and Bond Fire (12/2/20 – 12/10/20). The sampling site is ~ 15 km away from the main forest fire location: Santiago Canyon.

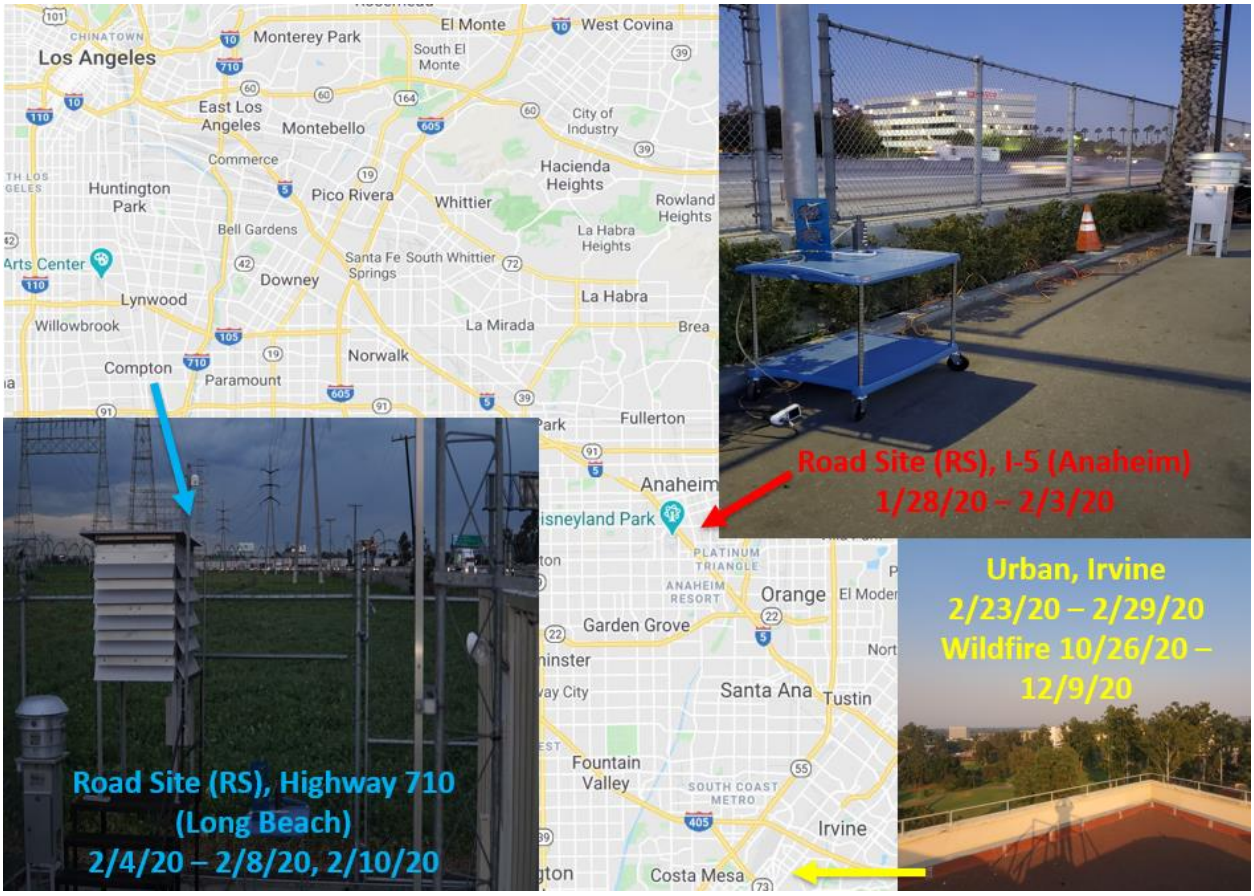

Figure 1.9: Ambient samples were collected at Anaheim, Long Beach, and Irvine from January to March and October to November 2020. (Google, n.d.) [Google Maps directions driving from Los Angeles to Irvine].

1.6.4. Continuous wave electron paramagnetic resonance spectrometer

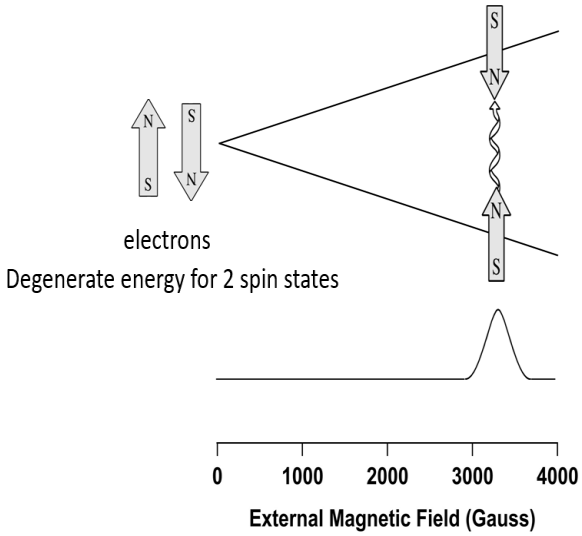

Figure 1.10: An electron has 2 spin states, and these spin states have same energy (degenerate). The energy of the spin states will differ once the electron is immersed in external magnetic field. (adopted from Weber)[91-92]

A radical is a molecule, atom, or ion with an unpaired electron and has been extensively studied due to its impact in atmospheric and physiological processes. The continuous wave electron paramagnetic resonance (CW-EPR) spectrometer was used to measure radicals from ambient samples. EPR spectroscopy is based on the Zeeman Effect which splits the energy of unpaired electron spin states in the presence of a magnetic field.[91-92] An electron is spinning charge subatomic particle that acts like a small magnet when it is exposed to an external magnetic field. A single unpaired electron can either align with the magnetic field (lower energy state) or against the magnetic field (higher energy state) as shown in Figure 1.10. The quantum mechanics potential energy of an electron (E) in interaction with the magnetic field (B_0) is given:

$$E = \frac{1}{2}\, g\, \mu_B B_0 \quad \text{(eq. 4)}$$

where g also known as g-factor is a value that depends on where the unpaired electron mainly resides in the molecule (g = 2.0023 for a free electron) and μ_B is the Bohr magneton, which the

natural unit of electronic magnetic moment. EPR measures the signal due to the transition of electron from lower energy state $E = -\frac{1}{2}\, g\, \mu_B B_0$ to higher energy state $E = \frac{1}{2}\, g\, \mu_B B_0$ when the electron is exposed to continuous microwave radiation (ν) in the presence of a magnetic field. This difference in energy (ΔE) is given by:

$$\Delta E = h\nu = \frac{1}{2}\, g\, \mu_B B_0 - \left(-\frac{1}{2}\, g\, \mu_B B_0\right) = g\, \mu_B B_0 \quad (\text{eq. } 5)$$

The population of electron of two spin states can be estimated at a given temperature (T) by the Boltzmann Equation:

$$\frac{n_{against}}{n_{align}} = e^{-\frac{\Delta E}{kT}} \quad (\text{eq. } 6)$$

where $n_{against}$ is the number of electrons in the higher energy state and n_{align} is the number of electrons in the lower energy state. The Boltzmann constant (k) is the constant that relates the energy of the system to the temperature.

1.6.5 EPR Signal

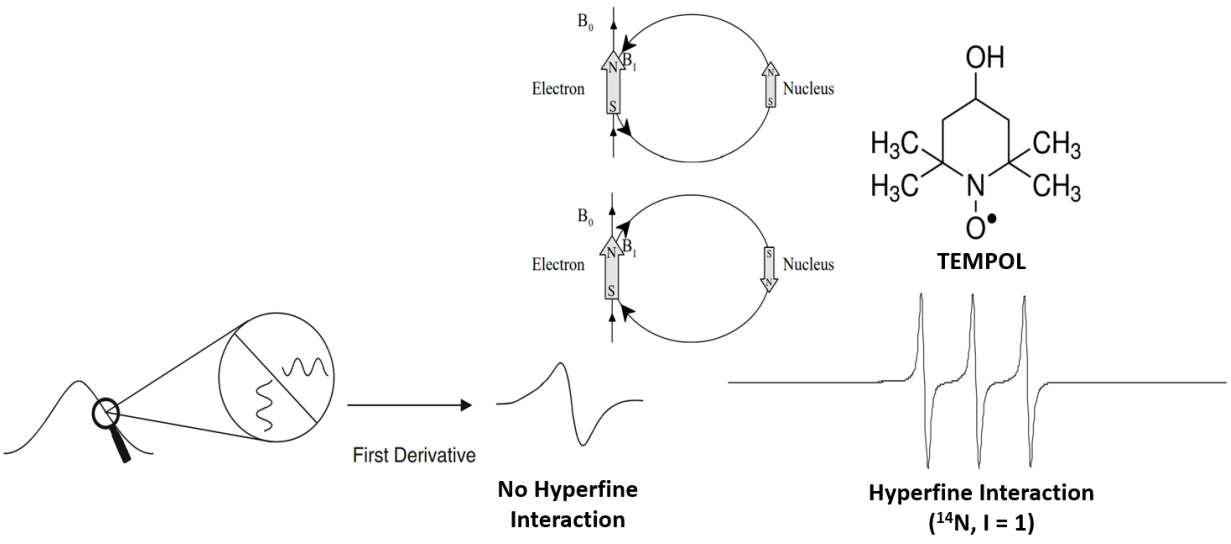

Figure 1.11: The modulation amplitude is applied to the magnetic field region where the sample absorbs the signal resulting in a first derivative EPR signal. The electron magnetic field is also influenced by the magnetic field exerted by the nucleus in a molecule. If the unpaired electron is influenced by nitrogen-14 isotope with a nuclear spin of 1 (for in the case of the molecule TEMPOL), the signal will split into three based on equation 6. (adopted from Weber)[91-92]

A typical EPR measurements begins as the magnetic field strength varies while simultaneously exposing the sample with a constant microwave radiation. The instrument also employs a weaker magnetic field ~ 35 mG as the external magnetic field (G) is scanned to the sample. This weaker magnetic field also known as modulation amplitude oscillate at the same frequency as the signal and the detector measures the change in slope of the absorption signal which eventually gives an output of the derivative EPR signal in the spectrum as shown in Figure 1.11.

1.6.6 Hyperfine Interaction

Isotope	Natural Abundance (%)	Nuclear Spin (I_n)
^{1}**H**	99.99	$\frac{1}{2}$
^{12}**C**	98.93	0
^{14}**N**	99.63	1
^{16}**O**	99.76	0

Table 1.2: Nucleus Spin of each isotope and their natural abundance.

For a single electron immersed in a magnetic field, the excitation of electrons to the higher energy state will result in a single first derivate peak in the EPR spectrum. However, electrons are also influence by the nucleus magnetic field in a molecule and will result in a different EPR signal as shown in Figure 1.11. This is called hyperfine interaction and can give an additional information about the structure of the molecule where the electron mainly resides. The nucleus is a spinning charged subatomic particle and has a nuclear spin (I_n) which depends on the isotope. Table 1 shows the nucleus spin of each isotope and their natural abundance that are relevant to this dissertation.[93] The number of lines (N_l) observed in the EPR spectrum can be predicted by the equation:

$$N_l = 2I_n + 1 \ (\text{eq. } 7)$$

In the case of the standard that was used in this study, 4-hydroxy-2,2,6,6-tetramethylpiperidin-1-oxyl, also known as TEMPOL. The unpaired electron is affected by the nitrogen (^{14}N) and oxygen

(^{16}O) nuclei that have the nuclear spins of 1 and 0, respectively, and the TEMPOL measurement will show 3 lines in the EPR spectrum (Figure 1.11).

1.6.7 EPR Calibration

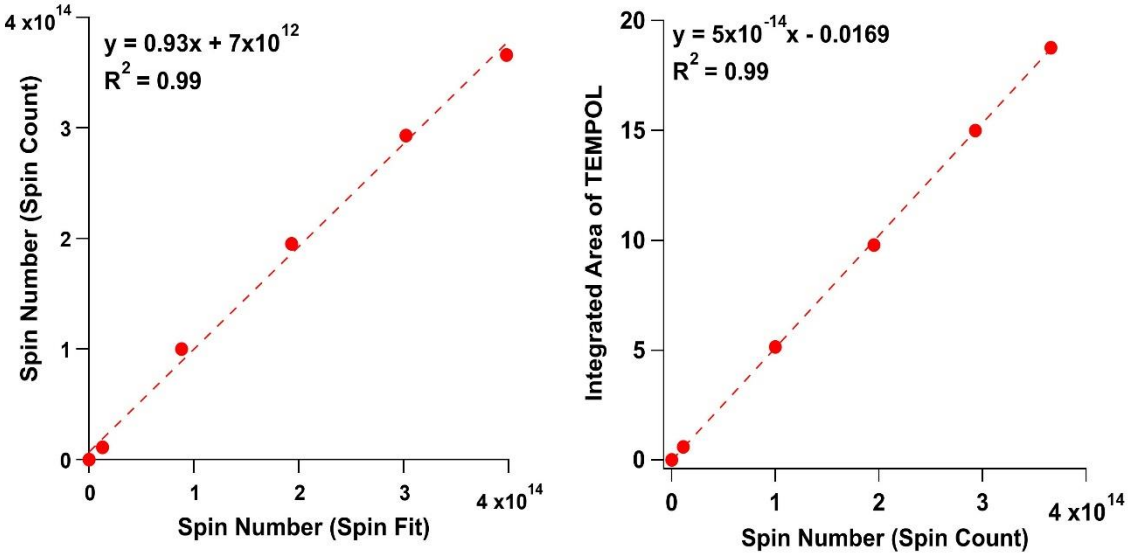

Figure 1.12: The spin number of the standard solution using SpinFit and Spin Count are consistent (left). The EPR signals of TEMPOL were integrated using Spin Count and calibration curve was used to quantify EPFR signal for our ambient samples.

2,2-diphenyl-1-picrylhydrazl (DPPH) and 4-hydroxy-2,2,6,6-tetramethylpiperidin-1-oxyl (TEMPOL) are often used as organic radical standards for EPR experiments.[91] TEMPOL was chosen as a standard in this study because it is stable and EPR parameters to quantify TEMPOL are provided in the EPR embedded software model, SpinFit. The spin number quantified using SpinFit was also compared with the results using another EPR embedded software program SpinCount which provides integrated area and spin number information (Fig 1.12). The results obtained using both software packages closely agree and the calibration curve shown in Figure 1.12 was used to quantify EPFR in our samples.

1.6.8 EPR Data Processing

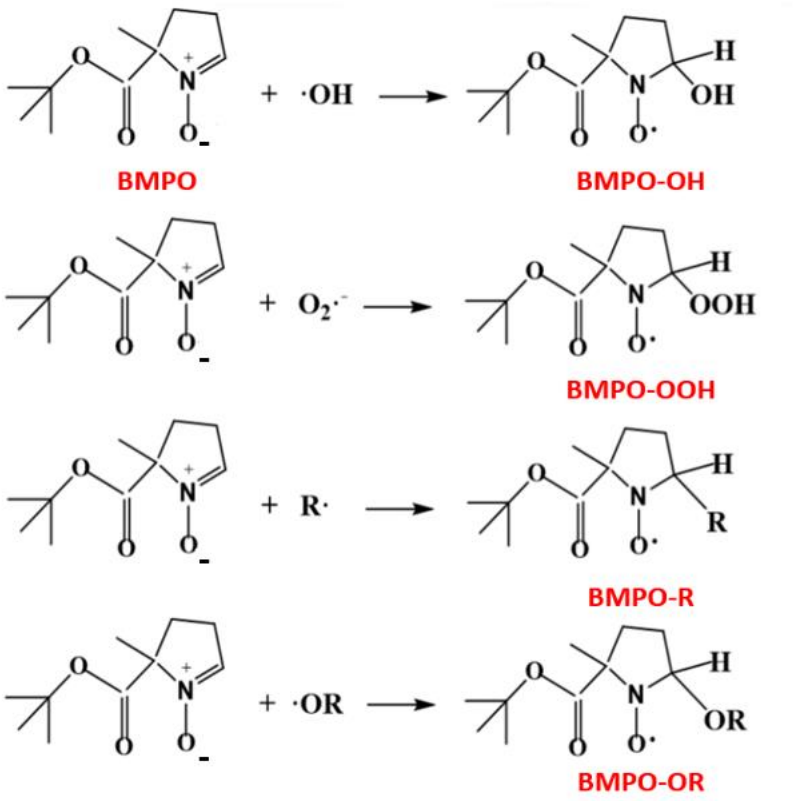

Figure 1.13: The chemical mechanism between radical of interest with the spin trap, BMPO. (Adopted from Wang et al.)[94]

The EPR embedded model, SpinFit, was used to identify and quantify the ROS observed in our sample spectrum. The spin trap, 5-*tert*-Butoxycarbonyl-5-methyl-1-pyrroline-N-oxide (BMPO), was used to react with ROS generated by the particles in solution to form more stable radical (BMPO-adducts) for measurements. The SpinFit simulates the observed spectrum result based on the inputted parameters: g-value, linewidth, line shape, and hyperfine splitting constants. This model also contains a library of selected radicals that were used as a reference: BMPO-OH, BMPO-OOH, and TEMPOL. The Figure 1.13 shows the list of radicals that were identified and quantified in this work. The BMPO-R and BMPO-OR are BMPO adducts that are formed from reacting with carbon-centered and oxygen-centered organic radicals, respectively. The difficulty

of synthesizing a pure and stable organic radical standard that can be used to react directly with the spin trap makes it difficult to define the BMPO-R and BMPO-OR radical adducts parameters. The more well characterized and chemically equivalent spin trap, 3,4-dihydro-2,3-dimethyl-2H-pyrrole 1-oxide (DMPO), has been studied with the organic radicals and similar parameters were used to simulate the spectrum for BMPO-R and BMPO-OR radical adducts.[95-96] The parameters used in this study to fit the observed signals are consistent with other studies. The exact identification of the organic radicals is not known in this study and should be further investigated for future studies.

1.6.9 Kinetic Modeling

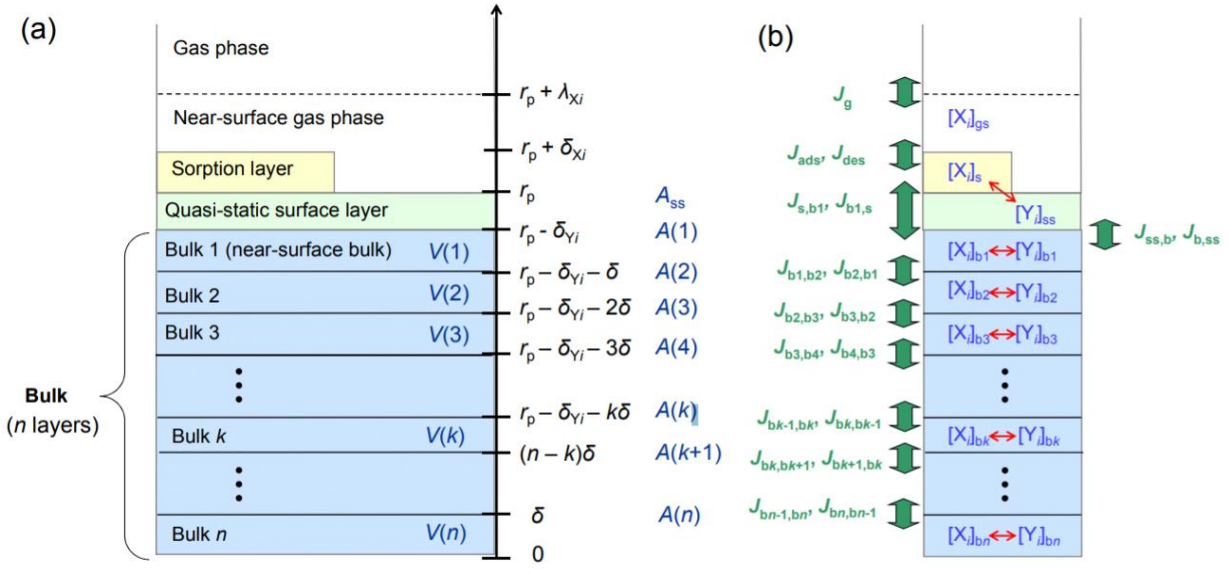

Figure 1.14: The kinetic multilayer model (KM-SUB) schematics, and this model was modified to study the thin film chemistry. The flux of chemical species (J) from the bulk to surface is shown in (b) and the red arrow indicates the chemical reactions between gas and condense-phase molecules. (Adapted from Shiraiwa et al)[97]

A kinetic multi-layer model of aerosol surface and bulk chemistry (KM-SUB) was used to simulate the experimental data provided by our collaborator (Figure 1.14). KM-SUB explicitly treats mass transport and chemical reactions at the surface and in the bulk of the system of interest, in this study: thin film. This model consists of multiple model compartments and layers

respectively: gas phase, near-surface gas phase, sorption layer, quasi-static surface layer, near-surface bulk, and a number of n bulk layers. The sorption layer is defined as the adsorption layer for gas-phase molecules and quasi-static surface layer is the surface layer of the thin film. The parameter (r_p) is defined as particle radius or in this study is the total film thickness. The λ_{xi} is the mean free path which is the distance the molecule travels before it makes a collision. The δ_{xi} and δ_{yi}, is defined as the size of the gas species X_i and condense phase species Y_i respectively. The δ, A, and V refers to the bulk thickness, area and volume of the film respectively.

1.6.10 Brief Description of Chemical Mechanisms in the Model

Experimental and modeling results show ozonolysis of PAHs follows the Langmuir-Hinselwood (LH) reaction pathway, in which the O_3 first adsorbs to the surface of PAHs and undergoes surface reaction.[98-100] Past kinetic modeling work demonstrated the adsorbed O_3 on PAH surfaces dissociates and forms a stronger chemisorbed oxygen species on the aromatic surface also known as reactive oxygen intermediate (ROI).[81, 89, 101] This reaction mechanism was treated in the model to be consistent with the short lifetime (nanoseconds) of O_3 on PAH surface calculated by the quantum mechanical calculations and explains the non-linear dependence of PAH decay against O_3 in the experiment data.[101]

Chapter 2: Environmentally Persistent Free Radicals, Reactive Oxygen Species Generation, and Oxidative Potential of Highway $PM_{2.5}$

This chapter is reproduced by permission from: Hwang, B.C.H.; Fang, T.; Pham, R.; Wei, J.; Gronstal, S.; Lopez, B.; Frederickson, C.; Galeazzo, T.; Wang, X.; Jung, H.; Shiraiwa, M., "Environmentally Persistent Free Radicals, Reactive Oxygen Species Generation, and Oxidative Potential of Highway $PM_{2.5}$."ACS Earth and Space Chemistry 2021, 5, 8, 1865–1875; DOI:10.1021/acsearthspacechem.1c00135

2.1 Abstract

In urban environments, vehicle exhaust and non-exhaust emissions represent important sources of fine particulate matter with an aerodynamic diameter less than 2.5 μm ($PM_{2.5}$). This plays a central role in adverse health effects and oxidative stress. We collected $PM_{2.5}$ filter samples from two highway sites (Anaheim and Long Beach, CA) and an urban site (Irvine, CA) to quantify environmentally persistent free radicals (EPFRs) contained in $PM_{2.5}$ and generation of radical forms of reactive oxygen species (ROS) in water using electron paramagnetic resonance spectroscopy. The EPFR concentrations were 36 ± 14 pmol m^{-3} at highway sites, which were about two times higher than those at the urban site. EPFRs correlated positively with CO, NOx, and elemental and organic carbon, indicating that EPFRs are emitted from vehicular exhaust. Good correlations of EPFRs and Fe and Cu may indicate that EPFRs are stabilized by Fe and Cu emitted from tire and brake wears. EPFRs are negatively correlated with ozone, suggesting that photochemistry does not play a large role in the formation of EPFRs and possibly also indicating that EPFRs are quenched by ozone. Highway $PM_{2.5}$ were found to generate mainly OH and organic radicals in the aqueous phase. The generated ROS were correlated with $PM_{2.5}$ mass concentrations and OH radicals showed a good correlation with EPFRs, implying the role of EPFRs in aqueous OH radical generation. The $PM_{2.5}$ oxidative potentials as quantified with the dithiothreitol (DTT) assay were correlated with ROS, OH and organic radicals for $PM_{2.5}$ collected in Anaheim, while little correlations were observed for Long Beach. These findings highlighted the interplay of various PM redox-active chemical components and complex relationship between ROS formation and DTT activity.

2.2 Introduction

Traffic-related emissions are one of the most important sources of particulate matter (PM) in urban environments. Exposure to the traffic-related fine PM is often associated with adverse health effects and oxidative stress.[102-106] Within the past two decades, many countries have implemented stringent regulations leading to a significant reduction in exhaust or tailpipe emissions and PM mass concentrations.[16, 27, 107] In contrast, non-exhaust emissions from brakes, tires, and road wear are currently not regulated, but their importance in urban air quality has been increasingly recognized.[19-20, 27, 108] Correlation analyses from recent studies suggest that non-exhaust emissions also contribute to fine PM toxicity, highlighting the importance of investigating relations among sources, chemical composition, and particle toxicity.[19-20] Recent epidemiological studies have shown strong associations of long-term exposure to non-tailpipe emissions with respiratory and cardiovascular diseases.[26, 109]

Ambient PM contains particle-bound free radicals, so-called environmentally persistent free radicals (EPFRs); in contrast to common free radicals with short lifetimes, EPFRs in atmospheric particles can persist for days or longer.[46, 55-56, 110] EPFRs may originate from both primary and secondary sources. Previous studies have found that particles emitted from coal combustion, traffic, and dust contain large amounts of EPFRs.[111-113] The chemical identity of EPFRs generated from incomplete combustion can be semiquinone, phenoxyl, and cyclopentadienyl radicals formed by thermal decomposition of organic precursors on metal-containing particles.[58, 114] EPFRs can also be formed in secondary processes such as heterogeneous oxidation of polycyclic aromatic hydrocarbons (PAHs) by ozone[59, 115] and oxidation of naphthalene followed by the formation of secondary organic aerosols (SOA).[116]

PM toxicity is related to its ability to cause oxidative stress[13, 117-118] by the formation of reactive oxygen species (ROS) upon inhalation and respiratory deposition of PM.[119-120] ROS include hydroxyl radical (OH▪), superoxide radical (▪O_2^-), hydrogen peroxide (H_2O_2), and organic radicals, which can deplete antioxidants and induce oxidative damage to lipids and tissues.[28, 37, 109, 120] PM contains redox-active components including quinones and transition metals,[45, 121-123] which can generate ROS via Fenton(-like) reactions, quinoid redox cycling, and decomposition of organic hydroperoxides.[39, 57, 116, 124-126] EPFRs are also shown to catalytically generate ROS by redox reactions.[57, 124, 127]

Oxidative potential of PM represents the redox activity of particles to generate ROS. One of the most commonly used methods to quantify PM oxidative potential is the dithiothreitol (DTT) assay.[71, 128-129] This method is sensitive to quinones,[130] transition metals,[68, 71, 131] humic-like substances (HULIS)[132-133] and it has also successfully applied to SOA formed by oxidation of naphthalene,[116, 134-136] toluene,[137] and isoprene SOA.[132-133, 138] Both exhaust and non-exhaust emissions have been identified as important sources contributing to PM DTT activities.[139-144] Studies have shown associations of DTT activities with various health outcomes,[68, 145-147] suggesting that controlling oxidative potential would add another dimension to the regulation of aerosol health effects in addition to reducing PM mass concentrations.[143] Note that DTT is not a physiological antioxidant in the human body and the robustness of the DTT assay in predicting PM health effects is still to be established. The similarity in PM chemical contributors to EPFRs, ROS generation, and DTT activities implies possibly close associations among them, but the link and interplay among them for causing oxidative stress are still unclear and warrant further investigations.

Traffic-related emissions contain high levels of EPFRs, quinones, and transition metals, providing a good source to study such associations to understand the contribution from exhaust and non-exhaust emissions. In this study, ambient PM with an aerodynamic diameter less than 2.5 μm ($PM_{2.5}$) was collected using a high-volume $PM_{2.5}$ sampler at highway sites in Anaheim and Long Beach as well as at an urban site in Irvine (all sites in Southern California, USA). The past chemical analyses at these locations have shown that the vehicle emissions cause poor air quality.[19-20] Particle-bound EPFRs were measured using a continuous wave electron paramagnetic resonance (EPR) spectrometer. The generation of ROS was quantified by extracting the particles in water and analyzing the extracts using EPR coupled with a spin-trapping technique. The DTT activity was measured by monitoring the consumption of DTT over time in $PM_{2.5}$ total extracts including the water-soluble and -insoluble fractions (hereafter called "total DTT activity"). We measured PM chemical components including organic carbon (OC), elemental carbon (EC), and transition metals. Gaseous pollutants including ozone (O_3), nitrogen monoxide (NO), nitrogen dioxide (NO_2), and carbon monoxide (CO) were also obtained. The correlations of EPFRs, ROS generation, and total DTT activity as well as $PM_{2.5}$ mass concentration were investigated for better understanding of aerosol health effects and oxidative stress by PM from traffic-related emissions.

2.3 Materials and methods

2.3.1 PM Collection. A high-volume sampler (Hi-Vol, Tisch Environmental, flow rate 1.13 m^3 min^{-1}) was used to collect ambient $PM_{2.5}$ onto prebaked 8" × 10" micro-quartz filters at an urban site (a campus building at the University of California, Irvine, 33°38'40.4"N 117°50'39.3"W, elevation 20 meters) and two highway sites in Anaheim (Interstate 5, 33°49'09.4"N 117°55'07.5"W) and Long Beach (Interstate 710, 33°51'34.0"N 118°12'01.0"W) within 20 meters from the highway roads. The Interstate 5 (I-5) is one of the busiest highways in Southern California and known as a commuter route from Orange County to the city of Los Angeles. The other highway site, Interstate 710 (I-710), is a major route that connects Long Beach and the Los Angeles city with a higher fraction of heavy-duty vehicles and known as heavy-duty corridor.[19] Particle filter samples were collected for 4 – 12 hours daily from 1/28/2020 to 2/3/2020 at the Anaheim site, for 6 – 12 hours per day from 2/4/2020 to 2/10/2020 (except on 2/9/2020) at the Long beach site, and for 8 – 11 hours at the urban site from 2/23/2020 to 2/29/2020 (except on 2/28/2020). Field blanks were collected every other day at each site. After the collection, all filters were wrapped in a prebaked aluminum foil and immediately stored in a freezer (-18 °C). Portions of the filters collected from the highway sites were cut using a circular punch with a diameter of 2.54 cm, and used for measurement of EPFRs, ROS, and DTT activities. Those from the urban sites were analyzed for EPFRs. Measurements of EPFRs, ROS, and DTT on each filter was repeated 3 – 5 times. EPFR measurements were conducted within two weeks of sample collection and ROS and DTT measurements were conducted within 4 – 6 months. Note that EPFRs are stable at least a year after collection (Fig. 2.2). Additionally, $PM_{2.5}$ samples were collected on one 47 mm Teflon-membrane filter and two 47 mm quartz-fiber filters in parallel using a medium-volume sampler with a Bendix Model 240 $PM_{2.5}$ cyclone at both highway sites. These filters were used to determine PM mass,

metals, OC, and EC at the highway sites. The sampling flow rate was 37.7 L min^{-1} for each filter channel and the sampling duration was four hours covering the following periods: 6:00 – 10:00, 10:00 – 14:00, and 14:00 – 18:00. The total sampling periods overlapped with the Hi-Vol sampling periods. The Teflon-membrane filters were analyzed for $PM_{2.5}$ mass and metal while the quartz fiber filters were analyzed for OC and EC.[148]

2.3.2 Environmentally Persistent Free Radicals (EPFRs). One or two circular punches from each filter sample was inserted into a quartz tube (9.17 mm I.D., SP Wilmad-LabGlass) for EPFR measurements using a continuous-wave electron paramagnetic resonance (CW-EPR) spectrometer (EMXplus, Bruker, Germany). The following parameters were used in EPR: a microwave frequency of 9.65 GHz; a microwave power of 36.18 mW (8 dB); a modulation frequency of 100 kHz; a modulation amplitude of 1.0 G; a receiver gain of 40 dB; a time constant of 10.24 ms; and a magnetic field scan of 1623.06 G. Ambient concentrations of EPFRs are presented as EPFR per volume of air (EPFRv, pmol m^{-3}) and per mass of $PM_{2.5}$ (EPFRm, pmol μg^{-1}). Paramagnetic species are characterized based on their g factor values: free electrons have a g factor value of 2.0023 and organic radicals have slightly higher values depending on the number of oxygen atoms in the molecule.[58]

2.3.3 Reactive Oxygen Species (ROS) Generation. EPR combined with a spin-trapping technique was applied to detect radicals in the aqueous particle extracts. Two circular punches from each filter sample were extracted in 1.3 mL of 10 mM spin-trapping agent 5-tert-butoxycarbonyl-5-methyl-1-pyrroline-N-oxide (BMPO) in Millipore water (>18 Ω cm^{-1}) for 8 – 10 minutes using an analog vortex mixer (VWR International LLC) and both water-soluble and insoluble compounds must have been extracted. The extracts were then concentrated by 5 to 20 times through blowing under N_2 gas for 10 – 13 minutes. The remaining solution was inserted into

a 50 µL micropipette and measured within 25 minutes from extraction. The EPR parameters used for ROS measurement were the same as those for EPFRs except: a microwave frequency of 9.86 GHz, a microwave power of 21.17 mW (10 dB); a time constant of 20.48 ms; a modulation amplitude of 2.0 G and a magnetic field scan of 150.0 G. The SpinFit and SpinCount modules in the Xenon software were applied to simulate each EPR spectrum to identify and quantify different radical adducts in the extracts. Data are normalized to the sampled volume of air (ROSv, pmol m^{-3}) and $PM_{2.5}$ mass (ROSm, pmol μg^{-1}).

2.3.4 Total Dithiothreitol (DTT) Activities. Two circular punches from each filter sample were extracted in 7 mL of Millipore water for 8 – 10 minutes using the vortex mixer. The DTT assay was conducted on the extracts and the filter following the same DTT protocol in Gao et al. (2017).[149] The measured total DTT activities include the contributions from both the water-soluble and water-insoluble fractions. In brief, 7 mL of the extracts and the filter were incubated at 37 °C with 2 mL potassium phosphate buffer and 1 mL DTT (1mM) and shaken continuously in a ThermoMixer (Eppendorf North America, Inc.). At specified time points (5, 10 ,15, 20, 25 min), a small aliquot (100 µL) of the incubated mixture was withdrawn and mixed with 1 mL trichloroacetic acid to quench the consumption of DTT. The quenched mixture was further mixed with 2mL Tris buffer (0.08 M with 4 mM EDTA (ethylenediaminetetraacetate)) and 0.5 mL of DTNB (0.2 mM, 5,5'-dithiobis-(2-nitrobenzoic acid)). 1 mL of this mixture was diluted with 9.5 mL of water and filtered using a 0.22 µm pore syringe filter (Millex). The filtered solution was immediately measured for absorbance at 412 nm and 700 nm wavelength using the Liquid Waveguide Capillary Cell with an optical path length of 100 cm (World Precision Instruments, Inc.) coupled to the ultraviolet-visible spectrophotometer (DH-MINI, Ocean Optics, Inc.) and the multi-wavelength light detector (FLAME-T-UV-VIS-ES, Ocean Optics, Inc.). The total DTT

activities were calculated from the linear regression of absorbance versus time, and presented as the total DTT activities per volume of air (total DTTv, pmol min^{-1} m^{-3}) and per mass of $PM_{2.5}$ (total DTTm, pmol min^{-1} μg^{-1}).[150]

2.3.5. Gaseous Pollutants. Real-time online measurements of gaseous pollutants were conducted at both sites. CO was measured with the Teledyne Model 300E CO analyzer every minute. NO and NO_2 were measured with an ECO Physics CLD 60 analyzer. Hourly O_3 was obtained from SCAQMD Long Beach - Signal Hill (33°47'37.4"N 118°10'15.7"W) and Anaheim - Loara School (33°49'50.2"N 117°56'18.6"W) sites (https://ww2.arb.ca.gov/).

2.3.6. PM2.5 Mass and Metals. Blank and exposed Teflon-membrane filters for the medium-volume sampler were equilibrated in a clean room with controlled temperature (21.5 ± 1.5 °C) and relative humidity (35 ± 5%) for > 24 hours before mass determination by gravimetry. Filters were weighed before and after sampling with a ±1 μg sensitivity microbalance (XP6, Mettler Toledo,LLC) to obtain gravimetric $PM_{2.5}$ mass.[151] Teflon-membrane filters were then analyzed for 51 elements (from sodium to uranium) by high sensitivity energy-dispersive X-ray fluorescence (XRF, Panalytical Epsilon 5).[152] Iron (Fe) and copper (Cu) are selected to discuss in this work, as they are known to be redox-active to cause ROS formation.

2.3.7. OC and EC. OC and EC were quantified from the quartz-fiber filters collected by the medium-volume sampler. The analysis followed the IMPROVE_A thermal/optical protocol using a multi-wavelength OC/EC analyzer (DRI Model 2015, Magee Scientific).[153-155] The table 2.1 lists the average concentration of selected pollutants measured at both highways in Anaheim and Long Beach.

Table 2.1. Average concentrations (±standard deviations) of OC, EC, O_3, NO, NO_2, CO, and metals at the Long Beach and Anaheim sites

	Long Beach	Anaheim
OC, µg m^{-3}	3.14 ± 1.10	3.39 ± 0.99
EC, µg m^{-3}	1.83 ± 0.58	1.48 ± 0.38
O_3, ppb	13.8 ± 12.8	9.4 ± 6.2
NO, ppb	33.3 ± 21.2	38.2 ± 12.4
NO_2, ppb	21.9 ± 7.0	24.4 ± 5.4
CO, ppm	0.56 ± 0.21	0.90 ± 0.15
Fe, µg m^{-3}	0.47 ± 0.16	0.68 ± 0.22
Cu, µg m^{-3}	0.02 ± 0.01	0.03 ± 0.01

2.4 Results and discussion

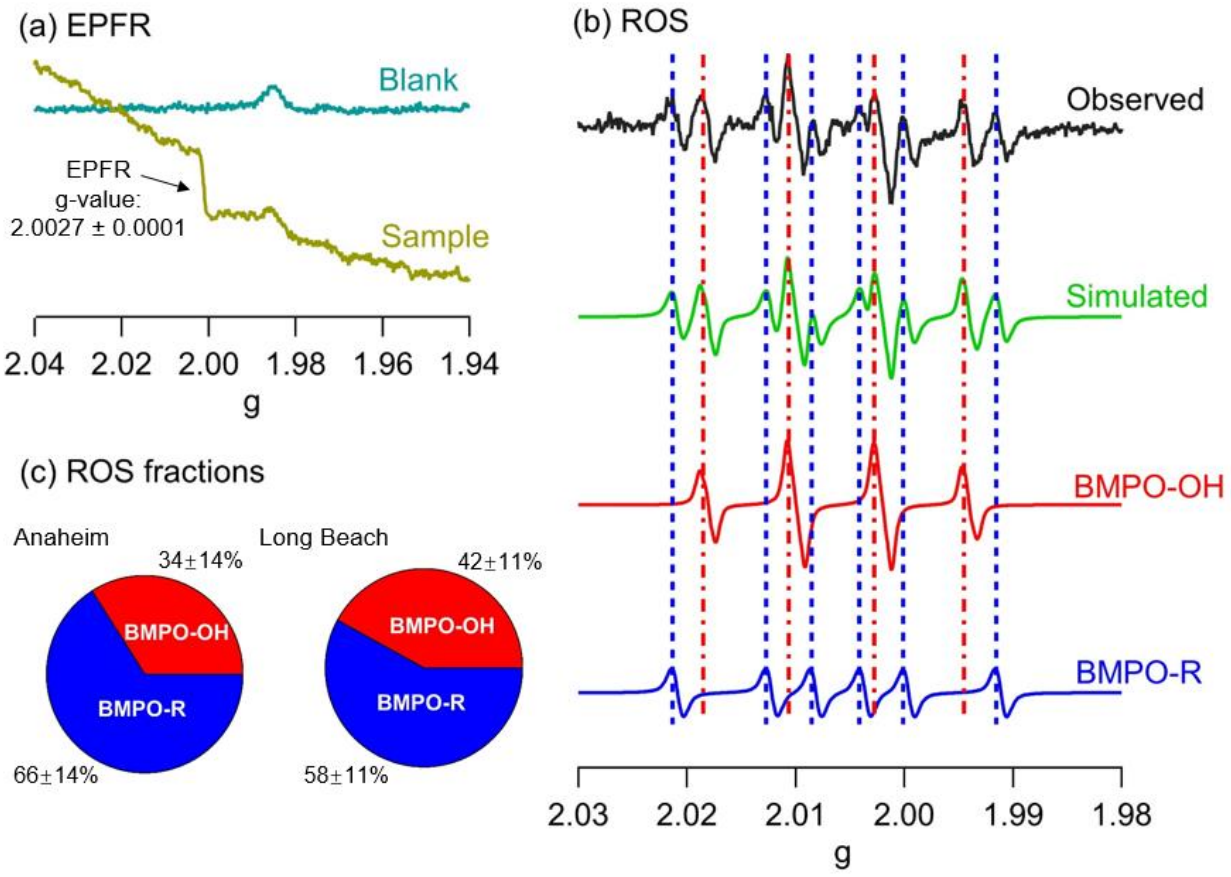

Figure 2.1: (a) Typical EPR spectra of a quartz blank filter and ambient $PM_{2.5}$ containing EPFRs. (b) The observed EPR spectrum (black) of the aqueous extracts of $PM_{2.5}$ collected at a highway site and the simulated spectrum (green) by deconvolution into OH radicals (red) and carbon-centered radicals (blue) trapped by spin-trapping agent BMPO. The vertical dashed lines indicate the position of each peak for BMPO-OH and BMPO-R adducts. (c) Averaged fractions of OH and carbon-centered radicals (R) as trapped by BMPO in aqueous extracts of $PM_{2.5}$ collected at highway sites in Anaheim and Long Beach.

2.4.1 Environmentally Persistent Free Radicals

Figure 2.1 (a) shows an example of EPR spectrum of the $PM_{2.5}$ particles and a blank filter. The EPR spectrum of ambient $PM_{2.5}$ particles exhibits a large signal with a g-factor of 2.0027 ± 0.0001 and a peak-to-peak distance of 4.4 ± 0.7 G, which are consistent with previously reported values for EPFRs and characteristics for semiquinone-type radicals.[55, 126, 156] The drift in the

spectrum in particle samples as opposed to the flat spectrum of the blank filters is likely due to the presence of transition metals.[57, 157]

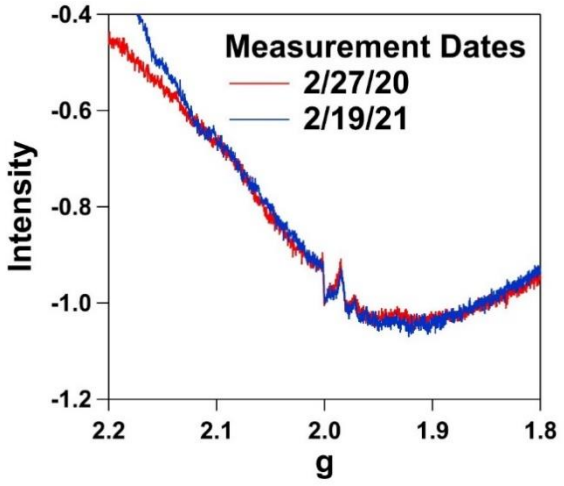

Figure 2.2: EPR spectra of $PM_{2.5}$ from a selected sample collected at Long Beach measured on 2/27/2020 and 2/19/2021, showing stability of EPFRs.

Figure 2.2 shows EPR measurements of the filter after roughly one year of storage at -18 ℃ show that the signals were almost unchanged, indicating the persistency of EPFRs. This is consistent with previous studies showing that some portions of EPFRs have lifetime longer than months to indefinite[56] as semiquinone-type radicals can be stabilized by their adsorption into a polymeric carbonaceous core of PM [158] or by electron transfer with transition metals.[110] In addition, a very recent study demonstrated the formation and stabilization of carbon-centered radicals in organic aerosols containing Fe ions.[159]

Figure 2.3 shows the average EPFRv and EPFRm concentrations at the highway and urban sites in comparison to those from other studies using the same analytical method. The two highway sites have similar levels of EPFRv (40 ± 11 and 31 ± 20 pmol m^{-3} at Anaheim and Long Beach, respectively) and are more than twice higher than EPFRv at the urban site (14 ± 12 pmol m^{-3}). The EPFRm at Anaheim (3.5 ± 1.0 pmol μg^{-1}) is higher than that at Long Beach (2.1 ± 1.4 pmol μg^{-1}).

Compared to reported values on EPFR concentrations at near-road and urban environments in US, Europe, and Asia, EPFRs at near-road sites are generally higher than those from urban background environments, except two studies reporting high levels of EPFRs in Linfen and Jinan, highly polluted urban cities in China.[113, 160] This suggests that EPFRs are likely associated with traffic-related emissions, consistent with many earlier studies.[114, 156, 160-161]

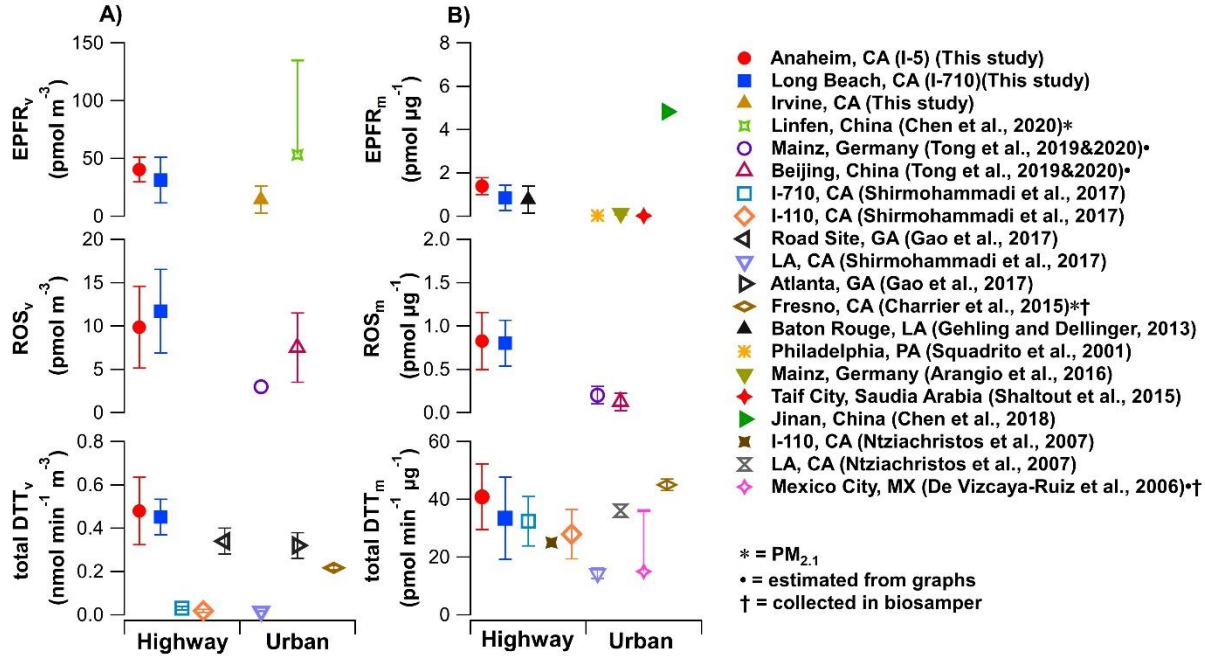

Figure 2.3: Air-volume- and $PM_{2.5}$-mass-normalized concentrations of EPFRs and ROS as well as total DTT activities of $PM_{2.5}$ collected at two highway sites and an urban site, CA, in comparison to ambient data from previous studies including Squadrito et al. (2001),[47] De Vizcaya-Ruiz et al. (2006),[162] Ntziachristos et al. (2007),[163] Gehling and Dellinger (2013),[56] Shaltout et al. (2015),[164] Charrier et al. (2015),[165] Arangio et al. (2016),[55] Shirmohammadi et al. (2017),[19] Gao et al. (2017),[149] Chen et al. (2018),[113] Tong et al. (2019),[125] Tong et al. (2020),[40, 43] and Chen et al. (2020).[160] Data in this study were averaged concentrations with error bars representing daily variability calculated from the standard deviations of the averaged data. Data from winter seasons (November to March) from previous studies were selected for comparisons. Markers with bars (Linfen, Mexico City) denote the range of ambient concentrations and markers with error bars are either reported values or estimated from previous studies.

Figure 2.4 shows the correlation between EPFRv and gaseous pollutants including CO, NO, NO_2, and O_3 as well as $PM_{2.5}$ components including OC, EC, and metals (Fe, Cu) at both highway sites. Summaries of correlation coefficients and p-values are given in Table 2.2 and 2.3. Note that the error bars on chemical species reflect the viability in their ambient concentrations which are averaged over the sampling time (e.g., 12 hours) of the $PM_{2.5}$ sampler. For both sites EPFRs show good positive correlations with a combustion marker CO and a traffic-emission marker NO. The strong positive correlations of EPFRs with soot particle EC suggest that EPFRs are likely associated with diesel exhaust particles.[50] A recent study showed that EPFRs measured from the $PM_{3.3}$ collected in China have a positive correlation with EC in winter and their source-receptor modeling suggested that EPFRs are mainly emitted from coal combustion.[160] In our study, the EC to TC (total carbon) ratio is slightly higher at the Long Beach site (0.37 ± 0.03) compared to the Anaheim site (0.31 ± 0.04), while the EC to CO ratio is much higher at the Long Beach site (3.4 ± 0.6 μg m^{-3} ppm^{-1}) than the Anaheim site (1.7 ± 0.3 μg m^{-3} ppm^{-1}). Diesel engines are known to emit less CO and more black carbon (BC), yielding higher EC fractions and EC to CO ratios.[166] The higher EC fractions and EC to CO ratios at the Long Beach site are consistent with the I-710 freeway serving as a major corridor accommodating a high volume of heavy-duty diesel trucks daily, while the I-5 freeway (Anaheim) has mainly light-duty vehicles fleet.[167]

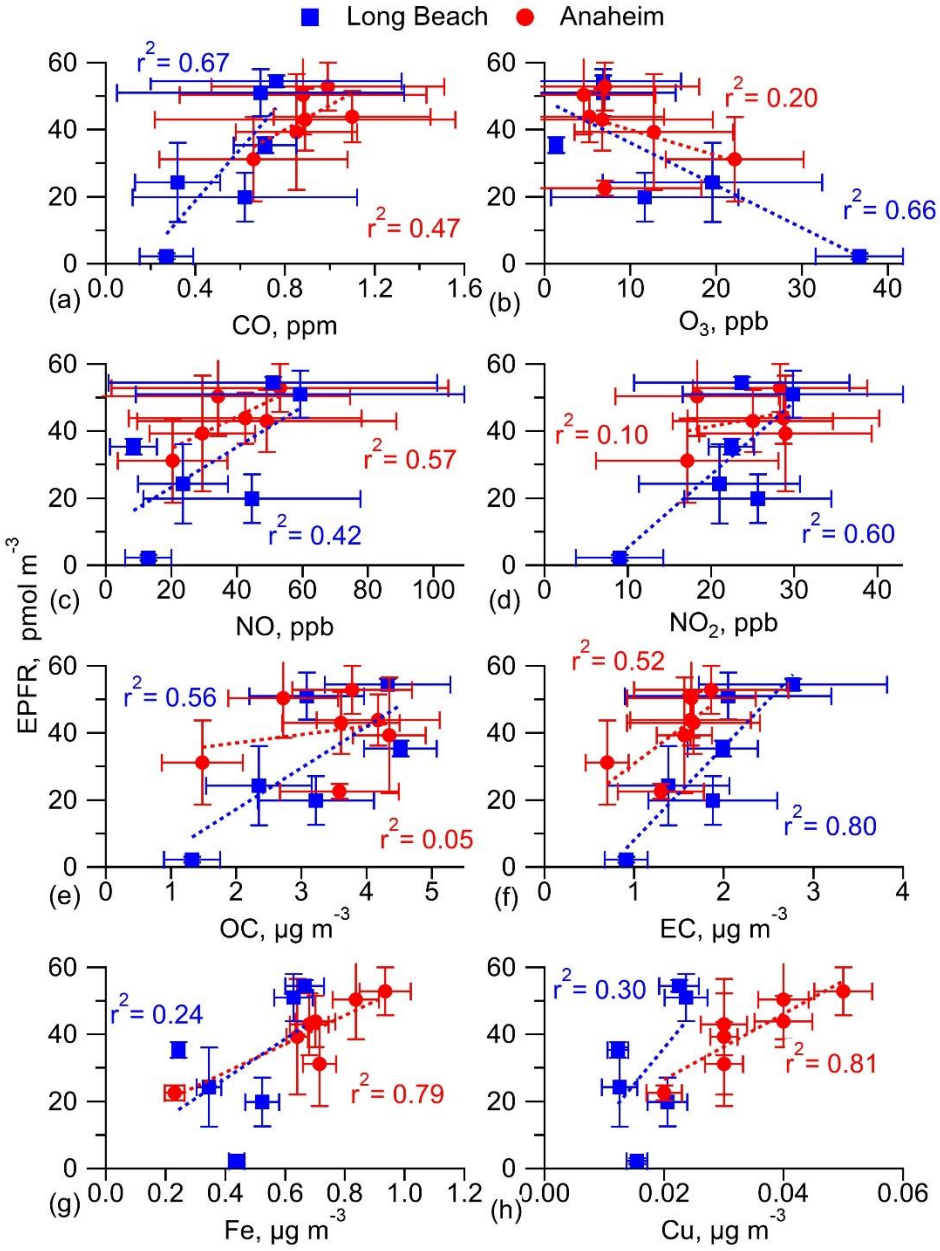

Figure 2.4: Correlations between volume-normalized EPFR concentrations and gaseous pollutants (CO, O_3, NO, NO_2) and chemical components (OC, EC, Fe, Cu) measured at the Anaheim and Long Beach highway sites. The error bars on EPFRs represent the standard deviations of multiple measurements. The error bars on gaseous pollutants are standard deviations of online measurements. The error bars for OC, EC, and metal measurements represent variability of their ambient concentrations and also are propagated from analytical and sampling volume uncertainties in these measurements.

Table 2.2. Correlation coefficient (r^2) of fine particle OP, ROS, and DTT activities with $PM_{2.5}$ mass and selected chemical species at two highway sites.

	Anaheim					Long Beach				
	EPFR	DTT	ROS	$OH^{\cdot}$	$R^{\cdot}$	EPFR	DTT	ROS	$OH^{\cdot}$	$R^{\cdot}$
EPFR	1.00					1.00				
DTT	0.03	1.00				0.01	1.00			
ROS	0.02	0.91	1.00			0.50	0.14	1.00		
$OH^{\cdot}$	0.12	0.71	0.83	1.00		0.73	0.07	0.81	1.00	
$R^{\cdot}$	0.00	0.85	0.90	0.54	1.00	0.26	0.16	0.90	0.52	1.00
$PM_{2.5}$	0.12	0.20	0.26	0.54	0.08	0.37	0.39	0.95	0.76	0.98
CO	0.47	0.07	0.14	0.31	0.05	0.67	0.13	0.75	0.95	0.45
O_3	0.20	0.13	0.22	0.21	0.17	0.66	0.01	0.47	0.87	0.18
NO	0.57	0.19	0.16	0.28	0.08	0.42	0.06	0.50	0.34	0.51
NO_2	0.10	0.10	0.07	0.01	0.21	0.60	0.08	0.41	0.66	0.20
OC	0.05	0.07	0.02	0.02	0.12	0.56	0.15	0.56	0.86	0.28
EC	0.52	0.00	0.00	0.00	0.00	0.80	0.06	0.86	0.93	0.62
Cu	0.81	0.00	0.01	0.07	0.01	0.30	0.00	0.53	0.30	0.60
Fe	0.79	0.05	0.08	0.29	0.01	0.24	0.00	0.43	0.17	0.58

Table 2.3. p-value of correlations of fine particle OP, ROS, and DTT activities with PM2.5 mass and selected chemical species at two highway sites.

	Anaheim					Long Beach				
	EPFR	DTT	ROS	$OH^{\cdot}$	$R^{\cdot}$	EPFR	DTT	ROS	$OH^{\cdot}$	$R^{\cdot}$
EPFR										
DTT	0.724					0.871				
ROS	0.740	0.001				0.117	0.472			
$OH^{\cdot}$	0.439	0.017	0.004			0.031	0.622	0.014		
$R^{\cdot}$	0.986	0.003	0.001	0.059		0.299	0.427	0.004	0.108	
$PM_{2.5}$	0.446	0.313	0.239	0.061	0.550	0.277	0.262	0.005	0.052	0.001
CO	0.131	0.619	0.468	0.253	0.670	0.045	0.479	0.027	0.001	0.142
O_3	0.315	0.434	0.289	0.296	0.353	0.048	0.852	0.130	0.007	0.400
NO	0.084	0.385	0.429	0.280	0.597	0.168	0.644	0.115	0.223	0.112
NO_2	0.540	0.543	0.619	0.842	0.355	0.072	0.587	0.167	0.051	0.379
OC	0.617	0.578	0.749	0.777	0.446	0.087	0.454	0.087	0.008	0.284
EC	0.066	0.892	0.995	0.958	0.953	0.017	0.641	0.007	0.002	0.062
Cu	0.006	0.973	0.861	0.561	0.880	0.258	0.947	0.099	0.264	0.069
Fe	0.008	0.614	0.527	0.211	0.879	0.325	0.971	0.154	0.424	0.077

At the Anaheim site, EPFRs are strongly correlated with Fe (r^2 = 0.79) and Cu (r^2 = 0.81). Fe and Cu are important metals emitted from tire or brake wear.[168] Both metals are more abundant at the Anaheim site than the Long Beach site (Table 2.1). The metal concentrations are found to be higher at the Anaheim site than the Long Beach site. Studies have shown that EPFRs are often associated with metals during combustion processes.[58, 114] PAHs can be oxidized and chemisorbed to the surface of metal particles to form EPFRs on the surface of particles.[110, 156] A recent study on chemical measurements on tire-wear particles showed that toxic quinones can be found in the tire-wear extracts.[169] The strong correlation of EPFRs with these metals may suggest that EPFRs at the Anaheim site are stabilized by interacting with transition metals such as Fe and Cu under ambient conditions.

The EPFRs measured at both highway sites show negative correlation with O_3, which may be stemmed from a negative correlation of O_3 with NO owing to the O_3 titration by NO (as NO correlates positively with EPFR). It may indicate that EPFRs are quenched by O_3 to form closed-shell organic compounds, which is in line with previous computational simulations suggesting that stabilized Criegee intermediates can react with ozone to form stable organic compounds.[170] It is however in contrast to previous studies showing that heterogeneous ozonolysis of PAHs can lead to the formation of persistent radicals.[59, 115] Weak positive relationships of EPFRs with solar radiation were observed previously[56] and a recent study also demonstrated that visible-light exposure of EPFRs contained in $PM_{2.5}$ can enhance the EPFR concentration and generate more oxidized organic radicals.[126] Laboratory experiments have shown that EPFRs formed from ozonolysis of PAHs decayed upon exposure to elevated concentrations of NO_2,[59] but negative correlations of EPFR and NO_2 are not observed in this study. A previous study has shown that the lifetime of EPFRs contained in naphthalene SOA is longer under dry conditions,[116] but we do not

observe a correlation between EPFRs and relative humidity as shown in Figure 2.5 ($r^2 \leq 0.18$). There may be complex competing effects for the fate of EPFRs by solar radiation, ambient conditions and interactions with oxidants. While our observations suggest that photochemical and secondary processes may not play a large role in the formation of EPFRs at these two highway sites, further laboratory studies are warranted to investigate interactions of EPFRs with gaseous pollutants to gain mechanistic understanding.

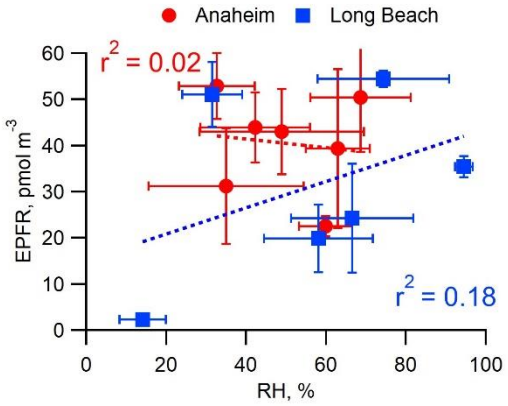

Figure 2.5: Correlation of EPFRs and relative humidity at Anaheim and Long Beach sites.

2.4.2 ROS Generation in Water and Relations with EPFRs and $PM_{2.5}$ Mass

Figure 2.1 (b) shows an example of the observed EPR spectrum (black) of the aqueous extracts of $PM_{2.5}$ collected at the Anaheim site. The EPR spectrum is composed of several peaks, indicating contributions from different types of radicals. The simulated EPR spectrum (green) reproduced the observed spectrum (black) very well and can be deconvoluted into four- and six-line signals due to the hyperfine splitting of BMPO-OH and BMPO-R adducts, respectively. It indicates that ambient $PM_{2.5}$ collected from the two highway sites form mainly OH and carbon-centered organic radicals upon interaction with water. Note that Fe(III) is known to withdraw an electron from nitric oxide spin trap and induce positive BMPO-OH artifacts.[44, 171] However, Fe(III) in atmospheric particles is likely largely complexed with organic ligands,[172] and our experiments

show that complexation leads to the stark suppression of BMPO-OH signals from Fe(III) (Figure 2.6); hence, such artifacts are likely to be minimum in our measurements.

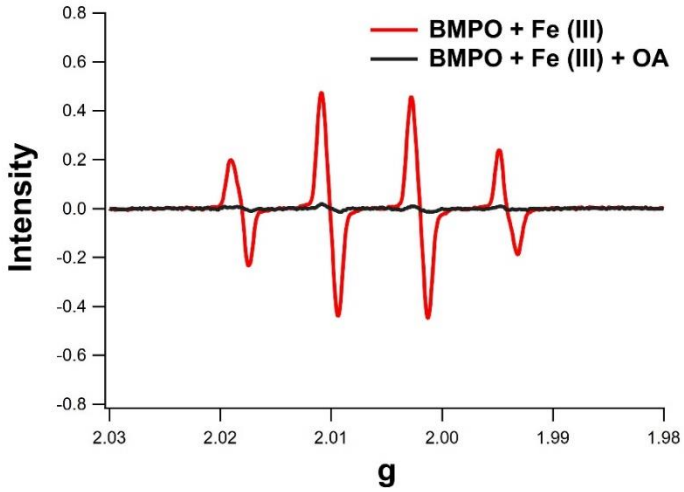

Figure 2.6: EPR spectra of mixtures of BMPO and Fe(III) (red line) as well as BMPO, Fe(III), and oxalic acid (OA) with the Fe(III):OA ratio of 1:3. It shows that the BMPO-OH signal is strongly suppressed upon complexation of Fe(III) with OA.

Figure 2.1 (c) shows the fraction of OH and carbon-centered radicals to total ROS is approximately 40% and 60%, respectively. Arangio et al. (2016) reported that OH and carbon-centered radicals contributed 10 – 87% and 9 – 62% of total radical forms of ROS, respectively, in Mainz, Germany.[55] Tong et al. also found large contributions from OH (20 – 50%) and organic radicals (35 – 80%) in ambient particles in multiple cities.[43, 125] ROSv and ROSm concentrations are similar at both highway sites to be ~10 (± 5) pmol m^{-3} and 0.8 (± 0.2) pmol μg^{-1}, respectively (Figure 2.3). Comparison of reported values from other studies shows that ROSv and ROSm from highway sites are higher than urban environments, suggesting that traffic-related emissions play an important role in ROS formation, although more studies on different locations are needed to provide better statistics.

Figure 2.7 (a) shows that total ROSv concentrations have a moderate positive correlation with $PM_{2.5}$ mass concentrations (r^2 = 0.59) at both highway sites, with the exclusion of one outliner from the measurement on 2/8/2020 at the Long Beach site (red triangle). This day has the highest relative humidity (RH = 95%) and is the only foggy day recorded during the campaign. The $PM_{2.5}$ concentration on this day reaches up to 35 μg m^{-3}, much higher than the other sampling days with mass concentrations less than 20 μg m^{-3}, while the ROS concentration on this day is within the range of other sampling days. $PM_{2.5}$ nitrate was the chemical composition with the largest increase (13.5 μg m^{-3}) on that day. It is likely that the foggy environment provided a favorable condition for aqueous chemistry to produce chemical compounds that add to the mass but did not contribute to ROS generation.[173] A recent study found that ROSv generated from fine PM showed a positive correlation with PM mass concentrations at forest sites (Amazon and Hyytiälä) and urban cities in China (Beijing, Guangzhou, Shanghai, and Xi'an).[125] Another study found that the superoxide generated from fine PM in Beijing also showed a positive correlation with $PM_{2.5}$ mass concentration in winter.[174]

Figure 2.7 (b) shows that OH radicals have a positive strong correlation with the EPFRs at the Long Beach site (r^2 = 0.73). OH radicals are also positively correlated with primary vehicle exhaust source markers including CO and EC, and negatively correlated with O_3 (Figure 2.8). This may suggest that OH radicals stem from the similar sources as EPFRs or are generated from EPFRs. In fact, past studies have shown that EPFR-containing combustion generated particles and atmospheric $PM_{2.5}$ can generate OH radicals in aqueous solutions.[57, 124, 127] OH radicals and EPFRs at the Anaheim site also show a positive, but much weaker (r^2 = 0.12) correlation, indicating that additional sources such as Fenton(-like) reactions and aqueous-phase decomposition of organic hydroperoxide[44] may contribute to OH formation at the Anaheim site. A slightly higher correlation

between Fe and OH radicals is observed at the Anaheim site (r^2 = 0.29) compared to the Long Beach site (r^2 = 0.17) (Figure 2.7 (c)).

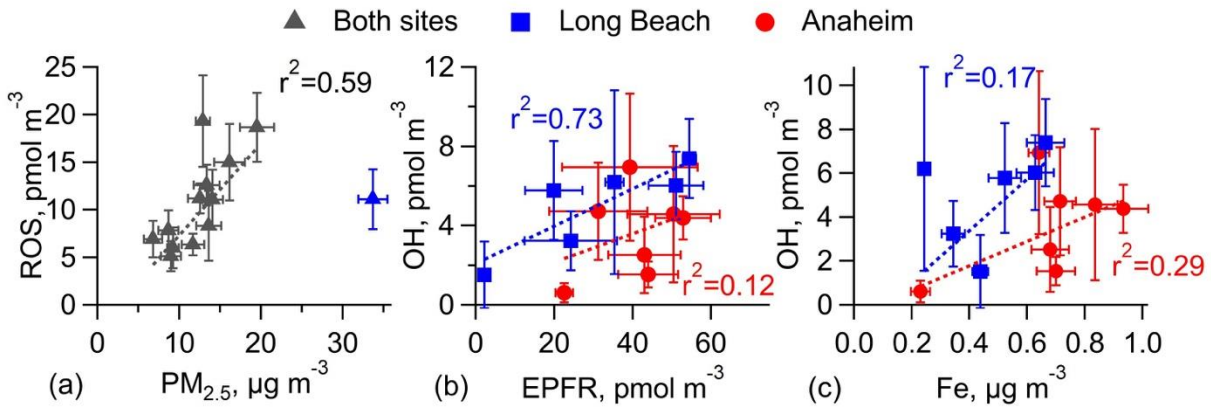

Figure 2.7: Correlations between (a) radical forms of ROS in the aqueous $PM_{2.5}$ extracts and $PM_{2.5}$ mass concentrations, (b) OH radicals in the aqueous $PM_{2.5}$ extracts and EPFR, and (c) OH radicals in the aqueous PM extracts and Fe. A red triangle in panel (a) denotes the measurement on Feb. 8, 2020 at Long Beach, which is considered as an outliner (see text). The error bars on ROS, OH, EPFR represent the standard deviations of multiple measurements, and those on $PM_{2.5}$ and Fe are propagated from analytical and sampling volume uncertainties in these measurements.

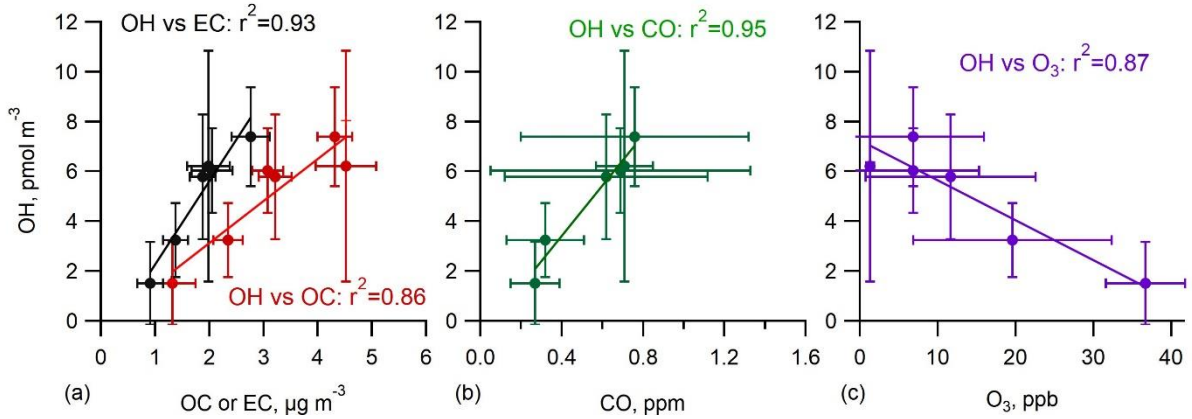

Figure 2.8: Correlation of OH generated from the aqueous extracts of $PM_{2.5}$ with EC, OC, CO, and O_3 measured at the Long Beach site.

2.4.3 DTT Activities and Relation with ROS Generation

The two highway sites have similar levels of total DTT activities (Figure 2.3) and the average total DTTv and DTTm are ~0.47 nmol min^{-1} m^{-3} and ~37 pmol min^{-1} μg^{-1} respectively.

These values are similar or slightly higher than previous measurements at highway or road sites.[19, 149, 165] Interestingly, the total DTTv activities at the Anaheim are strongly correlated with ROSv (r^2 = 0.91, Figure 2.9 (a)). For individual ROS species, the correlations of total DTTv with organic radicals (r^2 = 0.85, Figure 2.9 (b)) are stronger than OH radicals (r^2 = 0.71, Figure 2.9 (c)), suggesting that the DTT decay and the formation of organic radicals are contributed by similar organic compounds. This is consistent with a recent study reporting that organic hydroperoxides can consume DTT.[137] The lower correlation of total DTTv activities with OH radicals is expected as the DTT assay is less sensitive to Fe, which plays a large role in generating OH radicals through Fenton chemistry.[120] There is little correlation between total DTTv activities and ROSv or individual species at the Long Beach site ($r^2 \leq 0.16$, Figure 2.9).

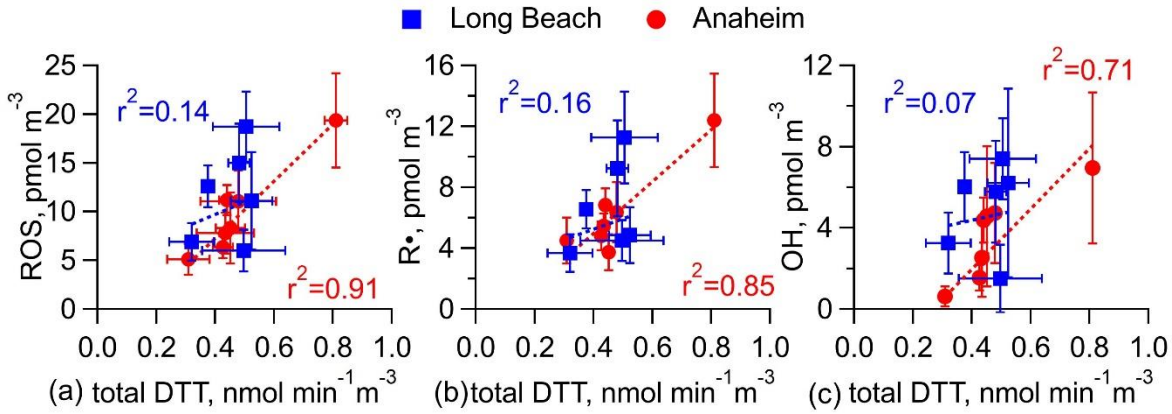

Figure 2.9: Correlation of total DTT activities with concentrations of (a) radical forms of ROS, (b) carbon-centered radicals (R·) and (c) OH radicals formed in aqueous extracts of $PM_{2.5}$ collected at the Anaheim and Long Beach sites.

A recent study found that secondary inorganic components, crustal material and biogenic secondary organic aerosols control PM mass concentrations, while oxidative potential is associated mostly with anthropogenic sources, in particular with residential biomass burning and metals from vehicular non-exhaust emissions.[143] Our previous study applied kinetic modeling[119] to estimate ROS formation from measured chemical components including OC, metals, and quinones, and the

results showed that the measured water-soluble DTT activities are correlated with the modelled formation rates of H_2O_2 and superoxide radicals.[120] The mixed results in this study provide promising but cautious implications from ambient data that DTT activities could represent ROS generation, but further studies are necessary to improve a mechanistic understanding of associations among DTT activities, ROS formation, and oxidative stress. Other OP assays such as ascorbic (AA) or glutathione (GSH) assays that measure the consumption of antioxidants could also be used to assess the relations of OP with ROS generation in future studies.

2.5 Conclusions

Exhaust and non-exhaust emissions contribute to ambient fine particulate matter, posing health risks. We collected $PM_{2.5}$ particles from highway and urban sites in Southern California and measured EPFRs, ROS generation, and total DTT activities. We find that $PM_{2.5}$ at highway sites contain substantial amounts of EPFRs with about two times higher concentrations than the urban site. Highway $PM_{2.5}$ is found to mainly generate OH and carbon-centered radicals upon extraction into water. Positive correlations of EPFRs with vehicle exhaust markers (CO, NO and EC) and non-exhaust markers (Fe and Cu) suggest that EPFRs are associated with diesel exhaust particles and they are semiquinone-type radicals stabilized by transition metals. Negative correlations of EPFRs with O_3 suggest the minor role of photochemistry on EPFR formation. We also find interesting links among EPFRs, ROS generation, and total DTT activities at the highway sites. EPFRs show a strong positive correlation with aqueous OH radical formation at one highway site, suggesting that EPFRs are redox-active to generate OH radicals in water. The atmospheric persistency of EPFRs and their ability to generate OH radicals make them highly relevant in studying the health impacts of highway emissions. The formation of radical forms of ROS is positively correlated with $PM_{2.5}$ mass concentrations and total DTT activities at one highway site,

providing rationale of the use of oxidative potential as an additional indicator of PM toxicity other than PM mass concentrations. As such correlation is weak at another site with different sources, further measurements with longer period of sampling times and also at various locations with different sources are necessary to better understand the associations of EPFRs, ROS generation, and DTT activities with oxidative stress induced by atmospheric particulate matter and its adverse effects on human health.

Chapter 3: Environmentally Persistent Free Radicals and Reactive Oxygen Species Generation Measurements from Wildfire Size-Segregated Particulate Matter

3.1 Abstract

The toxicity and health effects of particulate matter (PM) emitted by wildfires have yet to be fully elucidated. A hypothesis for the underlying mechanism of adverse health effects is oxidative stress induced by reactive oxygen species (ROS) generated from wildfire PM. The wildfire PM contains iron, copper, and environmentally persistent free radicals (EPFRs). These chemicals can generate ROS in water, but only a limited amount of studies have explored ROS formation associated with the chemical components in wildfire PM. In this study, EPFRs and ROS generated in aqueous extracts of size-segregated particles collected during the two Southern California wildfires using electron paramagnetic resonance (EPR) spectrometer. The ambient EPFR concentration in PM_1 was found to be approximately ten times higher during the wildfires compared to the urban background. Depending on the fire events, four different types of ROS ($OH\cdot$, $O_2^{\cdot-}$, carbon-centered and oxygen organic radicals) were generated from aqueous extracts PM_1 or PM_{10}. $OH\cdot$ and carbon-centered organic radicals were formed from aqueous extracts of coarse particles. $O_2^{\cdot-}$ was only detected in yellow-brownish aqueous wildfire PM extracts, which suggests redox-active components in brown carbon may be responsible for $O_2^{\cdot-}$ formation. These results indicate that the urban and wildfire PM redox-active chemical components differ, and further investigations on linking chemical components and ROS formation from the wildfire PM.

3.2 Introduction

Wildfires are becoming more intense and occurring more frequently in various parts of the world.[4, 9] Most notably between 2019 and 2020, western parts of the United States, Siberia, and Australia faced some of the worst wildfire disasters in modern history. Wildfires are projected to increase with climate change, which causes great concern regarding the wildfires' effects on air quality and public health.[21, 175] Exposure to intense wildfire emissions is well known to exacerbate asthma, and an increase in hospital admissions associated with asthmatic condition after heavy smoke exposure has been reported.[176-177] The toxicity mechanism in asthma associated with wildfire exposure continues to be explored. One of the plausible mechanisms involves oxidative stress induced by reactive oxygen species (ROS) generated from wildfire particulate matter (PM).[31, 178-179]

Wildfire PM contains iron, copper, and redox-active quinones, which are potential sources of ROS.[31, 176, 178] A study conducted in Singapore reported iron concentration to have roughly doubled during the bushfire events when compared to the concentration levels in Singapore's urban background. This study revealed hydroxyl radicals can be generated from wildfire PM in aqueous solution via Fenton-reaction with iron.[178] PAHs and molecules containing aromatic groups such as HUmic-LIke Substances (HULIS) are also present in wildfire PM and can be redox-active if oxidized.[52-54] The oxidized aromatic group can potentially form semiquinone and generate superoxide anion radical from wildfire PM.[52, 54] ROS generation from specific chemical components in wildfire PM have yet to be thoroughly understood and needs to be further explored.[30]

Environmentally persistent free radicals (EPFRs) are free radicals that are reportedly formed from oxidation of phenol, hydroquinone, catechol, or PAHs.[124] EPFRs have been detected

in biomass burning particles.[60] Pyrolysis of lignin produce substituted phenols that can potentially serve as a source of EPFR in wildfire PM.[60, 114, 180] Additionally, certain PAHs are found to be more abundant in wildfire emissions, which can potentially serve as an additional source of EPFR in PM during the wildfire.[31] EPFRs are known to produce a hydroxyl radical and cause DNA damage.[124, 181] The EPFR abundance in wildfire PM is still not well known and EPFR quantification must be made.

Size distributions of chemical species have provided insights into possible sources of particle toxicity.[131] Connecting size-resolved ROS measurements from wildfire PM to other chemical measurements can provide a better understanding of the chemical species that are potential ROS sources in wildfire PM. Here, we investigate the EPFRs and ROS size distributions of size-segregated particles collected from the two wildfire events.

3.3 Materials and methods

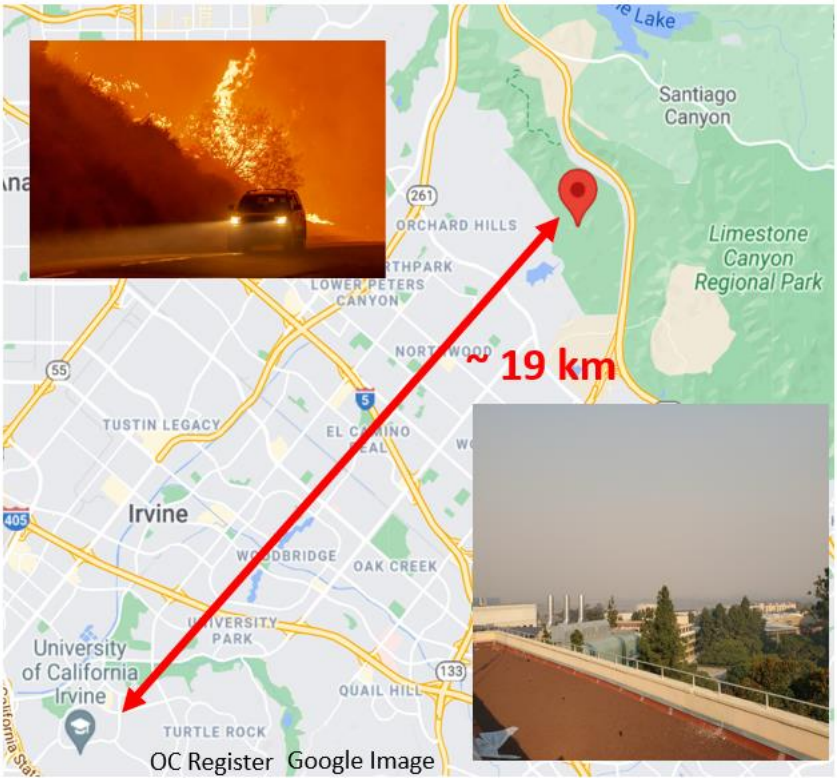

Figure 3.1 Map of the sampling location (University of California, Irvine) and approximate location where the wildfire occurred (Santiago Canyon). The sampling location is roughly 19 km away from the wildfire emission source and picture at the right shows the air quality is influenced by the wildfire (12/3/20, Bond Fire).

3.3.1 PM Collection

A Micro-Orifice Uniform Deposition Impactor (MOUDI, TSI, flow rate 30 L min^{-1}) was used to collect size-segregated ambient particles onto a Teflon filter at the sampling locations and dates mentioned in Chapters 1 and 2 for urban background samples. The size-segregated ambient particles were also collected onto a Teflon filter at an urban site (a campus building at the University of California, Irvine, 33°38'40.4"N 117°50'39.3"W, elevation 20 meters) during two wildfire events: Silverado Fire (10/26/20 to 11/7/20) and Bond Fire (12/2/20 to 12/10/20) (Figure 3.1). The wildfire samples were collected for two-and-a-half to three days from 10/26/20 to 11/16/20 and 12/3/20 to 12/6/20. and the flow rate did not significantly drop below 30 L min^{-1} during the sampling duration. The MOUDI stages were modified and collected at the urban and highway sites: $PM_{>18}$, PM_{10-18}, $PM_{3.2-10}$, $PM_{1-3.2}$, $PM_{0.56-1}$, and $PM_{0.056-0.56}$. The MOUDI stages were also modified for collecting wildfire particles: $PM_{>18}$, PM_{10-18}, PM_{1-10}, $PM_{0.18-1}$, and $PM_{0.056-0.18}$. The cut-off aerodynamic diameter of each stage may have been slightly altered by the modification. However, to avoid the confusion, the particle size ranges expected to be collected listed above will still be mentioned.

Figure 3.2 The left picture was taken on 10/27/20 (Silverado Fire, hazy day) and 11/7/20 (Silverado Fire mostly contained, no haze) at the roof of University of California, Irvine.

The brown haze was observed on 10/26/20 to 11/1/20, 11/10/20 to 11/13/20, and 12/6/20 to 12/9/20 while the sky was clear on 11/2/20 to 11/9/20 (Figure 3.2). This distinction was made for ROS data analysis.

3.3.2 Environmentally Persistent Free Radicals (EPFRs)

A whole filter was inserted into a quartz tube (9.17 mm I.D., SP Wilmad-LabGlass) for EPFR measurements using a continuous-wave electron paramagnetic resonance (CW-EPR) spectrometer (EMXplus, Bruker, Germany). The following parameters were used in EPR: a microwave frequency of 9.65 GHz; a microwave power of 36.18 mW or 20.00 mW (8 or 10 dB); a modulation frequency of 100 kHz; a modulation amplitude of 1.0 or 3.0 G; a receiver gain of 40 dB; a time constant of 10.24 ms; and a magnetic field scan of 1623.06 G. Ambient concentrations of EPFRs are presented as EPFR per volume of air (EPFRv, pmol m^{-3}).

3.3.3 Reactive Oxygen Species (ROS) Generation.

EPR combined with a spin-trapping technique was applied to detect radicals in the aqueous particle extracts. Half of a Teflon filter containing the sample was extracted in 300 μL of 10 mM spin-trapping agent 5-tert-butoxycarbonyl-5-methyl-1-pyrroline-N-oxide (BMPO) in Millipore water (>18 Ω cm^{-1}) for 8 minutes using an analog vortex mixer (VWR International LLC) and both water-soluble and insoluble compounds were thereby extracted. The extracts were then concentrated by 7 to 30 times through blowing under N_2 gas for approximately 20 minutes. The remaining solution was inserted into a 50 μL micropipette and measured at 46 minutes from extraction. The EPR parameters used for ROS measurement were the same as those for EPFRs except: a microwave frequency of 9.86 GHz, a microwave power of 21.17 mW (10 dB); a time constant of 20.48 ms; a modulation amplitude of 1.0 or 2.0 G and a magnetic field scan of 150.0 G. The SpinFit and SpinCount modules in the Xenon software were applied to simulate each EPR spectrum to identify and quantify different radical adducts formed in the aqueous extracts. Data were normalized to the sampled volume of air (ROSv, pmol m^{-3}).

ROS measurements were only conducted for the following dates at the highway and urban background due to time constraints for this dissertation: (2/24/20, and 2/25/20).

3.4 Results and discussion

3.4.1 Environmentally Persistent Free Radicals

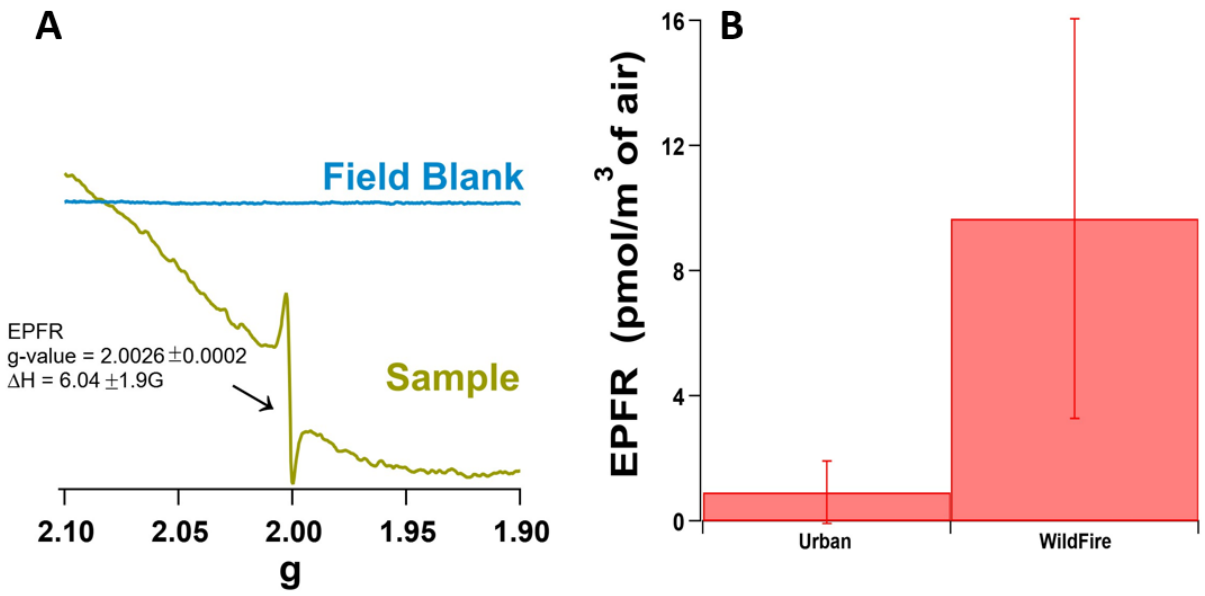

Figure 3.3: (A) Typical EPR spectra of a Teflon field blank filter and $PM_{0.18\text{-}1}$ containing EPFR during the Silverado Fire (10/26/20 to 10/29/20). **(B)** The average EPFRs concentration measured from ambient PM_1 before (urban) and during wildfires. The error bar represents the standard deviation of 5 sample measurements for urban background and wildfires. EPFRs were only detected in $PM_{0.056\text{-}0.56}$ for urban samples. The average EPFR concentration for wildfire samples are sum of the average EPFR measured in $PM_{0.056\text{-}0.18}$ and $PM_{0.18\text{-}1}$.

The EPR spectrum of wildfire size-segregated PM exhibit a single large peak with a g-factor of 2.0026 ± 0.0002 and a peak-to-peak distance (ΔH) of 6.04 ± 1.9 G (Figure 3.3, A). The sample signal looks like the signal is slowly decreasing because paramagnetic chemical species in the particle distorts the spectrum. The g-factor is consistent with fine PM mentioned in Chapter 2 while the peak-to-peak distance is slightly larger.[55, 58, 126, 182] However, these values are still consistent with previously reported values with a semiquinone-type radical observed in the EPR spectrum. After six months of storage at -18 °C, EPR measurements of the wildfire sample ($PM_{0.18\text{-}1}$) showed that the signal decreased by 36%, and yet no change in g-factor and peak-to-peak distance values were observable. The EPFRs decay with a lifetime of 21 days in fine PM was

reported.[56] The report also mentioned this decay may come from decomposition of organic radical at the surface.[56]

Figure 3.3(B) shows the sum of average ambient EPFRs concentration for PM_1 in urban background and wildfires. EPFRs measured during the wildfire (brown haze) can be 10.57 times higher than the urban background. Pyrolysis of lignin and burning biofuels such as sawgrass and pine are known to produce substituted phenols and oxygenated PAHs, which can potentially form EPFRs during the wildfire.[183] Certain PAHs concentration such as retene and dibenzo(ae)pyrene have been reported to increase by six folds during the 2007 Southern California event compared to the post fire measurements.[31] These PAHs can be oxidized and potentially become redox-active from chemical aging, which can form EPFRs during the wildfire observed in this study.

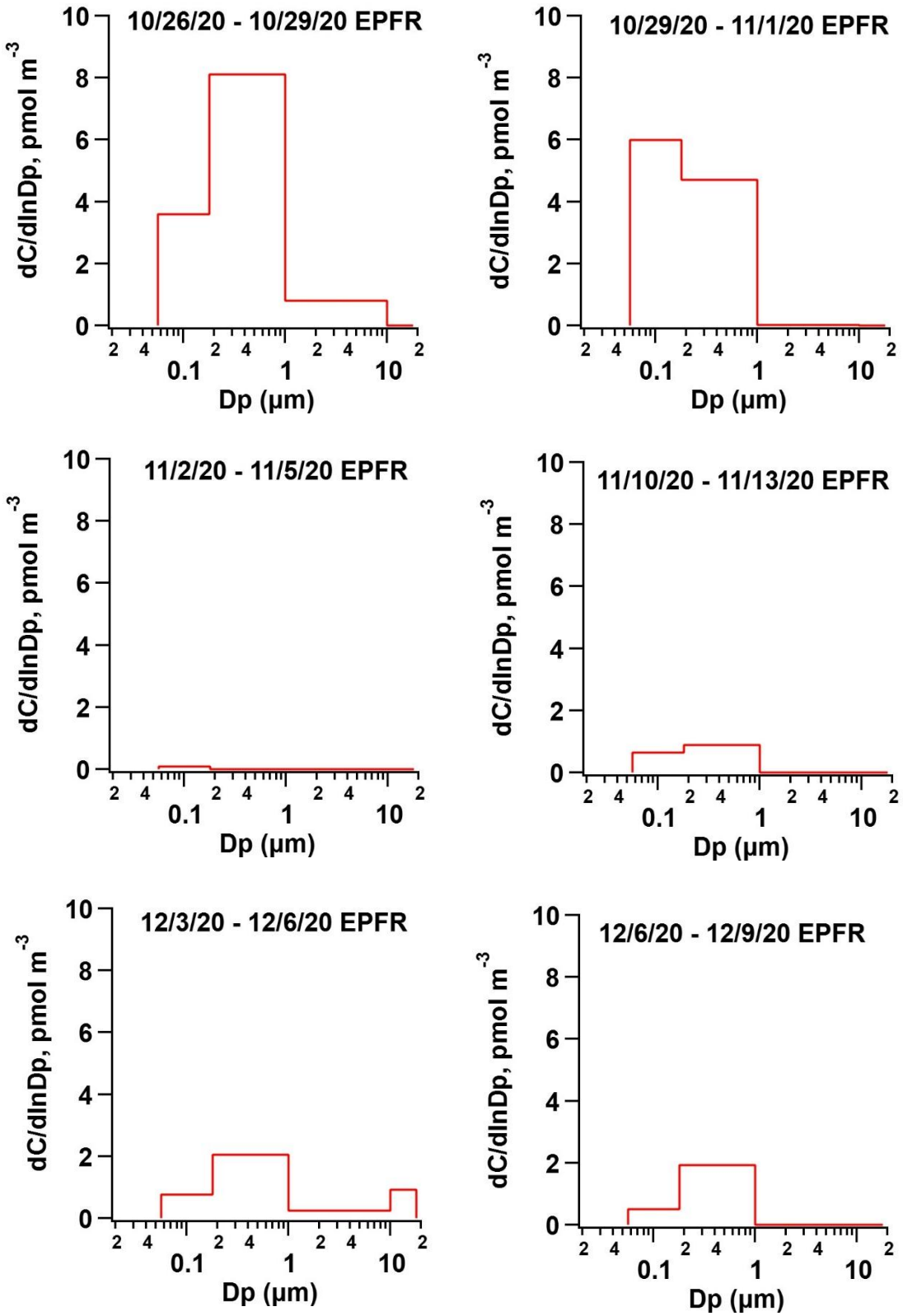

Figure 3.4 Ambient size distribution of EPFR detected in MOUDI samples collected on Nov to Dec 2020, when Silverado Fire (10/26/20 to 11/7/20) and Bond Fire (12/2/20 to 12/10/20) occurred.

Figure 3.4 shows the ambient size distribution of EPFRs measured from size-segregated samples collected between November and December of 2020 during two wildfire events: Silverado and Bond Fire. The size distributions show EPFRs are mainly found in $PM_{0.056\text{-}1}$ during the wildfire and are inconsistent with EPFRs size distribution measurements conducted in an urban environment at Mainz, Germany.[55] EPFRs were mainly found in $PM_{0.056\text{-}0.32}$ at Mainz, the size in range which the mass size distribution of combustion-generated particles typically is observed.[184] EPFRs have been detected in coarse particle during the winter season in China, when a large amount of coal is burned to keep households warm.[160] EPFRs were only detected in coarse particle during the initial fire events (10/26/20 to 10/29/20 and 12/3/20 to 12/6/20) when the fire to be at its most intense point. The sources of EPFRs in coarse particle are not known, and future studies investigating the source of EPFRs are necessary to obtain a better understanding of EPFRs and whether they contribute to uncomfortable health symptoms caused by coarse particles.

3.4.2 ROS generation from Urban and Wildfire Size-Segregated Particle

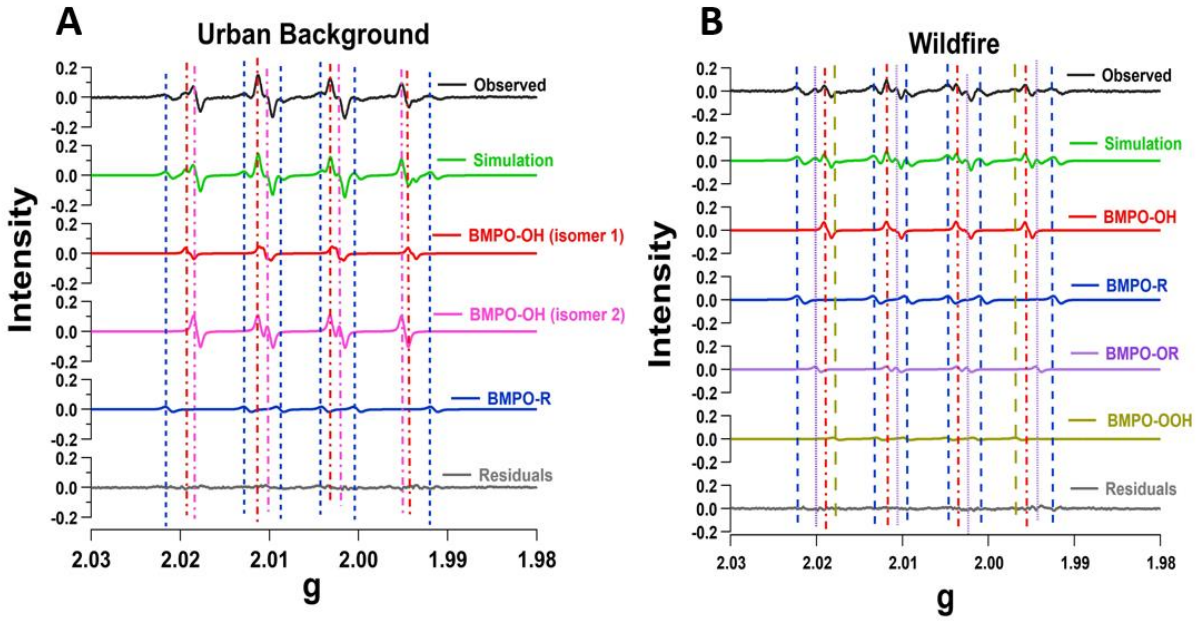

Figure 3.5 The observed EPR spectra (black) of the aqueous extracts of urban (A) and wildfire (B) $PM_{0.056\text{-}0.56}$ and $PM_{0.056\text{-}0.18}$ are shown. A) The deconvolution of simulated spectrum (green) of urban particle shows ·OH (red and pink) and carbon-centered radicals (blue) trapped by BMPO can fit the observed spectrum. The same type of ROS (BMPO-OH and BMPO-R) were observed for all sizes for urban samples measured. B) The deconvolution of simulated spectrum (green) of wildfire particle shows ·OH (red), carbon-centered radicals (blue), oxygen-centered radicals (purple), and superoxide anion radical (brown). The color dashed line represents the peak of the individual ROS needed to explain the observed spectrum. This result was consistent for $PM_{0.056\text{-}10}$ (10/26/20 to 10/29/20 and 10/29/20 to 11/1/20) and $PM_{0.056\text{-}1}$ (11/10/20 to11/13/20, 12/3/20 to12/6/20, and 12/6/20 to 12/9/20).

Figure 3.5 shows an example of the observed EPR spectrum (black) of the aqueous extracts of urban (A) and wildfire (B) $PM_{0.056\text{-}0.56}$ and $PM_{0.056\text{-}0.18}$ collected at Irvine. The same type of EPR spectrum was observed for all sizes for urban background samples. The EPR spectrum of particles collected during the wildfire was found to be size-dependent. The Figure 3.5(B) spectrum was only observed for wildfire $PM_{0.056\text{-}10}$ (10/26/20 to 10/29/20 and 10/29/20 ti 11/1/20) and $PM_{0.056\text{-}1}$ (11/10/20 ti 11/13/20, 12/3/20 to 12/6/20, and 12/6/20 to 12/9/20). Wildfire $PM_{>1}$ and $PM_{>10}$ were found to generate ·OH and carbon-centered organic radicals in water.

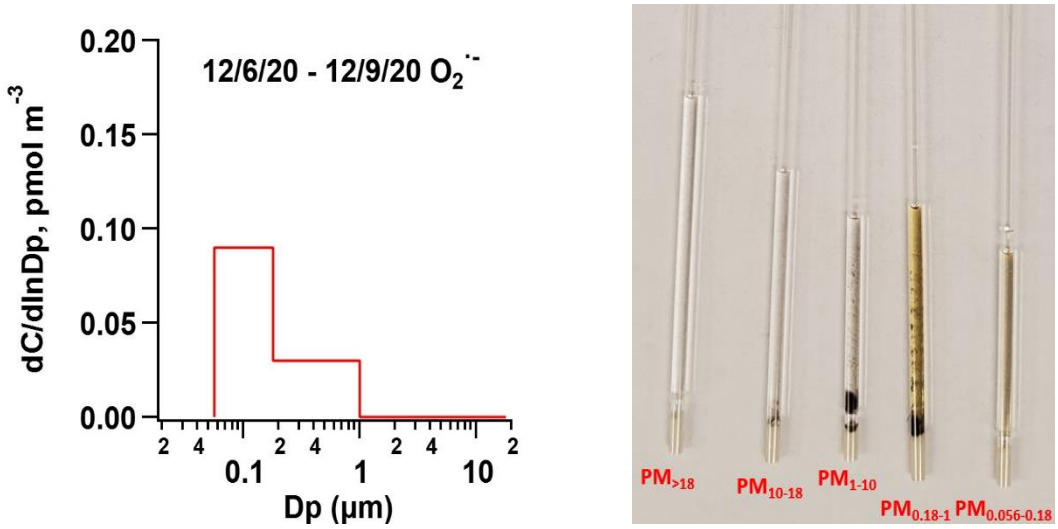

Figure 3.6 Superoxide anion radical ($O_2^{\cdot-}$) was only formed from aqueous extracts containing the yellow extracts ($PM_{0.056-0.18}$ and $PM_{0.18-1}$) for MOUDI samples collected on 12/6/20 to 12/9/20.

Figure 3.6 shows ambient size distribution of $O_2^{\cdot-}$ formed in the yellow-brownish aqueous extracts of the wildfire samples. A recent study reported chemical compounds that absorb light at 300 nm are predominately found in wildfire PM_1.[185] Brown carbon is a group of light absorbing compounds that their light-absorption coefficient has a strong wavelength dependence with absorption gets much higher near the UV region compared to visible light.[186] Brown carbons are also known to absorb light significantly at 300 nm and potentially can be found in this colored aqueous extract.[186] The main source of brown carbon is biomass burning and also can give this yellow-brownish coloring in the aqueous extract.[186] Brown carbon is composed of redox-active chemical components such as HUmic-LIke substance (HULIS) and oxygenated PAHs that can generate $O_2^{\cdot-}$ in aqueous solution.[186] Future studies connecting brown carbon measurements to ROS generation in size-segregated wildfire PM should be conducted to better understand the source of ROS in wildfire PM in water.

3.4.3 Future Studies

The air quality in the Los Angeles (L.A.) Basin is highly impacted by traffic emissions, but the degree to which wildfires influence the air quality is still in question.[31] Our preliminary results show urban PM generate hydroxyl and carbon-centered radicals in water. More interestingly, wildfire fine PM generated hydroxyl, superoxide anion, carbon-centered, and oxygen-centered organic radicals in water, which highlights chemical components from the wildfire can influence the ROS formation in the atmosphere. The $O_2^{\cdot-}$ was found to be formed only in yellow-brownish aqueous extract of wildfire PM, which suggests redox-active chemical components in brown carbon may be responsible for $O_2^{\cdot-}$ formation. DTT measurements would need to be conducted to quantify PM oxidative potential. This study was limited by the number of samples that can be collected during the wildfire and the results should be interpreted with a caution. However, our study provides qualitative picture on what type of ROS the public health may be exposed and motivates epidemiological studies to investigate the ROS observed in this study with health endpoints.

Chapter 4: Multiphase Reactivity of Polycyclic Aromatic Hydrocarbons is driven by Phase Separation and Diffusion Limitations

This chapter is reproduced by permission from: Hwang, B.C.H.; Zhou, S; Lakey, P. S. J.; Zuend, A.; Abbatt, J. P. D.; Shiraiwa, M, "Multiphase Reactivity of Polycyclic Aromatic Hydrocarbons is Driven by Phase Separation and Diffusion Limitations" Proceedings of the National Academy of Sciences 2019**,** *116*, (24), 11658;
DOI:10.1073/pnas.1902517116.

4.1 Abstract

Benzo[a]pyrene (BaP), a key polycyclic aromatic hydrocarbon often associated with soot particles coated by organic compounds, is a known carcinogen and mutagen. When mixed with organics, the kinetics and mechanisms of chemical transformations of BaP by ozone in indoor and outdoor environments are still not fully elucidated. Using direct analysis in real time mass spectrometry (DART-MS), kinetics studies of the ozonolysis of BaP in thin films exhibited fast initial loss of BaP followed by a slower decay at long exposure times, confirming long-standing unresolved observations of incomplete PAH decay upon prolonged ozone exposure. Kinetic multilayer modeling demonstrates that the slow decay of BaP over long times can be simulated if there is slow diffusion of BaP from the film interior to the surface. Phase separation drives the slow diffusion timescales in multicomponent systems. Specifically, thermodynamic modeling predicts that BaP phase separates from secondary organic aerosol material, so that the BaP-rich layer at the surface shields the inner BaP from ozone. Also, BaP is miscible with organic oils such as squalane, linoleic acid and cooking oil, but its oxidation products are virtually immiscible, resulting in the formation of a viscous surface crust that hinders diffusion of BaP from the film interior to the surface. These findings imply that phase separation and slow diffusion significantly prolong the chemical lifetime of PAHs, affecting long-range transport of PAHs in the atmosphere and their fates in indoor environments.

4.2 Introduction

Polycyclic aromatic hydrocarbons (PAHs), including benzo[a]pyrene (BaP), are among the most prominent toxic air pollutants, posing a threat to human health as their metabolites and oxidation products are carcinogenic and mutagenic.[32] PAHs are emitted into the atmosphere from incomplete combustion and biomass burning, and by smoking and cooking in indoor environments. Due to its low vapor pressure, BaP resides mostly in the condensed phase and heterogeneous oxidation of BaP by oxidants such as OH· and O_3 is a major atmospheric loss pathway.[187] Laboratory measurements show rapid degradation of BaP against ozone when adsorbed to a variety of substrates, such as water, ammonium sulfate, soot, and organic compounds.[88, 99, 188-189]

Upon chemical aging in the atmosphere, PAH-containing particles are likely coated by semi- or low-volatile organic compounds, which are formed by multigenerational gas-phase oxidation of volatile organic compounds. Laboratory experiments have shown that organic coatings can retard multiphase reactions of ozone with PAHs due to kinetic limitations of bulk diffusion.[88-89, 190] The extent of coating effects depends on the phase state of organic coatings, which can be liquid, amorphous semisolid or glassy solid, depending on chemical composition, relative humidity and temperature.[79] This shielding effect of PAHs from oxidation was recently implemented into regional and global air quality models, showing how regional and global distributions and transport of BaP can be affected by the temperature and humidity dependence of diffusivity and reactivity of BaP-containing particles. [80-81] These modeling results are consistent with observations of BaP at remote terrestrial and marine sites even in the polar regions. [191-192] Atmospheric aerosol particles are often mixtures of organics, inorganics and water, which are subject to complex and non-ideal behavior including liquid–liquid and/or liquid–solid phase separation, as predicted by thermodynamic models.[193-194] Experimental studies have demonstrated

the existence of multiple phases in model mixtures or laboratory-generated SOA particles as well as in field-collected organic aerosol particles.[74, 195-196] Liquid–liquid phase separation was also observed in SOA particles free of inorganic salts.[197-199] The interplay of phase state and non-ideality can affect aerosol mass concentration and the characteristic timescale of gas-particle mass transfer. [200] Changes in viscosity upon chemical aging of organic particles were observed [83] but it is not yet clear how the effects and interplay of non-ideality and phase state evolve upon multiphase chemical interactions to affect fates and atmospheric long-range transport of organic compounds. Although extensive laboratory measurements and modeling of PAHs have been conducted under atmospherically relevant conditions, chemical transformation of PAHs in indoor environments, where we spend ~90 % of the time, is poorly understood.[201] PAHs can be transported from outside air and they can also be emitted by indoor activities such as smoking, cooking, and burning of solid fuels. [202] Recent findings show that BaP diol-epoxide products, which are highly carcinogenic, can be formed in indoor environments and chronic exposure to these compounds can be detrimental to human health.[35] Thus, chemical transformation of PAHs with gaseous ozone under indoor-relevant conditions and PAH reactivity in mixtures of chemicals emitted from indoor sources need to be elucidated. A long-standing, unexplained issue in the field of environmental chemistry and health is the observation that although ozonolysis experiments show a rapid initial loss of condensed-phase PAHs, prolonged exposure to ozone does not necessarily lead to complete PAH decay. [203-206]

In this study, the decay kinetics of BaP upon exposure to ozone were measured using direct analysis in real time mass spectrometry (DART-MS). Three different sets of experimental and modeling scenarios were explored: i) the ozonolysis kinetics of pure BaP films (containing a small amount of an internal standard), ii) the effects of the reaction substrate by mixing BaP with α-

pinene secondary organic aerosol (SOA) material, a mixture of different oxidized organic compounds, and iii) the effects of mixing BaP with liquid substrates such as squalane, linoleic acid, and cooking oil. The experimental conditions were simulated using the kinetic multi-layer model of aerosol surface and bulk chemistry (KM-SUB), which resolves mass transport and chemical reactions at the surface and in the condensed phase explicitly [97], combined with the thermodynamic Aerosol Inorganic-Organic Mixtures Functional Groups Activity Coefficients (AIOMFAC) model [207-209] at the core of a thermodynamic equilibrium framework that predicts chemical composition of different co-existing phases. Together, the three sets of simulations and experimental results pinpoint the critical factors that control PAH ozonolysis loss rates in a variety of organic media.

4.3 The Kinetic Experiments

The kinetic experiments in this work were conducted by Dr. Shouming Zhou under Prof. Jonathan P. D. Abbatt.[210] BaP film containing bis(2-ethylhexyl) sebacate (BES) were prepared and deposited on the outside sealed end of capillary tubes. Similar procedures were conducted for α-pinene SOA and liquid organic mixtures. The BaP films were exposed to O_3 in a flow tube for selected time intervals. Then, the BaP and BES were measured using Direct Analysis in Real Time-Mass Spectrometry (DART-MS).[211]

4.4 Kinetic Modeling

4.4.1 Kinetic Model and Parameters:

The kinetic multi-layer model for aerosol surface and bulk chemistry (KM-SUB) [97] was applied to analyze the experimental data. KM-SUB consists of multiple model compartments and layers, respectively: gas phase, near-surface gas phase, sorption layer, quasi-static surface layer, near-surface bulk, and a number of *n* bulk layers. *n* was set to one for the BaP-BES system (Figure 4.2) and two for BaP-organic oil systems (Figure 4.4). For phase-separated α-pinene and BaP

mixtures, the BaP-rich phase was treated with one layer, while the SOA-rich phase was treated with six layers (Figure 4.3). KM-SUB treats gas-surface transport (reversible adsorption) of ozone, surface reaction, bulk diffusion of ozone and BaP, and bulk reaction between ozone and BaP. Surface reactions were treated with decomposition of ozone and formation of long-lived reactive oxygen intermediates (ROI; e.g., O atoms).[101] The weakly-bound physisorbed O_3 molecule can be desorbed thermally to the gas phase with a desorption lifetime of nanoseconds, or it can overcome an activation barrier ($E_{a,pc}$), undergo dissociation and enter into a state of stronger binding to the surface. The second activation barrier ($E_{a,ox}$) is the reaction between ROI and BaP to form stable oxidation products. The conversion of ROI to physisorbed ozone by surface reactions of ROI with adsorbed O_2 was also considered.

Bulk diffusion fluxes are treated with first-order transport velocities based on bulk diffusion coefficients. For mass transport fluxes in different phases in phase-separated cases, the first-order exchange rate coefficients were derived considering mass transport between two phases at equilibrium [200]. For bulk diffusion of O_3 and BaP in a product layer (i.e., surface crust), bulk diffusion coefficients were described by the Vignes-type equation [212-213]: $D_{X,p} = (D_{X,P})^{f_s} * (D_{X,oil})^{1-f_s}$, where f_s is the mole fraction of the product, $D_{X,P}$ and $D_{X,oil}$ are the bulk diffusion coefficients of X (O_3 or BaP) in pure products and pure organic oils, respectively. The temporal evolution of bulk diffusivities is shown in Figure 4.1. It shows that bulk diffusion coefficients of ozone and BaP decrease by several orders of magnitude during the time span from 10 - 200 s, when viscous effects start to become important.

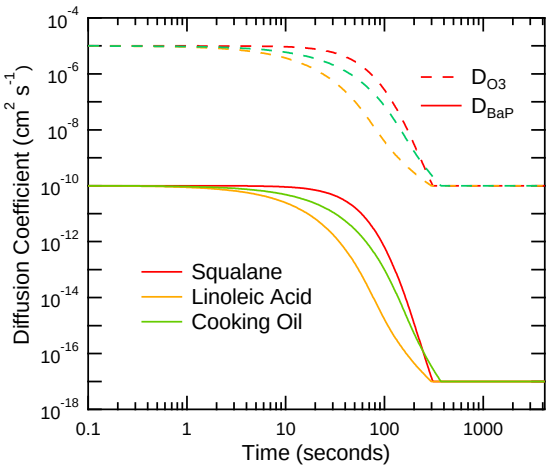

Figure 4.1: Temporal evolution of bulk diffusion coefficient of ozone (dashed lines) and BaP (solid lines) in the near-surface bulk of the films of squalane (red), linoleic acid (yellow), and cooking oil (green).

The initial concentrations of O_3 at the surface and in the bulk were set to zero. The initial surface and bulk concentrations of BaP were dependent on the composition of the film mixture. The film mixtures were composed of BES, BaP, and organics (α-pinene SOA, squalane, linoleic acid, or cooking oil) with the absolute amount of 0.5, 1, and 10 ng, respectively, as used in the experiments. For phase-separated BaP and α-pinene SOA mixtures, the initial amounts of BaP in the BaP-rich and α-pinene SOA-rich phases were set to 0.65 ng and 0.35 ng at RH <5%, 0.90 and 0.10 ng at 50% RH, and 1.0 ng and 0 ng (i.e., complete phase separation), respectively, based on AIOMFAC model predictions. Bulk concentrations were calculated using molar mass and density of each chemical component and for α-pinene SOA we assumed 250 g mol^{-1} and 1.4 g cm^{-3}, respectively. The density and the average molar mass of cooking oil were assumed to be 0.9 g cm^{-3} and ~600 – 800 g mol^{-1}, respectively. The surface concentrations were calculated from multiplying the thickness of a monolayer at the surface with the bulk concentrations.

The molecular depth of BaP is 0.3 nm. [214] For the base case scenario in Figure 4.2, we set the film thickness to be 0.61 nm, corresponding to approximately double layer of BaP on half of the surface area of the capillary. Due to non-uniform deposition of materials, the film thickness was varied in the model to explore its impact on simulation results. For example, KM-SUB can still reproduce the experimental data with the film thickness set to ~ 6 nm by increasing D_{BaP} by about two orders of magnitude.

The temporal evolution of the number of BaP molecules was modeled by numerically solving the differential equations for the mass balance of each model compartment with Matlab (ode23tb solver with 999 time steps). The thermal velocity of ozone (ω_{O3}) is 3.6×10^4 cm s^{-1} at 298 K and the surface accommodation coefficient of ozone on adsorbate-free surface ($\alpha_{s,0,O3}$) is set to 1 based on previous studies.[101,215] Other required input kinetic parameters value are summarized in Table 4.1, including the desorption lifetime of ozone ($\tau_{d,O3}$), the Henry's law constant for ozone ($K_{sol,cc}$) into the organic solution, the bulk diffusion coefficient of ozone (D_{O3}). $K_{sol,cc}$ into organics generally lies between ~ 10^{-4}–10^{-3} mol cm^{-3} atm^{-1}. [216-219] Molecular dynamics simulations suggest $\tau_{d,O3}$ should be on the order of nanoseconds.[215] The second-order bulk reaction rate coefficient between BaP and ozone (k_{BR}) and activation energies ($E_{a,pc}$, $E_{a,ox}$) are estimated based on previous studies.[89, 101, 220] For BaP in linoleic acid and cooking oil films, surface and bulk reactions between unsaturated fatty acids and ozone ($k_{SLR,O3,oil}$, $k_{BR,O3,oil}$) were included, which were reported to be within ~ 10^{-15} - 10^{-11} cm^2 s^{-1} and ~ 10^{-17} - 10^{-15} cm^2 s^{-1}, respectively. [97, 218, 221-223] These parameters and bulk diffusion coefficients of BaP in different matrices were varied in reported ranges to obtain optimal values to best fit the experimental data.

Table 4.1. Kinetic parameters used in the KM-SUB simulation for the ozonolysis of BaP.

Parameter	Description	Value
$\alpha_{s,0,O3}$	surface accommodation coefficient of O_3	1
$\alpha_{s,0,O2}$	surface accommodation coefficient of O_2	1
$\tau_{d,O3}$ (s)	Desorption lifetime of O_3	3.7×10^{-9}
$\tau_{d,O2}$ (s)	Desorption lifetime of O_2	1×10^{-10}
$E_{a,pc}$ (kJ mol^{-1})	Activation energy from physisorbed O_3 to ROI	40
$k_{SLR,BaP,ROI}$ (cm^2 s^{-1})	Second-order surface rate coefficient between BaP and ROI	3.0×10^{-17} (BaP-BES and α-pinene) 4.0×10^{-18} (for liquid organics)
$k_{SLR,O2,ROI}$ (cm^2 s^{-1})	Second-order surface rate coefficient between O_2 and ROI	9.2×10^{-15} (BaP-BES) 1.8×10^{-14} (BaP-SOA) 8.1×10^{-16} (Liquid Organics)
k_{BR} (cm^3 s^{-1})	Second-order bulk reaction rate coefficient between BaP and O_3	1×10^{-19}
$k_{SLR,O3,ROI}$ (cm^2 s^{-1})	Second-order surface reaction rate coefficient between O_3 and ROI	$< 1 \times 10^{-17}$
$k_{SLR,O3,oil}$ (cm^2 s^{-1})	Second-order surface reaction rate coefficient between O_3 and unsaturated organic oils	$> 1 \times 10^{-15}$
$k_{BR,O3,oil}$ (cm^3 s^{-1})	Second-order bulk reaction rate coefficient between O_3 and unsaturated organic oils	2×10^{-17} (linoleic acid) 1×10^{-17} (cooking oil)
$K_{sol,cc}$ (mol cm^{-3} atm^{-1})	Henry's law coefficient of O_3	6×10^{-4}
$D_{O3,BaP}$ (cm^2 s^{-1})	Bulk diffusivity of O_3 in BaP/BES	10^{-10}
$D_{O3,oil}$ (cm^2 s^{-1})	Bulk diffusivity of O_3 in organic oils	10^{-5}
$D_{BaP,\ BaP}$ (cm^2 s^{-1})	Bulk diffusivity of BaP in BaP/BES	2.1×10^{-19} - 1.9×10^{-17}
$D_{BaP,\ SOA}$ (cm^2 s^{-1})	Bulk diffusivity of BaP in SOA	1×10^{-14} (dry) 1×10^{-12} (50% RH)
$D_{BaP,\ oil}$ (cm^2 s^{-1})	Bulk diffusivity of BaP in organic oils	1×10^{-10}
$D_{BaP,O\text{-}BaP}$ (cm^2 s^{-1})	Bulk diffusivity of BaP in oxidized BaP	1×10^{-17}

4.4.2 Sensitivity Analysis

Note that some kinetic parameters were found to be co-dependent or non-orthogonal with other parameters, including the first-order rate coefficient of ROI formation from O_3 ($k_{SLR,O3}$) and τ_{O3}, second-order rate coefficient for surface layer reaction between ROI and O_2 ($k_{SLR,O,O2}$) and τ_{O2} ($< 10^{-8}$ s), as well as the reaction rate coefficient between ROI and BaP ($k_{SLR,BaP,ROI}$) and that between ROI and O_2 ($k_{SLR,O2,ROI}$). Sensitivity studies revealed D_{BaP}, $K_{sol,cc}$, and $k_{BR,BaP,O3}$ can be mutually adjusted to fit the experiment data which were also observed in previous studies [212, 224-225]. This indicates that certain pairs of kinetic parameters could lead to the same model output and such parameters may not be determined uniquely. Nevertheless, the model is still constrained to experiments and our main conclusion that crust formation and diffusion limitations will extend the lifetime of BaP is not affected.

To identify limiting steps of BaP ozonolysis, the following three properties were calculated that are fundamental to reactive uptake [226]: a) The ratio of surface and total loss rates of BaP (STLR) to distinguish the reaction location between the particle (or film) surface (STLR ≈ 1) and the bulk (STLR ≈ 0); b) Surface saturation ratio (SSR) of ROI to determine the abundance of ROI at the surface; c) Mixing Parameter (MP_{BaP}) as the ratio of BaP concentration at the surface and at the bottom of the bulk to indicate bulk concentration gradient. In the BaP film case, STLR and SSR approach ~ 0.9 – 1 within a minute indicating the reaction is limited by surface reactions including ROI formation and subsequent reactions of BaP with ROI. At longer reaction times, MP_{BaP} approaches ~ 0.01 while STLR and SSR still retain a high value of ~ 0.8, indicating that the surface is deprived of BaP as limited by bulk diffusion of BaP from the film interior to the surface. In the case of the organic oil film, the value of STLR remains high, while MP_{BaP} decreased from 1 to less

than 0.1 after ~10^3 s. This indicates that surface crust formation suppresses bulk diffusion of BaP to surface to retard surface reactions.

Sensitivity analysis of kinetic parameters was performed by varying each kinetic parameter by one order of magnitude to calculate normalized sensitivity coefficients with the modeled output of BaP concentration ratio, [BaP]/[BaP]$_0$. We found that for the BaP film $k_{SLR,O3}$ and $k_{SLR,O,BaP}$ are the most sensitive parameters, consistent with the BaP decay being initially limited by surface reactions. Initially D_{BaP} is insensitive, but becomes very sensitive at later reaction time, also indicating that the system becomes limited by bulk diffusion of BaP. D_{O3} and $D_{BaP,SOA}$ showed little influence on [BaP]/[BaP]$_0$, indicating O_3 and BaP diffusion in phase-separated SOA play a minor role. For the cooking oil film case, while ($D_{BaP,\,oil}$) has little sensitivity on BaP decay kinetics, $D_{BaP,O\text{-}BaP}$ was found to be very sensitive. It confirms that the system is limited by bulk diffusion of BaP through the surface crust.

4.5 Thermodynamic Model

Prof. Andreas Zuend used the Aerosol Inorganic-Organic Mixtures Functional groups Activity Coefficients (AIOMFAC) based liquid-liquid equilibrium (LLE) model to estimate how much BaP was present in α-pinene SOA film under dry and humid conditions.[210] This model was also used to predict the solubility of BaP oxidation products in liquid organic films.[210] A detail description of this model can be found elsewhere.[201-203]

4.6 Results and Discussion

4.6.1 BaP Film

Figure 4.2 shows the ozonolysis decays of pure BaP in thin films that only contain traces of bis(2-ethylhexyl) sebacate (BES) as an internal standard. There is a one hour exposure to 15-1000 ppb ozone (O_3) at < 5 % relative humidity (RH) and 296 K. If the BaP were uniformly deposited on

the capillary, then the resulting film would be roughly one monolayer thick. Much more likely, the film has inhomogeneous thickness leading to most of the BaP being present in multilayer amounts. The BaP concentration decayed slower at 15 ppb O_3 than at 100 ppb O_3, while BaP decay rates became saturated and very similar for 500 and 1000 ppb O_3. Interestingly, BaP was not entirely reacted away, leaving an unreacted fraction of ~20% at high O_3 mixing ratios (500 and 1000 ppb) after one hour, which has also been observed previously, but not explained for many decades.[203-206] The KM-SUB model was applied to simulate these data by considering surface adsorption of O_3, decomposition of O_3 into reactive oxygen intermediates (ROI; e.g., sorbed O atoms) and subsequent reactions with BaP[101], bulk diffusion of O_3 and BaP, and bulk reactions between O_3 and BaP. The time and concentration dependence of BaP decay can be reproduced by KM-SUB with the kinetic parameter values listed in table 4.1 as consistent with our previous work.[101] The film thickness was set in the model to be 0.61 nm, representing roughly a double layer of molecules. Note that qualitatively similar modeling results were obtained using a film thickness ten times larger (see section 4.4.1 for details).

The modeling results indicate that the decay of BaP is initially controlled by ROI formation and surface reactions with BaP, leading to fast initial BaP decay. Once surface BaP is depleted, the key aspect of the model prediction is that the oxidation of BaP becomes limited by bulk diffusion of BaP from the film interior to the surface at longer reaction times. This explains the subsequent slow BaP decay after ~10 minutes as well as saturation of BaP decay rates at higher O_3 mixing ratios. Bulk diffusivity of BaP was predicted to be in the range of ~10^{-17} to 10^{-19} cm^2 s^{-1}, which is consistent with an amorphous semi-solid state of the film. Note that the modeled kinetics are insensitive to the bulk diffusivity of O_3, as bulk reactions play a minor role in overall BaP degradation.[88-89] As a consequence, BaP in the deep bulk is protected from ozonolysis due to

this shielding effect arising from slow BaP diffusion to the surface, which explains the unreacted BaP fraction at long reaction times in these and previous experiments.[203-206]

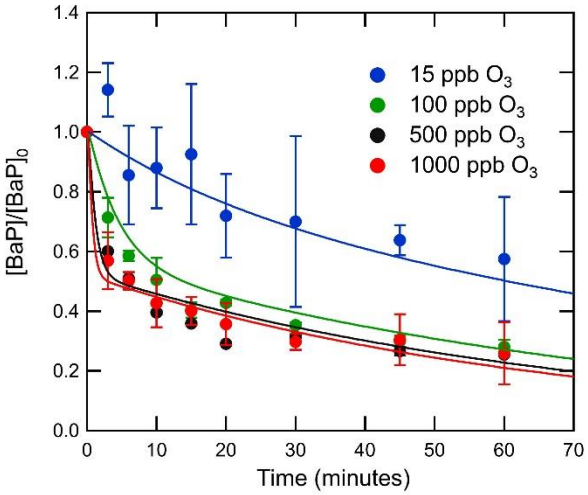

Figure 4.2. Decay of BaP concentration in BaP-BES films exposed to different mixing ratios of ozone (15 - 1000 ppb) at 296 K and RH < 5 %. Filled circles show the experimental data with error bars representing the standard deviation of ten measurements. The solid lines are KM-SUB model simulation results with a single kinetic parameter set shown in Table 4.1.

4.6.2 BaP in SOA Film at Dry and Humid Conditions

The results from the second reaction scenario are shown in Figure 4.3 (a), which illustrates the time-dependent oxidative decay of BaP mixed with α-pinene SOA exposed to 500 ppb O_3 at dry conditions, 50 % RH and 85 % RH. The BaP concentration decays at very similar rates at different relative humidities for up to ~10 minutes and then decays with faster rates and higher reacted fractions at higher RH. In theory this behavior could be due to a phase change of α-pinene SOA, which is expected to exist as an amorphous solid at a temperature of ~295 K and dry conditions, but becomes substantially less viscous at higher RH due to water uptake.[227] According to previous viscosity measurements [227] and kinetic experiments[89], the bulk diffusivity of PAH in α-pinene SOA at 85 % RH is expected to be as high as ~10^{-11} cm^2 s^{-1}. However, when PAH is assumed to be well-mixed and with such a high bulk diffusivity in the α-pinene SOA mixture, the KM-SUB

simulation failed to reproduce the experimental data, as shown by the red dashed line in Figure 4.3 (a). Under such assumptions, KM-SUB predicts complete depletion of BaP within less than 1 hour, indicating a lack of substantial kinetic limitations, even at 85 % RH. There is clearly an aspect to this modeling scenario that is not accurately representing the experimentally observed kinetics.

To probe this reaction system more deeply, the likelihood of phase separation was assessed using the AIOMFAC-based liquid–liquid equilibrium (LLE) model [207-209], where α-pinene SOA was simulated by a mixture of 14 representative oxidation products.[193, 200] Contrary to the assumption of full mixing which led to the dashed line in Figure 4.3a, the LLE model predicts that the mixtures separate into BaP-rich (see Fig. 4.3b upper panel) and SOA-rich (Fig. 4.3b lower panel) phases of distinct compositions, dependent on the water activity. Under dry conditions, ~65 % of the total particle-bound BaP mass is predicted to partition to the phase rich in BES and BaP, with the remaining ~35 % BaP present in the SOA-rich phase. BaP's phase preference becomes more distinct with increasing RH so that at 50 % RH about 90 % of its mass resides in the BaP-rich phase and at 85 % RH the partitioning to the BaP-rich phase approaches 100 %, i.e., virtually complete phase separation. The BaP-rich phase is most likely in the form of a film on top of the SOA-rich phase (i.e., full engulfing as opposed to partial engulfing), considering that BaP should have lower surface tension than polar SOA materials.

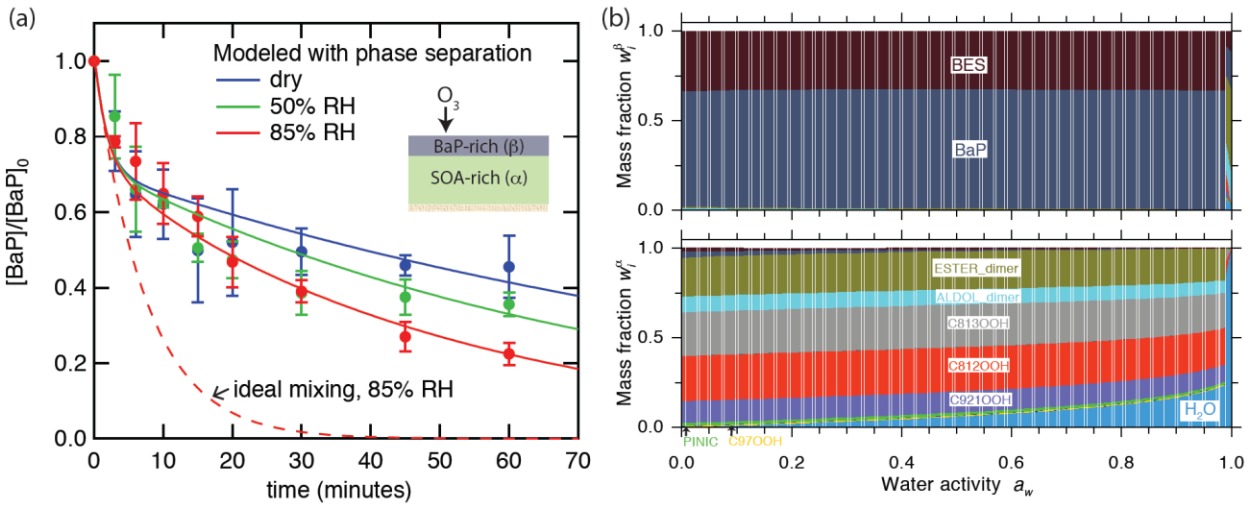

Figure 4.3. (a) Decay of BaP embedded in the films of α-pinene SOA upon exposure to 500 ppb O_3 at dry conditions (blue), 50% (green) and 85% (red) RH at 296 K. The circle markers are the experimental data and error bars represent the standard deviation of ten measurements. KM-SUB modeling results are presented with consideration of liquid–liquid phase separation (solid lines) and without (dashed line for 85% RH). (b) Thermodynamic modeling results by AIOMFAC, predicting phase compositions of the α-pinene SOA + BaP-BES system as a function of water activity (i.e. RH, assuming equilibrium conditions) for an initial amount of 10 ng α-pinene SOA, 1 ng BaP, and 0.5 ng BES in the particle phase. α-pinene SOA is treated with 14 representative oxidation products (Table 4.2). Predicted phase compositions are shown as stacked mass fractions of the individual components for the phase α enriched by SOA compounds (lower panel) and the phase β dominated by BaP and BES (upper panel).

By implementing the predicted phase compositions arising from phase separation in KM-SUB, the model reproduces experimental data very well as shown by the solid lines in Figure 4.3(a). The kinetic model simulations reveal that the BaP decay is initially controlled by surface reactions leading to fast BaP decay, followed by diffusion of BaP molecules from the bulk to its surface. The diffusion coefficients of BaP within the surface crust (i.e. a semi-solid surface layer of high viscosity) were found to have the most sensitivity in the modeling. Reactions at the surface are found to be faster than in the bulk[89], so BaP in the film interior needs to diffuse through the bulk to the surface to react. The BaP-rich layer at the surface hinders the BaP in the film interior to diffuse to the surface, resulting in significant fractions of BaP remaining unreacted after one hour of ozone exposure.

4.6.3 BaP in Cosmetic and Cooking Related Films

The final set of kinetic experiments measured the decay behavior of BaP embedded in other organic liquids, including squalane, linoleic acid, and cooking oil, as shown in Figure 4.4. Contrary to the SOA case, BaP is miscible with these organic compounds, as evident by visual inspection and also predicted by the thermodynamic phase equilibrium model. So, BaP should initially be homogenously mixed within the film. The KM-SUB modeling results for BaP decay in squalane upon exposure to 500 ppb O_3 are shown as the dashed red line in Figure 4.4. The model captures the initial BaP decay up to ~10 minutes but over-predicts the long-term BaP decay in the absence of kinetic limitations.

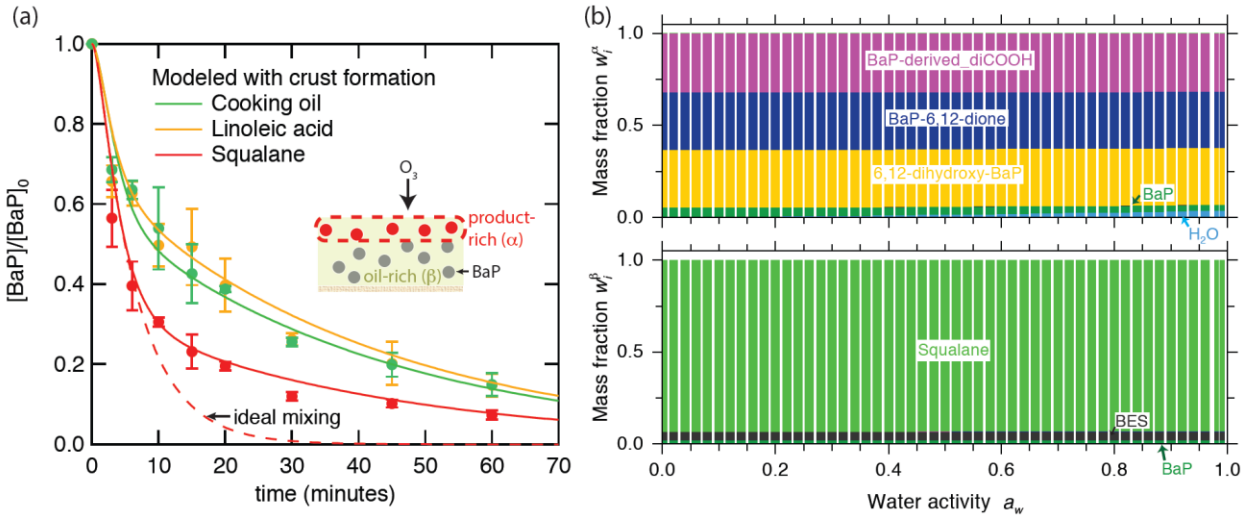

Figure 4.4 (a) Decay of BaP embedded in the films of squalane (red), linoleic acid (yellow), or cooking oil (green) upon exposure to 500 ppb O_3 under dry conditions. The circle markers are the experimental data and error bars represent the standard deviation of 10 measurements. The solid lines represent KM-SUB simulations with consideration of surface crust formation by BaP oxidation products and composition-dependent bulk diffusivity using a Vignes-type equation, while the dashed line for the squalane case does not consider this phase separation effect, failing to reproduce experiments. (b) The predicted phase compositions in mass fractions for mixtures of BaP, BaP oxidation products (BaP-6,2-dione, BaP-derived carboxylic acid, 6,12-dihydroxy BaP), and squalane after half of the BaP is degraded. (see Figure 4.3b caption for explanation of the plots). One phase consists of largely squalene, BES and BaP (β, lower panel), whereas the other consists largely of the BaP oxidation products (α, upper panel). Liquid–liquid phase equilibrium calculations with AIOMFAC predict for all RH (or water activities) that BaP oxidation products are virtually immiscible in squalane.

Although BaP may be miscible initially, its oxidation products may phase separate from the oily liquid reaction substrates. We considered three major BaP ozonolysis products, including 6,12-dihydroxy-BaP, BaP-6,12-dione, and a BaP-derived dicarboxylic acid[228], and cooking oil was treated as triolein. The AIOMFAC thermodynamic equilibrium modeling also predicts these oxidation products are immiscible in liquid organics. This suggests that the oxidation process, which leads to the formation of oxidation products that are more oxygenated than the BaP reactant, promotes phase separation. A viscous surface crust forms, which can hinder diffusion of BaP from the film interior to the surface. We note that a crusting effect has been observed in the uptake of organic nitrates [229] or ammonia to SOA, where carboxylates may also form a viscous crust at the surface of the reaction substrate.[230]

To consider this effect in the KM-SUB model, bulk diffusion coefficients of BaP were treated as composition-dependent using the Vignes type equation (Figure 4.1).[213] Linoleic acid and cooking oil compounds are unsaturated (i.e. with C=C double bonds) and ozone reacts with these compounds. Previous studies have shown that high molar mass compounds such as peroxidic oligomers can be formed especially under low RH[231-232], causing an increase of viscosity.[83] Thus, these products may also contribute to form the surface crust, which was explicitly treated in KM-SUB. With consideration of these effects, KM-SUB was able to capture a slow BaP decay at longer reaction times to fully reproduce the experimental data, as shown by the solid lines in Figure 4.4. Retardation of oleic acid ozonolysis from surface crust formation has been observed in mixed-component particles in previous studies.[85, 87, 233] These results demonstrate how phase separation leading to crust formation at the surface can affect the chemical transformation of PAH in multi-component mixtures.

4.6.4 Implications for Atmospheric and Indoor Chemistry

PAHs are often associated with soot particles that are subject to coating by semi-volatile primary organic emissions and by secondary organic materials formed by oxidation of anthropogenic and biogenic precursors. Our experimental and modeling study demonstrates that the multiphase reactivity of PAHs depends strongly on the interplay of phase state and non-ideal mixing with such organic materials.

In all three sets of reaction systems, it was found that slow diffusion through viscous phases is rate-limiting at long reaction times, because the BaP must diffuse to the surface to react. In the case of pure BaP films, the semi-solid substrate acts as the diffusion barrier, whereas in the mixtures with oils such as squalane, linoleic or cooking oils, the reaction products phase separate into a phase with low diffusivity. When mixed into SOA, the PAHs do not mix homogeneously with α-pinene SOA but are instead separated into different phases, affecting the multiphase reactivity of PAHs against ozone. RH controls the degree of non-ideality and phase separation, and also determines the phase state of PAH-SOA mixtures. In phase-separated particles with the PAH-rich phase on the particle surface, slow diffusion of PAH from the particle bulk to the surface limits PAH degradation by ozone. Moreover, the SOA-rich phase, which embeds a fraction of the PAHs, adopts an amorphous (semi-)solid state at low RH, posing additional kinetic limitations of bulk diffusion and retarding ozonolysis kinetics. Overall, these effects will prolong chemical lifetimes of PAHs, facilitating long-range transport of PAHs and affecting regional and global distributions in the atmosphere and their effects on air quality and public health.[80-81]

PAHs are also found in indoor environments and a BaP concentration of 38.8 μg per gram of dust has been reported.[234] PAHs are transported from outdoors to indoors and are directly emitted by indoor activities including cooking and smoking. With cooking, BaP may be deposited

and embedded into an organic film on indoor surfaces. The fate of low volatility PAHs will be controlled by surface oxidative processes considering the high surface-to-volume ratios in indoor environments and that organic films can persist for an indefinite time unless they are wiped off.[235]

To investigate PAH degradation kinetics with real indoor air, a BaP film was exposed to room air containing 10 ppb O_3 for up to five hours. Figure 4.5 shows the BaP decay rate by room air is remarkably similar to the one when BaP is exposed to 15 ppb O_3 in a controlled flow tube setting, and it is modeled well (the solid red line) with the same kinetic parameters used to model (Figure 4.2). These results indicate that ozone will be the most important indoor oxidant among others (e.g., OH, NO_3) for determining the fate of these compounds in indoor environments.

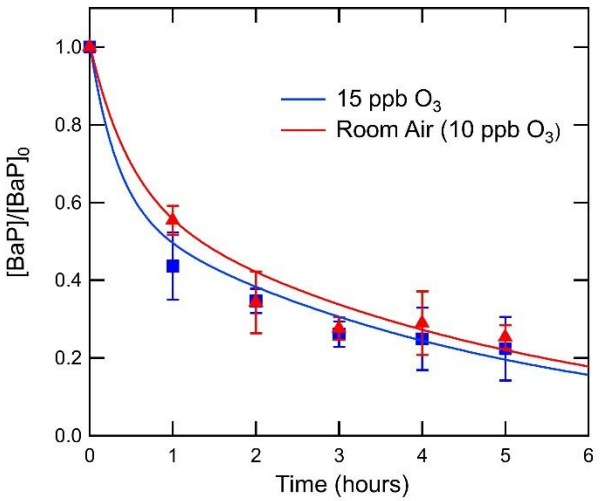

Figure 4.5: Experimental measurements (circles) and KM-SUB modeling results (lines) of decay of BaP in BaP-BES films exposed to 15 ppb O_3 and room air (10 ppb O_3).

To illustrate the chemical fate of BaP embedded in an indoor surface film consisting of cooking oil, we simulated the molar fraction of unreacted BaP after exposure to 0.1 to 100 ppb O_3 for one hour, twelve hours, one day and one week. The parameters used in the model are those that successfully modeled the experimental data in Figure 4.4 (Table 4.1). The mass concentration of BaP in cooking oil was assumed to be 1200 ng cm^{-3} and the film thickness was set to be 8 nm

based on previous observations in indoor environments.[236-238] Figure 4.6 shows the results of such KM-SUB simulations. At O_3 concentration of 10 ppb, ~80 % and ~10 % of the BaP remain unreacted after one hour and a half day, respectively, while the BaP is expected to be fully reacted away after one week. Typical indoor O_3 concentrations ranges from 5 ppb to over 50 ppb (depending on air exchange rates and outdoor air pollution)[239] and the unreacted fraction of BaP molecules considering surface crust formation is larger than the case with an ideal mixing assumption, especially at higher O_3 concentrations. Thus, the fate of PAH in indoor environments is strongly influenced by multiphase reactivity as impacted by surface crust formation and diffusion limitations. The true BaP lifetime may be even longer, dependent upon the mass transfer rates that prevail under genuine indoor conditions.

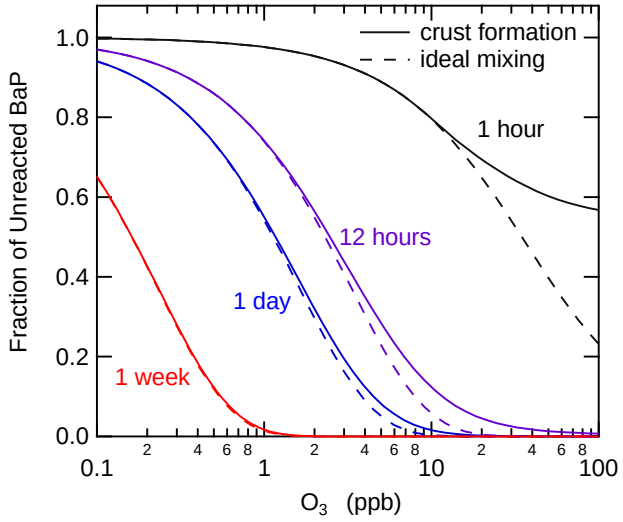

Figure 4.6. Fraction of BaP remaining in a 8 nm-thick cooking oil film exposed to different gas-phase ozone mixing ratios after one hour (black), twelve hours (purple), one day (blue), and one week (red) at 295 K and dry conditions, as simulated by KM-SUB considering phase separation and crust formation by BaP oxidation products (solid lines) or assuming ideal mixing (dashed lines).

5. Summary of the Dissertation

Fine particulate matter ($PM_{2.5}$) was collected at the two highways: Interstate 5 (I-5) and 710 (I-710) located in Anaheim and Long Beach, respectively. Government agencies and other groups have previously conducted chemical measurements at these two sites. Their findings determined that DTT activities did not significantly change over the years while pollutants that contribute to redox activity of fine PM decreased.[19-20] Their findings further hypothesized that an increase in contribution of metals in $PM_{2.5}$ may explain the consistent DTT activities measured at the Southern California highways.

This study has chosen highways I-5 and I-710 to explore whether metals, most likely emitted from non-exhaust emission, play a role in ROS formation near highways. EPFRs, ROS generation, and total DTT activities from $PM_{2.5}$ were measured in this study. The ambient EPFR concentrations ($EPFR_v$) measured from $PM_{2.5}$ at the highway sites were found to be more than two times higher than the urban site in Irvine. The mass normalized EPFR concentrations ($EPFR_m$) were found to be approximately six to ten times higher in comparison to that of the urban sites mentioned in the literature.[47, 55] The highway $PM_{2.5}$ was found to mainly generate ·OH and carbon-centered radicals in water, which is in contrast with superoxide anion and oxygenated organic radical generation from fine PM collected from major cities in China.[42] The ROS concentrations (ROS_v and ROS_m) generated from fine PM at Anaheim and Long Beach were found to be similar at both sites. This study shows communities living near the highway are exposed to twice the amount of these radicals, compared to communities living in suburban areas. The total DTT activities did not significantly differ when compared to past studies conducted at I-710 and Anaheim around the same season.[19-20] The univariate correlation analysis shows a ·OH radical generated in aqueous solution and EPFR at Long Beach are positively correlated with primary

pollutants (CO and NO_2) along with elemental carbon (EC). The formed ·OH and EPFR were also found to be positively correlated with each other. These correlation results suggest that formed ·OH radical and EPFR may have similar sources at Long Beach and redox-active EPFR possibly contributed to ·OH generation in aqueous solutions. EPFR was found to be positively correlated with Fe and Cu at the Anaheim site, which suggests non-exhaust emissions may play a role in stabilizing EPFR. Interestingly, the total DTT activity showed positive correlations with ROS generated from fine PM in water.

In chapter 3, EPFR and ROS generated from size-segregated urban and wildfire particles were measured. The preliminary results show that EPFR can be approximately ten times higher during the wildfire compared to urban environments. ·OH, superoxide anion, carbon-centered, and oxygen-centered organic radicals were found to be formed in aqueous solutions depending on wildfire particle sizes, while urban particles showed no size-dependence of hydroxyl and carbon-centered organic radical formation in water.

Chapter 4 explores the reaction mechanism and kinetics of ozonolysis of BaP in a multicomponent film. Incomplete BaP decay was observed upon prolonged ozone exposure. This phenomenon was also observed in past studies under similar experimental conditions dating back to the 1970s and could not be explained.[203-205] In this study, the unreacted fraction of BaP in the film upon prolonged ozone exposure can be explained by the slow bulk diffusivity of BaP to the surface. For a multichemical component system, α-pinene SOA was mixed with BaP and BES to form a film, which was exposed to O_3 under different humidity conditions. The kinetic model was able to reproduce the experimental data sets only when BaP is immiscible in SOA. The BaP decay was found to be limited by bulk diffusivity of BaP to the surface at the immiscible BaP layer on top of SOA film. This assumption was also supported by the thermodynamic model AIOMFAC.

Lastly, a multicomponent film was also generated from mixing BaP and BES with organic liquids including squalene, linoleic acid, and cooking oil. The kinetic model further showed that BaP oxidized product are immiscible with the organic liquids to form a viscous layer at the surface, which also slows diffusivity of BaP from the film bulk to the surface. Oxidation products of linoleic acid and triolein also contribute to the formation of surface viscous layer. Simulation of BaP in cooking oil film was conducted using the kinetic parameters to fit the experimental data, showing that ~80% and ~10% of BaP would remain unreacted after 1 and 12 hours of 10 ppb O_3 exposure, respectively. These findings demonstrate that phase separation and slow diffusion significantly prolong the chemical lifetime of PAHs, affecting their fates in indoor environments.

6. Future Studies

The water-soluble $PM_{2.5}$ DTT activity revealed to be strongly associated with emergency department visits for asthma/wheezing and congestive heart failure.[240] This study's source contribution analysis showed the gasoline vehicle emissions exhibited the highest DTT activity, which highlights the importance of tailpipe regulations. The total DTT activity can be significantly impacted by insoluble redox-active components from non-exhaust emissions. The positive correlation between the total DTT activity and ROS formation in our study suggests similar epidemiological studies should be conducted with the total DTT activity measurements.

The redox-active chemical components that are responsible for ROS formation from wildfire PM are still not well known. The $O_2^{\cdot-}$ was only generated in yellow-brownish aqueous extract of wildfire PM in this dissertation. Chemical measurements of these yellow-brownish aqueous extract should be made the better understand the $O_2^{\cdot-}$ source in wildfire PM.

The oxidation products from ozonolysis of BaP and unsaturated compounds at the surface layer were explicitly treated in the kinetic model to fit the experimental data for BaP in linoleic acid and cooking oil films. Oleic acid, a compound chemically similar to linoleic acid, has been reported to form peroxidic oligomer upon exposure to the ozone.[231-232] The current hypothesis is that the ozonolysis products of oleic acid are non-polar and are immiscible with polar compounds.[83] However, our kinetic, experimental, and thermodynamic results also discovered polar oxidation BaP products contribute to the surface layer. The interactions between BaP and linoleic acid ozonolysis products are not known, and how these products' interactions can affect the phase state should be investigated in future studies.

7. Bibliography

1. Kelvin, C., Cheng, Kelvin. Silverado Fire in Irvine taken last night. https://www.reddit.com/r/orangecounty/comments/jj8ail/silverado_fire_in_irvine_taken_last_night/?utm_medium=android_app&utm_source=share. 2020.

2. Houghton, J., Global warming. *Reports on Progress in Physics* **2005,** *68* (6), 1343-1403.

3. McKinnon, K. A.; Poppick, A.; Simpson, I. R., Hot extremes have become drier in the United States Southwest. *Nature Climate Change* **2021,** *11* (7), 598-604.

4. Abatzoglou, J. T.; Williams, A. P., Impact of anthropogenic climate change on wildfire across western US forests. *Proceedings of the National Academy of Sciences* **2016,** *113* (42), 11770-11775.

5. Westerling, A. L.; Hidalgo, H. G.; Cayan, D. R.; Swetnam, T. W., Warming and Earlier Spring Increase Western U.S. Forest Wildfire Activity. *Science* **2006,** *313* (5789), 940-943.

6. Gordon, S. B.; Bruce, N. G.; Grigg, J.; Hibberd, P. L.; Kurmi, O. P.; Lam, K.-b. H.; Mortimer, K.; Asante, K. P.; Balakrishnan, K.; Balmes, J.; Bar-Zeev, N.; Bates, M. N.; Breysse, P. N.; Buist, S.; Chen, Z.; Havens, D.; Jack, D.; Jindal, S.; Kan, H.; Mehta, S.; Moschovis, P.; Naeher, L.; Patel, A.; Perez-Padilla, R.; Pope, D.; Rylance, J.; Semple, S.; Martin, W. J., Respiratory risks from household air pollution in low and middle income countries. *The Lancet Respiratory Medicine* **2014,** *2* (10), 823-860.

7. Lelieveld, J.; Evans, J. S.; Fnais, M.; Giannadaki, D.; Pozzer, A., The contribution of outdoor air pollution sources to premature mortality on a global scale. *Nature* **2015,** *525* (7569), 367-371.

8. Manisalidis, I.; Stavropoulou, E.; Stavropoulos, A.; Bezirtzoglou, E., Environmental and Health Impacts of Air Pollution: A Review. *Frontiers in Public Health* **2020,** *8* (14).

9. Jaffe, D. A.; O'Neill, S. M.; Larkin, N. K.; Holder, A. L.; Peterson, D. L.; Halofsky, J. E.; Rappold, A. G., Wildfire and prescribed burning impacts on air quality in the United States. *Journal of the Air & Waste Management Association* **2020,** *70* (6), 583-615.

10. Kuklinska, K.; Wolska, L.; Namiesnik, J., Air quality policy in the U.S. and the EU – a review. *Atmospheric Pollution Research* **2015,** *6* (1), 129-137.

11. Zanobetti, A.; Coull, B. A.; Gryparis, A.; Kloog, I.; Sparrow, D.; Vokonas, P. S.; Wright, R. O.; Gold, D. R.; Schwartz, J., Associations between arrhythmia episodes and temporally and spatially resolved black carbon and particulate matter in elderly patients. *Occupational and Environmental Medicine* **2014,** *71* (3), 201-207.

12. Schaumann, F.; Borm, P. J.; Herbrich, A.; Knoch, J.; Pitz, M.; Schins, R. P.; Luettig, B.; Hohlfeld, J. M.; Heinrich, J.; Krug, N., Metal-rich ambient particles (particulate matter 2.5)

cause airway inflammation in healthy subjects. *American journal of respiratory and critical care medicine* **2004,** *170* (8), 898-903.

13. Nel, A., Air pollution-related illness: Effects of particles. *Science* **2005,** *308* (5723), 804-806.

14. Araujo, J. A.; Barajas, B.; Kleinman, M.; Wang, X.; Bennett, B. J.; Gong, K. W.; Navab, M.; Harkema, J.; Sioutas, C.; Lusis, A. J.; Nel, A. E., Ambient Particulate Pollutants in the Ultrafine Range Promote Early Atherosclerosis and Systemic Oxidative Stress. *Circulation Research* **2008,** *102* (5), 589-596.

15. Verma, V.; Sioutas, C.; Weber, R. J., Oxidative Properties of Ambient Particulate Matter - An Assessment of the Relative Contributions from Various Aerosol Components and Their Emission Sources. In *Multiphase Environmental Chemistry in the Atmosphere,* American Chemical Society: 2018; Vol. 1299, pp 389-416.

16. Hasheminassab, S.; Daher, N.; Ostro, B. D.; Sioutas, C., Long-term source apportionment of ambient fine particulate matter (PM2.5) in the Los Angeles Basin: A focus on emissions reduction from vehicular sources. *Environmental Pollution* **2014,** *193*, 54-64.

17. RISTOVSKI, Z. D.; MILJEVIC, B.; SURAWSKI, N. C.; MORAWSKA, L.; FONG, K. M.; GOH, F.; YANG, I. A., Respiratory health effects of diesel particulate matter. *Respirology* **2012,** *17* (2), 201-212.

18. Li, N.; Hao, M.; Phalen, R. F.; Hinds, W. C.; Nel, A. E., Particulate air pollutants and asthma: A paradigm for the role of oxidative stress in PM-induced adverse health effects. *Clinical Immunology* **2003,** *109* (3), 250-265.

19. Shirmohammadi, F.; Wang, D.; Hasheminassab, S.; Verma, V.; Schauer, J. J.; Shafer, M. M.; Sioutas, C., Oxidative potential of on-road fine particulate matter (PM2.5) measured on major freeways of Los Angeles, CA, and a 10-year comparison with earlier roadside studies. *Atmospheric Environment* **2017,** *148*, 102-114.

20. Shirmohammadi, F.; Hasheminassab, S.; Wang, D.; Schauer, J. J.; Shafer, M. M.; Delfino, R. J.; Sioutas, C., The relative importance of tailpipe and non-tailpipe emissions on the oxidative potential of ambient particles in Los Angeles, CA. *Faraday Discussions* **2016,** *189* (0), 361-380.

21. Enayati Ahangar, F.; Pakbin, P.; Hasheminassab, S.; Epstein, S. A.; Li, X.; Polidori, A.; Low, J., Long-term trends of PM2.5 and its carbon content in the South Coast Air Basin: A focus on the impact of wildfires. *Atmospheric Environment* **2021,** *255*, 118431.

22. Kukutschová, J.; Moravec, P.; Tomášek, V.; Matějka, V.; Smolík, J.; Schwarz, J.; Seidlerová, J.; Šafářová, K.; Filip, P., On airborne nano/micro-sized wear particles released from low-metallic automotive brakes. *Environmental Pollution* **2011,** *159* (4), 998-1006.

23. Gustafsson, M.; Blomqvist, G.; Gudmundsson, A.; Dahl, A.; Swietlicki, E.; Bohgard, M.; Lindbom, J.; Ljungman, A., Properties and toxicological effects of particles from the interaction between tyres, road pavement and winter traction material. *Science of The Total Environment* **2008,** *393* (2), 226-240.

24. Grigoratos, T.; Martini, G., Brake wear particle emissions: a review. *Environmental Science and Pollution Research* **2015,** *22* (4), 2491-2504.

25. Thorpe, A.; Harrison, R. M., Sources and properties of non-exhaust particulate matter from road traffic: A review. *Science of The Total Environment* **2008,** *400* (1), 270-282.

26. Zhang, Z.; Weichenthal, S.; Kwong, J. C.; Burnett, R. T.; Hatzopoulou, M.; Jerrett, M.; van Donkelaar, A.; Bai, L.; Martin, R. V.; Copes, R.; Lu, H.; Lakey, P.; Shiraiwa, M.; Chen, H., A Population-Based Cohort Study of Respiratory Disease and Long-Term Exposure to Iron and Copper in Fine Particulate Air Pollution and Their Combined Impact on Reactive Oxygen Species Generation in Human Lungs. *Environmental Science & Technology* **2021,** *55* (6), 3807-3818.

27. Fuzzi, S.; Baltensperger, U.; Carslaw, K.; Decesari, S.; Denier van der Gon, H.; Facchini, M. C.; Fowler, D.; Koren, I.; Langford, B.; Lohmann, U.; Nemitz, E.; Pandis, S.; Riipinen, I.; Rudich, Y.; Schaap, M.; Slowik, J. G.; Spracklen, D. V.; Vignati, E.; Wild, M.; Williams, M.; Gilardoni, S., Particulate matter, air quality and climate: lessons learned and future needs. *Atmos. Chem. Phys.* **2015,** *15* (14), 8217-8299.

28. Lakey, P. S. J.; Berkemeier, T.; Tong, H.; Arangio, A. M.; Lucas, K.; Pöschl, U.; Shiraiwa, M., Chemical exposure-response relationship between air pollutants and reactive oxygen species in the human respiratory tract. *Scientific Reports* **2016,** *6* (1), 32916.

29. Aclima, Aclima. PM 2.5 Surges As Wildfires Rage in California https://www.aclima.io/blog/a-wildfire-driven-rise-of-orange-skies-falling-ash-and-fine-particulate-matter-in-california-9dc2261ff437. 2021. **2021**.

30. Aguilera, R.; Corringham, T.; Gershunov, A.; Benmarhnia, T., Wildfire smoke impacts respiratory health more than fine particles from other sources: observational evidence from Southern California. *Nature Communications* **2021,** *12* (1), 1493.

31. Verma, V.; Polidori, A.; Schauer, J. J.; Shafer, M. M.; Cassee, F. R.; Sioutas, C., Physicochemical and Toxicological Profiles of Particulate Matter in Los Angeles during the October 2007 Southern California Wildfires. *Environmental Science & Technology* **2009,** *43* (3), 954-960.

32. Finlayson-Pitts, B. J.; Pitts, J. N., Tropospheric Air Pollution: Ozone, Airborne Toxics, Polycyclic Aromatic Hydrocarbons, and Particles. *Science* **1997,** *276* (5315), 1045-1051.

33. Liu, Y.; Zhu, L.; Shen, X., Polycyclic Aromatic Hydrocarbons (PAHs) in Indoor and Outdoor Air of Hangzhou, China. *Environmental Science & Technology* **2001,** *35* (5), 840-844.

34. Ohura, T.; Amagai, T.; Fusaya, M.; Matsushita, H., Polycyclic Aromatic Hydrocarbons in Indoor and Outdoor Environments and Factors Affecting Their Concentrations. *Environmental Science & Technology* **2004,** *38* (1), 77-83.

35. Zhou, S.; Yeung, Leo W. Y.; Forbes, M. W.; Mabury, S.; Abbatt, J. P. D., Epoxide formation from heterogeneous oxidation of benzo[a]pyrene with gas-phase ozone and indoor air. *Environmental Science: Processes & Impacts* **2017,** *19* (10), 1292-1299.

36. Kazerouni, N.; Sinha, R.; Hsu, C.-H.; Greenberg, A.; Rothman, N., Analysis of 200 food items for benzo[a]pyrene and estimation of its intake in an epidemiologic study. *Food and Chemical Toxicology* **2001,** *39* (5), 423-436.

37. Winterbourn, C. C., Reconciling the chemistry and biology of reactive oxygen species. *Nature Chem. Biol.* **2008,** *4* (5), 278-286.

38. Betteridge, D. J., What is oxidative stress? *Metabolism* **2000,** *49* (2, Supplement 1), 3-8.

39. Tong, H.; Arangio, A. M.; Lakey, P. S. J.; Berkemeier, T.; Liu, F.; Kampf, C. J.; Brune, W. H.; Pöschl, U.; Shiraiwa, M., Hydroxyl radicals from secondary organic aerosol decomposition in water. *Atmos. Chem. Phys.* **2016,** *16* (3), 1761-1771.

40. Tong, H.; Lakey, P. S. J.; Arangio, A. M.; Socorro, J.; Shen, F.; Lucas, K.; Brune, W. H.; Pöschl, U.; Shiraiwa, M., Reactive Oxygen Species Formed by Secondary Organic Aerosols in Water and Surrogate Lung Fluid. *Environmental Science & Technology* **2018,** *52* (20), 11642-11651.

41. Seinfeld, J. H.; Pandis, S. N., *Atmospheric chemistry and physics : from air pollution to climate change / John H. Seinfeld, Spyros N. Pandis*. Third edition. ed.; John Wiley & Sons, Incorporated: Hoboken, New Jersey, 2016.

42. Tong, H.; Zhang, Y.; Filippi, A.; Wang, T.; Li, C.; Liu, F.; Leppla, D.; Kourtchev, I.; Wang, K.; Keskinen, H.-M.; Levula, J. T.; Arangio, A. M.; Shen, F.; Ditas, F.; Martin, S. T.; Artaxo, P.; Godoi, R. H. M.; Yamamoto, C. I.; de Souza, R. A. F.; Huang, R.-J.; Berkemeier, T.; Wang, Y.; Su, H.; Cheng, Y.; Pope, F. D.; Fu, P.; Yao, M.; Pöhlker, C.; Petäjä, T.; Kulmala, M.; Andreae, M. O.; Shiraiwa, M.; Pöschl, U.; Hoffmann, T.; Kalberer, M., Radical Formation by Fine Particulate Matter Associated with Highly Oxygenated Molecules. *Environmental Science & Technology* **2019,** *53* (21), 12506-12518.

43. Tong, H.; Liu, F.; Filippi, A.; Wilson, J.; Arangio, A. M.; Zhang, Y.; Yue, S.; Lelieveld, S.; Shen, F.; Keskinen, H. M. K.; Li, J.; Chen, H.; Zhang, T.; Hoffmann, T.; Fu, P.; Brune, W. H.; Petäjä, T.; Kulmala, M.; Yao, M.; Berkemeier, T.; Shiraiwa, M.; Pöschl, U., Reactive species formed upon interaction of water with fine particulate matter from remote forest and polluted urban air. *Atmos. Chem. Phys. Discuss.* **2020,** *2020*, 1-40.

44. Fang, T.; Lakey, P. S. J.; Rivera-Rios, J. C.; Keutsch, F. N.; Shiraiwa, M., Aqueous-Phase Decomposition of Isoprene Hydroxy Hydroperoxide and Hydroxyl Radical Formation by

Fenton-like Reactions with Iron Ions. *The Journal of Physical Chemistry A* **2020,** *124* (25), 5230-5236.

45. Wei, J.; Fang, T.; Wong, C.; Lakey, P. S. J.; Nizkorodov, S. A.; Shiraiwa, M., Superoxide Formation from Aqueous Reactions of Biogenic Secondary Organic Aerosols. *Environmental Science & Technology* **2021,** *55* (1), 260-270.

46. Dellinger, B.; Pryor, W. A.; Cueto, R.; Squadrito, G. L.; Hegde, V.; Deutsch, W. A., Role of Free Radicals in the Toxicity of Airborne Fine Particulate Matter. *Chemical Research in Toxicology* **2001,** *14* (10), 1371-1377.

47. Squadrito, G. L.; Cueto, R.; Dellinger, B.; Pryor, W. A., Quinoid redox cycling as a mechanism for sustained free radical generation by inhaled airborne particulate matter. *Free Radical Biology and Medicine* **2001,** *31* (9), 1132-1138.

48. Schuetzle, D., Sampling of vehicle emissions for chemical analysis and biological testing. *Environ Health Perspect* **1983,** *47*, 65-80.

49. Zelinkova, Z.; Wenzl, T., The Occurrence of 16 EPA PAHs in Food - A Review. *Polycycl Aromat Compd* **2015,** *35* (2-4), 248-284.

50. Cho, A. K.; Di Stefano, E.; You, Y.; Rodriguez, C. E.; Schmitz, D. A.; Kumagai, Y.; Miguel, A. H.; Eiguren-Fernandez, A.; Kobayashi, T.; Avol, E.; Froines, J. R., Determination of Four Quinones in Diesel Exhaust Particles, SRM 1649a, and Atmospheric PM2.5 Special Issue of Aerosol Science and Technology on Findings from the Fine Particulate Matter Supersites Program. *Aerosol Science and Technology* **2004,** *38* (sup1), 68-81.

51. Chung, M. Y.; Lazaro, R. A.; Lim, D.; Jackson, J.; Lyon, J.; Rendulic, D.; Hasson, A. S., Aerosol-Borne Quinones and Reactive Oxygen Species Generation by Particulate Matter Extracts. *Environmental Science & Technology* **2006,** *40* (16), 4880-4886.

52. Antiñolo, M.; Willis, M. D.; Zhou, S.; Abbatt, J. P. D., Connecting the oxidation of soot to its redox cycling abilities. *Nature Communications* **2015,** *6* (1), 6812.

53. Graber, E. R.; Rudich, Y., Atmospheric HULIS: How humic-like are they? A comprehensive and critical review. *Atmos. Chem. Phys.* **2006,** *6* (3), 729-753.

54. Dou, J.; Lin, P.; Kuang, B.-Y.; Yu, J. Z., Reactive Oxygen Species Production Mediated by Humic-like Substances in Atmospheric Aerosols: Enhancement Effects by Pyridine, Imidazole, and Their Derivatives. *Environmental Science & Technology* **2015,** *49* (11), 6457-6465.

55. Arangio, A. M.; Tong, H.; Socorro, J.; Pöschl, U.; Shiraiwa, M., Quantification of Environmentally Persistent Free Radicals and Reactive Oxygen Species in Atmospheric Aerosol Particles. *Atmos. Chem. Phys.* **2016,** *16* (20), 13105-13119.

56. Gehling, W.; Dellinger, B., Environmentally Persistent Free Radicals and Their Lifetimes in PM2.5. *Environmental Science & Technology* **2013,** *47* (15), 8172-8178.

57. Gehling, W.; Khachatryan, L.; Dellinger, B., Hydroxyl Radical Generation from Environmentally Persistent Free Radicals (EPFRs) in PM2.5. *Environmental Science & Technology* **2014,** *48* (8), 4266-4272.

58. Dellinger, B.; Lomnicki, S.; Khachatryan, L.; Maskos, Z.; Hall, R. W.; Adounkpe, J.; McFerrin, C.; Truong, H., Formation and stabilization of persistent free radicals. *Proceedings of the Combustion Institute* **2007,** *31* (1), 521-528.

59. Borrowman, C. K.; Zhou, S.; Burrow, T. E.; Abbatt, J. P. D., Formation of environmentally persistent free radicals from the heterogeneous reaction of ozone and polycyclic aromatic compounds. *Physical Chemistry Chemical Physics* **2016,** *18* (1), 205-212.

60. Valavanidis, A.; Fiotakis, K.; Bakeas, E.; Vlahogianni, T., Electron paramagnetic resonance study of the generation of reactive oxygen species catalysed by transition metals and quinoid redox cycling by inhalable ambient particulate matter. *Redox Report* **2005,** *10* (1), 37-51.

61. Pryor, W. A.; Hales, B. J.; Premovic, P. I.; Church, D. F., The radicals in cigarette tar: their nature and suggested physiological implications. *Science* **1983,** *220* (4595), 425-427.

62. Sigmund, G.; Santín, C.; Pignitter, M.; Tepe, N.; Doerr, S. H.; Hofmann, T., Environmentally persistent free radicals are ubiquitous in wildfire charcoals and remain stable for years. *Communications Earth & Environment* **2021,** *2* (1), 68.

63. Garg, B. D.; Cadle, S. H.; Mulawa, P. A.; Groblicki, P. J.; Laroo, C.; Parr, G. A., Brake Wear Particulate Matter Emissions. *Environmental Science & Technology* **2000,** *34* (21), 4463-4469.

64. Bates, J. T.; Fang, T.; Verma, V.; Zeng, L.; Weber, R. J.; Tolbert, P. E.; Abrams, J. Y.; Sarnat, S. E.; Klein, M.; Mulholland, J. A.; Russell, A. G., Review of Acellular Assays of Ambient Particulate Matter Oxidative Potential: Methods and Relationships with Composition, Sources, and Health Effects. *Environmental Science & Technology* **2019,** *53* (8), 4003-4019.

65. Shiraiwa, M.; Ueda, K.; Pozzer, A.; Lammel, G.; Kampf, C. J.; Fushimi, A.; Enami, S.; Arangio, A. M.; Fröhlich-Nowoisky, J.; Fujitani, Y.; Furuyama, A.; Lakey, P. S. J.; Lelieveld, J.; Lucas, K.; Morino, Y.; Pöschl, U.; Takahama, S.; Takami, A.; Tong, H.; Weber, B.; Yoshino, A.; Sato, K., Aerosol Health Effects from Molecular to Global Scales. *Environmental Science & Technology* **2017,** *51* (23), 13545-13567.

66. Kumagai, Y.; Koide, S.; Taguchi, K.; Endo, A.; Nakai, Y.; Yoshikawa, T.; Shimojo, N., Oxidation of Proximal Protein Sulfhydryls by Phenanthraquinone, a Component of Diesel Exhaust Particles. *Chemical Research in Toxicology* **2002,** *15* (4), 483-489.

67. Cho, A. K.; Sioutas, C.; Miguel, A. H.; Kumagai, Y.; Schmitz, D. A.; Singh, M.; Eiguren-Fernandez, A.; Froines, J. R., Redox activity of airborne particulate matter at different sites in the Los Angeles Basin. *Environmental Research* **2005,** *99* (1), 40-47.

68. Fang, T.; Verma, V.; Bates, J. T.; Abrams, J.; Klein, M.; Strickland, M. J.; Sarnat, S. E.; Chang, H. H.; Mulholland, J. A.; Tolbert, P. E.; Russell, A. G.; Weber, R. J., Oxidative potential of ambient water-soluble PM2.5 in the southeastern United States: contrasts in sources and health associations between ascorbic acid (AA) and dithiothreitol (DTT) assays. *Atmos. Chem. Phys.* **2016,** *16* (6), 3865-3879.

69. Zhang, Y.; Dai, M.; Yuan, Z., Methods for the detection of reactive oxygen species. *Analytical Methods* **2018,** *10* (38), 4625-4638.

70. Kumagai, Y.; Arimoto, T.; Shinyashiki, M.; Shimojo, N.; Nakai, Y.; Yoshikawa, T.; Sagai, M., Generation of Reactive Oxygen Species during Interaction of Diesel Exhaust Particle Components with NADPH-Cytochrome p450 Reductase and Involvement of the Bioactivation in the DNA Damage. *Free Radical Biology and Medicine* **1997,** *22* (3), 479-487.

71. Charrier, J. G.; Anastasio, C., On dithiothreitol (DTT) as a measure of oxidative potential for ambient particles: evidence for the importance of soluble transition metals. *Atmos. Chem. Phys.* **2012,** *12* (19), 9321-9333.

72. Xiong, Q.; Yu, H.; Wang, R.; Wei, J.; Verma, V., Rethinking Dithiothreitol-Based Particulate Matter Oxidative Potential: Measuring Dithiothreitol Consumption versus Reactive Oxygen Species Generation. *Environmental Science & Technology* **2017,** *51* (11), 6507-6514.

73. Virtanen, A.; Joutsensaari, J.; Koop, T.; Kannosto, J.; Yli-Pirilä, P.; Leskinen, J.; Mäkelä, J. M.; Holopainen, J. K.; Pöschl, U.; Kulmala, M.; Worsnop, D. R.; Laaksonen, A., An amorphous solid state of biogenic secondary organic aerosol particles. *Nature* **2010,** *467* (7317), 824-827.

74. You, Y.; Renbaum-Wolff, L.; Carreras-Sospedra, M.; Hanna, S. J.; Hiranuma, N.; Kamal, S.; Smith, M. L.; Zhang, X.; Weber, R. J.; Shilling, J. E.; Dabdub, D.; Martin, S. T.; Bertram, A. K., Images reveal that atmospheric particles can undergo liquid–liquid phase separations. *Proceedings of the National Academy of Sciences* **2012,** *109* (33), 13188-13193.

75. Perraud, V.; Bruns, E. A.; Ezell, M. J.; Johnson, S. N.; Yu, Y.; Alexander, M. L.; Zelenyuk, A.; Imre, D.; Chang, W. L.; Dabdub, D.; Pankow, J. F.; Finlayson-Pitts, B. J., Nonequilibrium atmospheric secondary organic aerosol formation and growth. *Proceedings of the National Academy of Sciences* **2012,** *109* (8), 2836-2841.

76. Shiraiwa, M.; Seinfeld, J. H., Equilibration timescale of atmospheric secondary organic aerosol partitioning. *Geophysical Research Letters* **2012,** *39* (24).

77. Shiraiwa, M.; Ammann, M.; Koop, T.; Pöschl, U., Gas uptake and chemical aging of semisolid organic aerosol particles. *Proceedings of the National Academy of Sciences* **2011,** *108* (27), 11003-11008.

78. Koop, T.; Bookhold, J.; Shiraiwa, M.; Pöschl, U., Glass transition and phase state of organic compounds: dependency on molecular properties and implications for secondary organic aerosols in the atmosphere. *Physical Chemistry Chemical Physics* **2011,** *13* (43), 19238-19255.

79. Shiraiwa, M.; Li, Y.; Tsimpidi, A. P.; Karydis, V. A.; Berkemeier, T.; Pandis, S. N.; Lelieveld, J.; Koop, T.; Pöschl, U., Global distribution of particle phase state in atmospheric secondary organic aerosols. *Nature Communications* **2017,** *8* (1), 15002.

80. Shrivastava, M.; Lou, S.; Zelenyuk, A.; Easter, R. C.; Corley, R. A.; Thrall, B. D.; Rasch, P. J.; Fast, J. D.; Massey Simonich, S. L.; Shen, H.; Tao, S., Global long-range transport and lung cancer risk from polycyclic aromatic hydrocarbons shielded by coatings of organic aerosol. *Proceedings of the National Academy of Sciences* **2017,** *114* (6), 1246-1251.

81. Mu, Q.; Shiraiwa, M.; Octaviani, M.; Ma, N.; Ding, A.; Su, H.; Lammel, G.; Pöschl, U.; Cheng, Y., Temperature effect on phase state and reactivity controls atmospheric multiphase chemistry and transport of PAHs. *Science Advances* **2018,** *4* (3), eaap7314.

82. King, M. D.; Rennie, A. R.; Thompson, K. C.; Fisher, F. N.; Dong, C. C.; Thomas, R. K.; Pfrang, C.; Hughes, A. V., Oxidation of oleic acid at the air–water interface and its potential effects on cloud critical supersaturations. *Physical Chemistry Chemical Physics* **2009,** *11* (35), 7699-7707.

83. Hosny, N. A.; Fitzgerald, C.; Vyšniauskas, A.; Athanasiadis, A.; Berkemeier, T.; Uygur, N.; Pöschl, U.; Shiraiwa, M.; Kalberer, M.; Pope, F. D.; Kuimova, M. K., Direct imaging of changes in aerosol particle viscosity upon hydration and chemical aging. *Chemical Science* **2016,** *7* (2), 1357-1367.

84. Kidd, C.; Perraud, V.; Wingen, L. M.; Finlayson-Pitts, B. J., Integrating phase and composition of secondary organic aerosol from the ozonolysis of α-pinene. *Proceedings of the National Academy of Sciences* **2014,** *111* (21), 7552-7557.

85. Pfrang, C.; Shiraiwa, M.; Pöschl, U., Chemical ageing and transformation of diffusivity in semi-solid multi-component organic aerosol particles. *Atmos. Chem. Phys.* **2011,** *11* (14), 7343-7354.

86. Lucic, B.; Bašic, I.; Nadramija, D.; Milicevic, A.; Trinajstic, N.; Suzuki, T.; Petrukhin, R.; Karelson, M.; Katritzky, A. R., Correlation of liquid viscosity with molecular structure for organic compounds using different variable selection methods. *ARKIVOC* **2002,** *2002* (4), 45-59.

87. Nash, D. G.; Tolocka, M. P.; Baer, T., The uptake of O3 by myristic acid–oleic acid mixed particles: evidence for solid surface layers. *Physical Chemistry Chemical Physics* **2006,** *8* (38), 4468-4475.

88. Zhou, S.; Lee, A. K. Y.; McWhinney, R. D.; Abbatt, J. P. D., Burial Effects of Organic Coatings on the Heterogeneous Reactivity of Particle-Borne Benzo[a]pyrene (BaP) toward Ozone. *The Journal of Physical Chemistry A* **2012,** *116* (26), 7050-7056.

89. Zhou, S.; Shiraiwa, M.; McWhinney, R. D.; Pöschl, U.; Abbatt, J. P. D., Kinetic limitations in gas-particle reactions arising from slow diffusion in secondary organic aerosol. *Faraday Discussions* **2013,** *165* (0), 391-406.

90. Baron, P. A.; Kulkarni, P.; Willeke, K., *Aerosol measurement : principles, techniques, and applications / edited by Pramod Kulkarni and Paul A. Baron, Klaus Willeke*. 3rd ed ed.; Wiley: Hoboken, N.J, 2011.

91. Eaton, G. R.; Eaton, S. S.; Barr, D. P.; Weber, R. T., *Quantitative EPR / Gareth R. Eaton, Sandra S. Eaton, David P. Barr, Ralph T. Weber*. Springer: Wien ;, 2010.

92. Weber, R. T., Xenon User's Guide. 328.

93. WebElement, WebElements. The Periodic Table of the Elements. https://www.webelements.com/nitrogen/isotopes.html. 2021.

94. Wang, S.; Takhar, M.; Zhao, Y.; Al Rashdi, L. N. S.; Chan, A. W. H., Dynamic Oxidative Potential of Organic Aerosol from Heated Cooking Oil. *ACS Earth and Space Chemistry* **2021,** *5* (5), 1150-1162.

95. Zhu, B.-Z.; Zhao, H.-T.; Kalyanaraman, B.; Liu, J.; Shan, G.-Q.; Du, Y.-G.; Frei, B., Mechanism of metal-independent decomposition of organic hydroperoxides and formation of alkoxyl radicals by halogenated quinones. *Proceedings of the National Academy of Sciences* **2007,** *104* (10), 3698-3702.

96. Huang, C.-H.; Ren, F.-R.; Shan, G.-Q.; Qin, H.; Mao, L.; Zhu, B.-Z., Molecular Mechanism of Metal-Independent Decomposition of Organic Hydroperoxides by Halogenated Quinoid Carcinogens and the Potential Biological Implications. *Chemical Research in Toxicology* **2015,** *28* (5), 831-837.

97. Shiraiwa, M.; Pfrang, C.; Pöschl, U., Kinetic multi-layer model of aerosol surface and bulk chemistry (KM-SUB): the influence of interfacial transport and bulk diffusion on the oxidation of oleic acid by ozone. *Atmos. Chem. Phys.* **2010,** *10* (8), 3673-3691.

98. Kwamena, N.-O. A.; Thornton, J. A.; Abbatt, J. P. D., Kinetics of Surface-Bound Benzo[a]pyrene and Ozone on Solid Organic and Salt Aerosols. *The Journal of Physical Chemistry A* **2004,** *108* (52), 11626-11634.

99. Pöschl, U.; Letzel, T.; Schauer, C.; Niessner, R., Interaction of Ozone and Water Vapor with Spark Discharge Soot Aerosol Particles Coated with Benzo[a]pyrene: O3 and H2O Adsorption, Benzo[a]pyrene Degradation, and Atmospheric Implications. *The Journal of Physical Chemistry A* **2001,** *105* (16), 4029-4041.

100. Kahan, T. F.; Kwamena, N. O. A.; Donaldson, D. J., Heterogeneous ozonation kinetics of polycyclic aromatic hydrocarbons on organic films. *Atmospheric Environment* **2006,** *40* (19), 3448-3459.

101. Shiraiwa, M.; Sosedova, Y.; Rouvière, A.; Yang, H.; Zhang, Y.; Abbatt, J. P. D.; Ammann, M.; Pöschl, U., The role of long-lived reactive oxygen intermediates in the reaction of ozone with aerosol particles. *Nature Chemistry* **2011,** *3* (4), 291-295.

102. Brauer, M.; Hoek, G.; Smit, H. A.; de Jongste, J. C.; Gerritsen, J.; Postma, D. S.; Kerkhof, M.; Brunekreef, B., Air pollution and development of asthma, allergy and infections in a birth cohort. *The European respiratory journal* **2007,** *29* (5), 879-88.

103. Simkhovich, B. Z.; Kleinman, M. T.; Kloner, R. A., Air Pollution and Cardiovascular Injury: Epidemiology, Toxicology, and Mechanisms. *Journal of the American College of Cardiology* **2008,** *52* (9), 719-726.

104. Brook Robert, D.; Rajagopalan, S.; Pope, C. A.; Brook Jeffrey, R.; Bhatnagar, A.; Diez-Roux Ana, V.; Holguin, F.; Hong, Y.; Luepker Russell, V.; Mittleman Murray, A.; Peters, A.; Siscovick, D.; Smith Sidney, C.; Whitsel, L.; Kaufman Joel, D., Particulate Matter Air Pollution and Cardiovascular Disease. *Circulation* **2010,** *121* (21), 2331-2378.

105. Ostro, B.; Malig, B.; Hasheminassab, S.; Berger, K.; Chang, E.; Sioutas, C., Associations of Source-Specific Fine Particulate Matter With Emergency Department Visits in California. *American Journal of Epidemiology* **2016,** *184* (6), 450-459.

106. Shkirkova, K.; Lamorie-Foote, K.; Connor, M.; Patel, A.; Barisano, G.; Baertsch, H.; Liu, Q.; Morgan, T. E.; Sioutas, C.; Mack, W. J., Effects of ambient particulate matter on vascular tissue: a review. *Journal of toxicology and environmental health. Part B, Critical reviews* **2020,** *23* (7), 319-350.

107. Zhang, Q.; Zheng, Y.; Tong, D.; Shao, M.; Wang, S.; Zhang, Y.; Xu, X.; Wang, J.; He, H.; Liu, W.; Ding, Y.; Lei, Y.; Li, J.; Wang, Z.; Zhang, X.; Wang, Y.; Cheng, J.; Liu, Y.; Shi, Q.; Yan, L.; Geng, G.; Hong, C.; Li, M.; Liu, F.; Zheng, B.; Cao, J.; Ding, A.; Gao, J.; Fu, Q.; Huo, J.; Liu, B.; Liu, Z.; Yang, F.; He, K.; Hao, J., Drivers of improved PM_{2.5} air quality in China from 2013 to 2017. *Proceedings of the National Academy of Sciences* **2019,** *116* (49), 24463.

108. Harrison, R. M.; Jones, A. M.; Gietl, J.; Yin, J.; Green, D. C., Estimation of the contributions of brake dust, tire wear, and resuspension to nonexhaust traffic particles derived from atmospheric measurements. *Environmental Science & Technology* **2012,** *46* (12), 6523-6529.

109. Zhang, Z.; Weichenthal, S.; Kwong, J. C.; Burnett, R. T.; Hatzopoulou, M.; Jerrett, M.; van Donkelaar, A.; Bai, L.; Martin, R. V.; Copes, R.; Lu, H.; Lakey, P.; Shiraiwa, M.; Chen, H., Long-term exposure to iron and copper in fine particulate air pollution and their combined impact on reactive oxygen species concentration in lung fluid: a population-based cohort study of cardiovascular disease incidence and mortality in Toronto, Canada. *Int. J. Epidemiol.* **2020**, dyaa230.

110. Truong, H.; Lomnicki, S.; Dellinger, B., Potential for Misidentification of Environmentally Persistent Free Radicals as Molecular Pollutants in Particulate Matter. *Environmental Science & Technology* **2010,** *44* (6), 1933-1939.

111. Yang, L.; Liu, G.; Zheng, M.; Jin, R.; Zhu, Q.; Zhao, Y.; Wu, X.; Xu, Y., Highly Elevated Levels and Particle-Size Distributions of Environmentally Persistent Free Radicals in Haze-Associated Atmosphere. *Environmental Science & Technology* **2017,** *51* (14), 7936-7944.
112. Wang, P.; Pan, B.; Li, H.; Huang, Y.; Dong, X.; Ai, F.; Liu, L.; Wu, M.; Xing, B., The Overlooked Occurrence of Environmentally Persistent Free Radicals in an Area with Low-Rank Coal Burning, Xuanwei, China. *Environmental Science & Technology* **2018,** *52* (3), 1054-1061.

113. Chen, Q.; Wang, M.; Sun, H.; Wang, X.; Wang, Y.; Li, Y.; Zhang, L.; Mu, Z., Enhanced health risks from exposure to environmentally persistent free radicals and the oxidative stress of PM2.5 from Asian dust storms in Erenhot, Zhangbei and Jinan, China. *Environment International* **2018,** *121,* 260-268.

114. Lomnicki, S.; Truong, H.; Vejerano, E.; Dellinger, B., Copper Oxide-Based Model of Persistent Free Radical Formation on Combustion-Derived Particulate Matter. *Environmental Science & Technology* **2008,** *42* (13), 4982-4988.

115. Chen, Q.; Sun, H.; Mu, Z.; Wang, Y.; Li, Y.; Zhang, L.; Wang, M.; Zhang, Z., Characteristics of environmentally persistent free radicals in PM2.5: Concentrations, species and sources in Xi'an, Northwestern China. *Environmental Pollution* **2019,** *247,* 18-26.

116. Tong, H.; Lakey, P. S. J.; Arangio, A. M.; Socorro, J.; Shen, F.; Lucas, K.; Brune, W. H.; Pöschl, U.; Shiraiwa, M., Reactive Oxygen Species Formed by Secondary Organic Aerosols in Water and Surrogate Lung Fluid. *Environ. Sci. Technol.* **2018,** *52* (20), 11642-11651.

117. Davies, K. J. A., Oxidative stress: the paradox of aerobic life. *Biochemical Society Symposium* **1995,** *61,* 1.

118. Kelly, F. J., Oxidative stress: its role in air pollution and adverse health effects. *Occupational and environmental medicine* **2003,** *60* (8), 612-6.

119. Lakey, P. S.; Berkemeier, T.; Tong, H.; Arangio, A. M.; Lucas, K.; Poschl, U.; Shiraiwa, M., Chemical Exposure-response Relationship between Air Pollutants and Reactive Oxygen Species in the Human Respiratory Tract. *Sci. Rep.* **2016,** *6*, 32916.

120. Fang, T.; Lakey, P. S. J.; Weber, R. J.; Shiraiwa, M., Oxidative Potential of Particulate Matter and Generation of Reactive Oxygen Species in Epithelial Lining Fluid. *Environmental Science & Technology* **2019,** *53* (21), 12784-12792.

121. Shi, T.; Schins, R. P.; Knaapen, A. M.; Kuhlbusch, T.; Pitz, M.; Heinrich, J.; Borm, P. J., Hydroxyl radical generation by electron paramagnetic resonance as a new method to monitor ambient particulate matter composition. *Journal of environmental monitoring : JEM* **2003,** *5* (4), 550-6.

122. Jung, H.; Guo, B.; Anastasio, C.; Kennedy, I. M., Quantitative measurements of the generation of hydroxyl radicals by soot particles in a surrogate lung fluid. *Atmospheric Environment* **2006,** *40* (6), 1043-1052.

123. DiStefano, E.; Eiguren-Fernandez, A.; Delfino, R. J.; Sioutas, C.; Froines, J. R.; Cho, A. K., Determination of metal-based hydroxyl radical generating capacity of ambient and diesel exhaust particles. *Inhal Toxicol* **2009,** *21* (9), 731-8.

124. Khachatryan, L.; Vejerano, E.; Lomnicki, S.; Dellinger, B., Environmentally Persistent Free Radicals (EPFRs). 1. Generation of Reactive Oxygen Species in Aqueous Solutions. *Environmental Science & Technology* **2011,** *45* (19), 8559-8566.

125. Tong, H.; Zhang, Y.; Filippi, A.; Wang, T.; Li, C.; Liu, F.; Leppla, D.; Kourtchev, I.; Wang, K.; Keskinen, H.-M.; Levula, J. T.; Arangio, A. M.; Shen, F.; Ditas, F.; Martin, S. T.; Artaxo, P.; Godoi, R. H. M.; Yamamoto, C. I.; de Souza, R. A. F.; Huang, R.-J.; Berkemeier, T.; Wang, Y.; Su, H.; Cheng, Y.; Pope, F. D.; Fu, P.; Yao, M.; Pöhlker, C.; Petäjä, T.; Kulmala, M.; Andreae, M. O.; Shiraiwa, M.; Pöschl, U.; Hoffmann, T.; Kalberer, M., Radical Formation by Fine Particulate Matter Associated with Highly Oxygenated Molecules. *Environ. Sci. Technol.* **2019,** *53* (21), 12506-12518.

126. Chen, Q.; Sun, H.; Wang, M.; Wang, Y.; Zhang, L.; Han, Y., Environmentally Persistent Free Radical (EPFR) Formation by Visible-Light Illumination of the Organic Matter in Atmospheric Particles. *Environmental Science & Technology* **2019,** *53* (17), 10053-10061.

127. Khachatryan, L.; Dellinger, B., Environmentally Persistent Free Radicals (EPFRs)-2. Are Free Hydroxyl Radicals Generated in Aqueous Solutions? *Environmental Science & Technology* **2011,** *45* (21), 9232-9239.

128. Cho, A. K.; Sioutas, C.; Miguel, A. H.; Kumagai, Y.; Schmitz, D. A.; Singh, M.; Eiguren-Fernandez, A.; Froines, J. R., Redox activity of airborne particulate matter at different sites in the Los Angeles Basin. *Environ. Res.* **2005,** *99* (1), 40-47.

129. Verma, V.; Fang, T.; Guo, H.; King, L. E.; Bates, J. T.; Peltier, R. E.; Edgerton, E. S.; Russell, A. G.; Weber, R. J., Reactive oxygen species associated with water-soluble PM2.5 in the southeastern United States: spatiotemporal trends and source apportionment. *Atmos. Chem. Phys.* **2014,** *14* (23), 12915-12930.

130. Kumagai, Y.; Koide, S.; Taguchi, K.; Endo, A.; Nakai, Y.; Yoshikawa, T.; Shimojo, N., Oxidation of proximal protein sulfhydryls by phenanthraquinone, a component of diesel exhaust particles. *Chem. Res. Toxicol.* **2002,** *15* (4), 483-489.

131. Fang, T.; Zeng, L.; Gao, D.; Verma, V.; Stefaniak, A. B.; Weber, R. J., Ambient Size Distributions and Lung Deposition of Aerosol Dithiothreitol-Measured Oxidative Potential: Contrast between Soluble and Insoluble Particles. *Environmental Science & Technology* **2017,** *51* (12), 6802-6811.

132. Lin, P.; Yu, J. Z., Generation of reactive oxygen species mediated by Humic-like Substances in atmospheric aerosols. *Environ. Sci. Technol.* **2011,** *45* (24), 10362-10368.

133. Dou, J.; Lin, P.; Kuang, B.-Y.; Yu, J. Z., Reactive Oxygen Species Production Mediated by Humic-like Substances in Atmospheric Aerosols: Enhancement Effects by Pyridine, Imidazole, and Their Derivatives. *Environ. Sci. Technol.* **2015,** *49* (11), 6457-6465.

134. McWhinney, R. D.; Zhou, S.; Abbatt, J. P. D., Naphthalene SOA: redox activity and naphthoquinone gas–particle partitioning. *Atmos. Chem. Phys.* **2013,** *13* (19), 9731-9744.

135. Tuet, W. Y.; Chen, Y.; Xu, L.; Fok, S.; Gao, D.; Weber, R. J.; Ng, N. L., Chemical oxidative potential of secondary organic aerosol (SOA) generated from the photooxidation of biogenic and anthropogenic volatile organic compounds. *Atmos. Chem. Phys.* **2017,** *17* (2), 839-853.

136. Wang, S.; Ye, J.; Soong, R.; Wu, B.; Yu, L.; Simpson, A. J.; Chan, A. W. H., Relationship between chemical composition and oxidative potential of secondary organic aerosol from polycyclic aromatic hydrocarbons. *Atmos. Chem. Phys.* **2018,** *18* (6), 3987-4003.

137. Jiang, H.; Jang, M.; Sabo-Attwood, T.; Robinson, S. E., Oxidative potential of secondary organic aerosols produced from photooxidation of different hydrocarbons using outdoor chamber under ambient sunlight. *Atmospheric Environment* **2016,** *131*, 382-389.

138. Kramer, A. J.; Rattanavaraha, W.; Zhang, Z.; Gold, A.; Surratt, J. D.; Lin, Y.-H., Assessing the oxidative potential of isoprene-derived epoxides and secondary organic aerosol. *Atmospheric Environment* **2016,** *130*, 211-218.

139. Fang, T.; Guo, H.; Zeng, L.; Verma, V.; Nenes, A.; Weber, R. J., Highly acidic ambient particles, soluble metals, and oxidative potential: a link between sulfate and aerosol toxicity. *Environ. Sci. Technol.* **2017,** *51*, 2611-2620.

140. Gao, D.; Fang, T.; Verma, V.; Zeng, L.; Weber, R., A method for measuring total aerosol oxidative potential (OP) with the dithiothreitol (DTT) assay and comparisons between an urban and roadside site of water-soluble and total OP. *Atmos. Meas. Tech. Discuss.* **2017,** *2017*, 1-25.

141. Saffari, A.; Daher, N.; Shafer, M. M.; Schauer, J. J.; Sioutas, C., Seasonal and spatial variation in dithiothreitol (DTT) activity of quasi-ultrafine particles in the Los Angeles Basin and its association with chemical species. *J. Environ. Sci. Health, Part A: Toxic/Hazard. Subst. Environ. Eng.* **2014,** *49* (4), 441-451.

142. Zhang, X.; Staimer, N.; Tjoa, T.; Gillen, D. L.; Schauer, J. J.; Shafer, M. M.; Hasheminassab, S.; Pakbin, P.; Longhurst, J.; Sioutas, C.; Delfino, R. J., Associations between microvascular function and short-term exposure to traffic-related air pollution and particulate matter oxidative potential. *Environmental Health* **2016,** *15* (1), 81.

143. Daellenbach, K. R.; Uzu, G.; Jiang, J.; Cassagnes, L.-E.; Leni, Z.; Vlachou, A.; Stefenelli, G.; Canonaco, F.; Weber, S.; Segers, A.; Kuenen, J. J. P.; Schaap, M.; Favez, O.;

Albinet, A.; Aksoyoglu, S.; Dommen, J.; Baltensperger, U.; Geiser, M.; El Haddad, I.; Jaffrezo, J.-L.; Prévôt, A. S. H., Sources of particulate-matter air pollution and its oxidative potential in Europe. *Nature* **2020,** *587* (7834), 414-419.

144. Xue, J.; Hu, S.; Quiros, D.; Ayala, A.; Jung, H. S., How do particle number, surface area, and mass correlate with toxicity of diesel particle emissions as measured in chemical and cellular assays? *Chemosphere* **2019,** *229*, 559-569.

145. Abrams, J. Y.; Weber, R. J.; Klein, M.; Samat, S. E.; Chang, H. H.; Strickland, M. J.; Verma, V.; Fang, T.; Bates, J. T.; Mulholland, J. A.; Russell, A. G.; Tolbert, P. E., Associations between Ambient Fine Particulate Oxidative Potential and Cardiorespiratory Emergency Department Visits. *Environ Health Perspec* **2017,** *125* (10), 107008.

146. Yang, A.; Janssen, N. A.; Brunekreef, B.; Cassee, F. R.; Hoek, G.; Gehring, U., Children's respiratory health and oxidative potential of PM2.5: the PIAMA birth cohort study. *Occup. Environ. Med.* **2016,** *73* (3), 154-60.

147. Bates, J. T.; Weber, R. J.; Abrams, J.; Verma, V.; Fang, T.; Klein, M.; Strickland, M. J.; Sarnat, S. E.; Chang, H. H.; Mulholland, J. A.; Tolbert, P. E.; Russell, A. G., Reactive Oxygen Species Generation Linked to Sources of Atmospheric Particulate Matter and Cardiorespiratory Effects. *Environ. Sci. Technol.* **2015,** *49* (22), 13605-13612.

148. Wang, X.; Ho, K.-F.; Chow, J. C.; Kohl, S. D.; Chan, C. S.; Cui, L.; Lee, S.-c. F.; Chen, L.-W. A.; Ho, S. S. H.; Cheng, Y.; Watson, J. G., Hong Kong vehicle emission changes from 2003 to 2015 in the Shing Mun Tunnel. *Aerosol Science and Technology* **2018,** *52* (10), 1085-1098.

149. Gao, D.; Fang, T.; Verma, V.; Zeng, L.; Weber, R. J., A method for measuring total aerosol oxidative potential (OP) with the dithiothreitol (DTT) assay and comparisons between an urban and roadside site of water-soluble and total OP. *Atmos. Meas. Tech.* **2017,** *10* (8), 2821-2835.

150. Fang, T.; Verma, V.; Guo, H.; King, L. E.; Edgerton, E. S.; Weber, R. J., A semi-automated system for quantifying the oxidative potential of ambient particles in aqueous extracts using the dithiothreitol (DTT) assay: results from the Southeastern Center for Air Pollution and Epidemiology (SCAPE). *Atmos. Meas. Tech.* **2015,** *8* (1), 471-482.

151. Watson, J. G.; Tropp, R. J.; Kohl, S. D.; Wang, X.; Chow, J. C., Filter Processing and Gravimetric Analysis for Suspended Particulate Matter Samples. *Aerosol Science and Engineering* **2017,** *1* (2), 93-105.

152. Watson, J. G.; Chow, J. C.; Frazier, C. A., *X-ray fluorescence analysis of ambient air samples*. Gordon and Breach Science Publishers: Amsterdam, Netherlands, 1999; p 67-96.

153. Chow, J. C.; Watson, J. G.; Pritchett, L. C.; Pierson, W. R.; Frazier, C. A.; Purcell, R. G., The dri thermal/optical reflectance carbon analysis system: description, evaluation and

applications in U.S. Air quality studies. *Atmospheric Environment. Part A. General Topics* **1993,** *27* (8), 1185-1201.

154. Chow, J. C.; Watson, J. G.; Chen, L. W. A.; Chang, M. C. O.; Robinson, N. F.; Trimble, D.; Kohl, S., The IMPROVE_A Temperature Protocol for Thermal/Optical Carbon Analysis: Maintaining Consistency with a Long-Term Database. *Journal of the Air & Waste Management Association* **2007,** *57* (9), 1014-1023.

155. Chen, L. W. A.; Chow, J. C.; Wang, X. L.; Robles, J. A.; Sumlin, B. J.; Lowenthal, D. H.; Zimmermann, R.; Watson, J. G., Multi-wavelength optical measurement to enhance thermal/optical analysis for carbonaceous aerosol. *Atmos. Meas. Tech.* **2015,** *8* (1), 451-461.

156. Dellinger, B.; Lomnicki, S.; Khachatryan, L.; Maskos, Z.; Hall, R. W.; Adounkpe, J.; McFerrin, C.; Truong, H., Formation and stabilization of persistent free radicals. *Proc. Combust. Inst.* **2007,** *31* (1), 521-528.

157. Ledoux, F.; Zhilinskaya, E.; Bouhsina, S.; Courcot, L.; Bertho, M.-L.; Aboukaïs, A.; Puskaric, E., EPR investigations of Mn2+, Fe3+ ions and carbonaceous radicals in atmospheric particulate aerosols during their transport over the eastern coast of the English Channel. *Atmospheric Environment* **2002,** *36* (6), 939-947.

158. Valavanidis, A.; Fiotakis, K.; Bakeas, E.; Vlahogianni, T., Electron paramagnetic resonance study of the generation of reactive oxygen species catalysed by transition metals and quinoid redox cycling by inhalable ambient particulate matter. *Redox Rep.* **2005,** *10* (1), 37-51.

159. Alpert, P. A.; Dou, J.; Corral Arroyo, P.; Schneider, F.; Xto, J.; Luo, B.; Peter, T.; Huthwelker, T.; Borca, C. N.; Henzler, K. D.; Schaefer, T.; Herrmann, H.; Raabe, J.; Watts, B.; Krieger, U. K.; Ammann, M., Photolytic radical persistence due to anoxia in viscous aerosol particles. *Nat. Commun.* **2021,** *12* (1), 1769.

160. Chen, Q.; Sun, H.; Song, W.; Cao, F.; Tian, C.; Zhang, Y. L., Size-resolved exposure risk of persistent free radicals (PFRs) in atmospheric aerosols and their potential sources. *Atmos. Chem. Phys.* **2020,** *20* (22), 14407-14417.

161. Wang, Y.; Li, S.; Wang, M.; Sun, H.; Mu, Z.; Zhang, L.; Li, Y.; Chen, Q., Source apportionment of environmentally persistent free radicals (EPFRs) in PM2.5 over Xi'an, China. *Science of The Total Environment* **2019,** *689*, 193-202.

162. De Vizcaya-Ruiz, A.; Gutiérrez-Castillo, M. E.; Uribe-Ramirez, M.; Cebrián, M. E.; Mugica-Alvarez, V.; Sepúlveda, J.; Rosas, I.; Salinas, E.; Garcia-Cuéllar, C.; Martínez, F.; Alfaro-Moreno, E.; Torres-Flores, V.; Osornio-Vargas, A.; Sioutas, C.; Fine, P. M.; Singh, M.; Geller, M. D.; Kuhn, T.; Miguel, A. H.; Eiguren-Fernandez, A.; Schiestl, R. H.; Reliene, R.; Froines, J., Characterization and in vitro biological effects of concentrated particulate matter from Mexico City. *Atmospheric Environment* **2006,** *40, Supplement 2*, 583-592.

163. Ntziachristos, L.; Froines, J. R.; Cho, A. K.; Sioutas, C., Relationship between redox activity and chemical speciation of size-fractionated particulate matter. *Part. Fibre Toxicol.* **2007,** *4* (1), 5.

164. Shaltout, A. A.; Boman, J.; Shehadeh, Z. F.; Al-Malawi, D.-a. R.; Hemeda, O. M.; Morsy, M. M., Spectroscopic investigation of PM2.5 collected at industrial, residential and traffic sites in Taif, Saudi Arabia. *Journal of Aerosol Science* **2015,** *79*, 97-108.

165. Charrier, J. G.; Richards-Henderson, N. K.; Bein, K. J.; McFall, A. S.; Wexler, A. S.; Anastasio, C., Oxidant production from source-oriented particulate matter – Part 1: Oxidative potential using the dithiothreitol (DTT) assay. *Atmos. Chem. Phys.* **2015,** *15* (5), 2327-2340.

166. Schauer, J. J., Evaluation of elemental carbon as a marker for diesel particulate matter. *Journal of Exposure Science & Environmental Epidemiology* **2003,** *13* (6), 443-453.

167. Zhu, Y.; Hinds, W. C.; Kim, S.; Shen, S.; Sioutas, C., Study of ultrafine particles near a major highway with heavy-duty diesel traffic. *Atmospheric Environment* **2002,** *36* (27), 4323-4335.

168. Fang, T.; Guo, H.; Verma, V.; Peltier, R. E.; Weber, R. J., PM2.5 water-soluble elements in the southeastern United States: automated analytical method development, spatiotemporal distributions, source apportionment, and implications for heath studies. *Atmos. Chem. Phys.* **2015,** *15* (20), 11667-11682.

169. Tian, Z.; Zhao, H.; Peter, K. T.; Gonzalez, M.; Wetzel, J.; Wu, C.; Hu, X.; Prat, J.; Mudrock, E.; Hettinger, R.; Cortina, A. E.; Biswas, R. G.; Kock, F. V. C.; Soong, R.; Jenne, A.; Du, B.; Hou, F.; He, H.; Lundeen, R.; Gilbreath, A.; Sutton, R.; Scholz, N. L.; Davis, J. W.; Dodd, M. C.; Simpson, A.; McIntyre, J. K.; Kolodziej, E. P., A ubiquitous tire rubber–derived chemical induces acute mortality in coho salmon. *Science* **2021,** *371* (6525), 185.

170. Kjaergaard, H. G.; Kurtén, T.; Nielsen, L. B.; Jørgensen, S.; Wennberg, P. O., Criegee Intermediates React with Ozone. *The Journal of Physical Chemistry Letters* **2013,** *4* (15), 2525-2529.

171. Makino, K.; Hagiwara, T.; Hagi, A.; Nishi, M.; Murakami, A., Cautionary Note for DMPO Spin Trapping in the Presence of Iron Ion. *Biochem. Biophys. Res. Commun.* **1990,** *172* (3), 1073-1080.

172. Al-Abadleh, H. A., Review of the Bulk and Surface Chemistry of Iron in Atmospherically Relevant Systems Containing Humic-like Substances. *RSC Advances* **2015,** *5* (57), 45785-45811.

173. Ervens, B.; Turpin, B. J.; Weber, R. J., Secondary Organic Aerosol Formation in Cloud Droplets and Aqueous Particles (aqSOA): a Review of Laboratory, Field and Model Studies. *Atmos. Chem. Phys.* **2011,** *11* (21), 11069-11102.

174. Campbell, S. J.; Wolfer, K.; Utinger, B.; Westwood, J.; Zhang, Z.; Bukiowiecki, N.; Steimer, S. S.; Vu, T. V.; Xu, J.; Straw, N.; Thomson, S.; Elzein, A.; Sun, Y.; Liu, D.; Li, L.; Fu, P.; Lewis, A. C.; Harrison, R. M.; Bloss, W. J.; Loh, M.; Miller, M. R.; Shi, Z.; Kalberer, M., Atmospheric conditions and composition that influence PM2.5 oxidative potential in Beijing, China. *Atmos. Chem. Phys. Discuss.* **2020,** *2020*, 1-40.

175. Liu, J. C.; Peng, R. D., The impact of wildfire smoke on compositions of fine particulate matter by ecoregion in the Western US. *J Expo Sci Environ Epidemiol* **2019,** *29* (6), 765-776.

176. Adetona, O.; Reinhardt, T. E.; Domitrovich, J.; Broyles, G.; Adetona, A. M.; Kleinman, M. T.; Ottmar, R. D.; Naeher, L. P., Review of the health effects of wildland fire smoke on wildland firefighters and the public. *Inhalation Toxicology* **2016,** *28* (3), 95-139.

177. Delfino, R. J.; Brummel, S.; Wu, J.; Stern, H.; Ostro, B.; Lipsett, M.; Winer, A.; Street, D. H.; Zhang, L.; Tjoa, T.; Gillen, D. L., The relationship of respiratory and cardiovascular hospital admissions to the southern California wildfires of 2003. *Occupational and Environmental Medicine* **2009,** *66* (3), 189-197.

178. Karthikeyan, S.; Balasubramanian, R.; Iouri, K., Particulate Air Pollution from Bushfires: Human Exposure and Possible Health Effects. *Journal of Toxicology and Environmental Health, Part A* **2006,** *69* (21), 1895-1908.

179. Williams, K. M.; Franzi, L. M.; Last, J. A., Cell-specific oxidative stress and cytotoxicity after wildfire coarse particulate matter instillation into mouse lung. *Toxicology and Applied Pharmacology* **2013,** *266* (1), 48-55.

180. Mazzoleni, L. R.; Zielinska, B.; Moosmüller, H., Emissions of Levoglucosan, Methoxy Phenols, and Organic Acids from Prescribed Burns, Laboratory Combustion of Wildland Fuels, and Residential Wood Combustion. *Environmental Science & Technology* **2007,** *41* (7), 2115-2122.

181. Dizdaroglu, M.; Jaruga, P., Mechanisms of free radical-induced damage to DNA. *Free Radical Research* **2012,** *46* (4), 382-419.

182. Hwang, B.; Fang, T.; Pham, R.; Wei, J.; Gronstal, S.; Lopez, B.; Frederickson, C.; Galeazzo, T.; Wang, X.; Jung, H.; Shiraiwa, M., Environmentally Persistent Free Radicals, Reactive Oxygen Species Generation, and Oxidative Potential of Highway PM2.5. *ACS Earth and Space Chemistry* **2021**.

183. Lin, P.; Aiona, P. K.; Li, Y.; Shiraiwa, M.; Laskin, J.; Nizkorodov, S. A.; Laskin, A., Molecular Characterization of Brown Carbon in Biomass Burning Aerosol Particles. *Environmental Science & Technology* **2016,** *50* (21), 11815-11824.

184. Bond, T. C.; Doherty, S. J.; Fahey, D. W.; Forster, P. M.; Berntsen, T.; DeAngelo, B. J.; Flanner, M. G.; Ghan, S.; Kärcher, B.; Koch, D.; Kinne, S.; Kondo, Y.; Quinn, P. K.; Sarofim, M. C.; Schultz, M. G.; Schulz, M.; Venkataraman, C.; Zhang, H.; Zhang, S.; Bellouin, N.; Guttikunda, S. K.; Hopke, P. K.; Jacobson, M. Z.; Kaiser, J. W.; Klimont, Z.; Lohmann, U.;

Schwarz, J. P.; Shindell, D.; Storelvmo, T.; Warren, S. G.; Zender, C. S., Bounding the role of black carbon in the climate system: A scientific assessment. *Journal of Geophysical Research: Atmospheres* **2013,** *118* (11), 5380-5552.

185. Di Lorenzo, R. A.; Place, B. K.; VandenBoer, T. C.; Young, C. J., Composition of Size-Resolved Aged Boreal Fire Aerosols: Brown Carbon, Biomass Burning Tracers, and Reduced Nitrogen. *ACS Earth and Space Chemistry* **2018,** *2* (3), 278-285.

186. Laskin, A.; Laskin, J.; Nizkorodov, S. A., Chemistry of Atmospheric Brown Carbon. *Chemical Reviews* **2015,** *115* (10), 4335-4382.

187. Keyte, I. J.; Harrison, R. M.; Lammel, G., Chemical reactivity and long-range transport potential of polycyclic aromatic hydrocarbons - a review. *Chem. Soc. Rev.* **2013,** *42* (24), 9333-9391.

188. Kwamena, N. O. A.; Staikova, M. G.; Donaldson, D. J.; George, I. J.; Abbatt, J. P. D., Role of the Aerosol Substrate in the Heterogeneous Ozonation Reactions of Surface-Bound PAHs. *The Journal of Physical Chemistry A* **2007,** *111* (43), 11050-11058.

189. Mmereki, B. T.; Donaldson, D. J., Direct Observation of the Kinetics of an Atmospherically Important Reaction at the Air−Aqueous Interface. *The Journal of Physical Chemistry A* **2003,** *107* (50), 11038-11042.

190. Henderson, E. A.; Donaldson, D. J., Influence of Organic Coatings on Pyrene Ozonolysis at the Air–Aqueous Interface. *The Journal of Physical Chemistry A* **2012,** *116* (1), 423-429.

191. Keyte, I. J.; Harrison, R. M.; Lammel, G., Chemical reactivity and long-range transport potential of polycyclic aromatic hydrocarbons – a review. *Chemical Society Reviews* **2013,** *42* (24), 9333-9391.

192. Halsall, C. J.; Barrie, L. A.; Fellin, P.; Muir, D. C. G.; Billeck, B. N.; Lockhart, L.; Rovinsky, F. Y.; Kononov, E. Y.; Pastukhov, B., Spatial and Temporal Variation of Polycyclic Aromatic Hydrocarbons in the Arctic Atmosphere. *Environmental Science & Technology* **1997,** *31* (12), 3593-3599.

193. Zuend, A.; Seinfeld, J. H., Modeling the gas-particle partitioning of secondary organic aerosol: the importance of liquid-liquid phase separation. *Atmos. Chem. Phys.* **2012,** *12* (9), 3857-3882.

194. Chang, E. I.; Pankow, J. F., Prediction of activity coefficients in liquid aerosol particles containing organic compounds, dissolved inorganic salts, and water - Part 2: Consideration of phase separation effects by an X-UNIFAC model. *Atmos. Environ.* **2006,** *40* (33), 6422-6436.

195. Pöhlker, C.; Wiedemann, K. T.; Sinha, B.; Shiraiwa, M.; Gunthe, S. S.; Smith, M.; Su, H.; Artaxo, P.; Chen, Q.; Cheng, Y.; Elbert, W.; Gilles, M. K.; Kilcoyne, A. L. D.; Moffet, R. C.; Weigand, M.; Martin, S. T.; Pöschl, U.; Andreae, M. O., Biogenic Potassium Salt Particles as Seeds for Secondary Organic Aerosol in the Amazon. *Science* **2012,** *337* (6098), 1075-1078.

196. Krieger, U. K.; Marcolli, C.; Reid, J. P., Exploring the complexity of aerosol particle properties and processes using single particle techniques. *Chemical Society Reviews* **2012,** *41* (19), 6631-6662.

197. Song, M.; Ham, S.; Andrews, R. J.; You, Y.; Bertram, A. K., Liquid–liquid phase separation in organic particles containing one and two organic species: importance of the average O:C. *Atmos. Chem. Phys.* **2018,** *18* (16), 12075-12084.

198. Song, M.; Liu, P.; Martin, S. T.; Bertram, A. K., Liquid–liquid phase separation in particles containing secondary organic material free of inorganic salts. *Atmos. Chem. Phys.* **2017,** *17* (18), 11261-11271.

199. Renbaum-Wolff, L.; Song, M.; Marcolli, C.; Zhang, Y.; Liu, P. F.; Grayson, J. W.; Geiger, F. M.; Martin, S. T.; Bertram, A. K., Observations and implications of liquid–liquid phase separation at high relative humidities in secondary organic material produced by α-pinene ozonolysis without inorganic salts. *Atmos. Chem. Phys.* **2016,** *16* (12), 7969-7979.

200. Shiraiwa, M.; Zuend, A.; Bertram, A. K.; Seinfeld, J. H., Gas-particle partitioning of atmospheric aerosols: interplay of physical state, non-ideal mixing and morphology. *Phys. Chem. Chem. Phys.* **2013,** *15* (27), 11441-11453.

201. Gligorovski, S.; Abbatt, J. P. D., An indoor chemical cocktail. *Science* **2018,** *359* (6376), 632-633.

202. Shen, H.; Huang, Y.; Wang, R.; Zhu, D.; Li, W.; Shen, G.; Wang, B.; Zhang, Y.; Chen, Y.; Lu, Y.; Chen, H.; Li, T.; Sun, K.; Li, B.; Liu, W.; Liu, J.; Tao, S., Global Atmospheric Emissions of Polycyclic Aromatic Hydrocarbons from 1960 to 2008 and Future Predictions. *Environ. Sci. Technol.* **2013,** *47* (12), 6415-6424.

203. Pitts, J. N.; Paur, H.-R.; Zielinska, B.; Arey, J.; Winer, A. M.; Ramdahl, T.; Mejia, V., Factors influencing the reactivity of polycyclic aromatic hydrocarbons adsorbed on filters and ambient POM with ozone. *Chemosphere* **1986,** *15* (6), 675-685.

204. Wu, C. H.; Salmeen, I.; Niki, H., Fluorescence spectroscopic study of reactions between gaseous ozone and surface-adsorbed polycyclic aromatic hydrocarbons. *Environmental Science & Technology* **1984,** *18* (8), 603-607.

205. Katz, M.; Lane, D. A., PHOTOMODIFICATION OF BENZO(a) PYRENE UNDER SIMULATED ATMOSPHERIC CONDITIONS. 1975; Vol. 15, pp 181-183.

206. Van Vaeck, L.; Van Cauwenberghe, K., Conversion of polycyclic aromatic hydrocarbons on diesel particulate matter upon exposure to ppm levels of ozone. *Atmospheric Environment (1967)* **1984,** *18* (2), 323-328.

207. Zuend, A.; Marcolli, C.; Luo, B. P.; Peter, T., A thermodynamic model of mixed organic-inorganic aerosols to predict activity coefficients. *Atmos. Chem. Phys.* **2008,** *8* (16), 4559-4593.

208. Zuend, A.; Marcolli, C.; Booth, A. M.; Lienhard, D. M.; Soonsin, V.; Krieger, U. K.; Topping, D. O.; McFiggans, G.; Peter, T.; Seinfeld, J. H., New and extended parameterization of the thermodynamic model AIOMFAC: calculation of activity coefficients for organic-inorganic mixtures containing carboxyl, hydroxyl, carbonyl, ether, ester, alkenyl, alkyl, and aromatic functional groups. *Atmos. Chem. Phys.* **2011,** *11* (17), 9155-9206.

209. Zuend, A.; Seinfeld, J. H., A practical method for the calculation of liquid–liquid equilibria in multicomponent organic–water–electrolyte systems using physicochemical constraints. *Fluid Phase Equilib.* **2013,** *337* (0), 201-213.

210. Zhou, S.; Hwang, B. C. H.; Lakey, P. S. J.; Zuend, A.; Abbatt, J. P. D.; Shiraiwa, M., Multiphase reactivity of polycyclic aromatic hydrocarbons is driven by phase separation and diffusion limitations. *Proceedings of the National Academy of Sciences* **2019,** *116* (24), 11658.

211. Zhou, S.; Forbes, M. W.; Abbatt, J. P. D., Application of Direct Analysis in Real Time-Mass Spectrometry (DART-MS) to the Study of Gas–Surface Heterogeneous Reactions: Focus on Ozone and PAHs. *Analytical Chemistry* **2015,** *87* (9), 4733-4740.

212. Berkemeier, T.; Steimer, S.; Krieger, U. K.; Peter, T.; Poschl, U.; Ammann, M.; Shiraiwa, M., Ozone uptake on glassy, semi-solid and liquid organic matter and the role of reactive oxygen intermediates in atmospheric aerosol chemistry. *Phys. Chem. Chem. Phys.* **2016,** *18*, 12662-12674.

213. Lienhard, D. M.; Huisman, A. J.; Krieger, U. K.; Rudich, Y.; Marcolli, C.; Luo, B. P.; Bones, D. L.; Reid, J. P.; Lambe, A. T.; Canagaratna, M. R.; Davidovits, P.; Onasch, T. B.; Worsnop, D. R.; Steimer, S. S.; Koop, T.; Peter, T., Viscous organic aerosol particles in the upper troposphere: diffusivity-controlled water uptake and ice nucleation? *Atmos. Chem. Phys.* **2015,** *15* (23), 13599-13613.

214. Lewis, D. F. V.; Ioannides, C.; Parke, D. V., Molecular modelling of cytochrome CYP1A1: a putative access channel explains differences in induction potency between the isomers benzo (a) pyrene and benzo (e) pyrene, and 2-and 4-acetylaminofluorene. *Toxicol. Lett.* **1994,** *71* (3), 235-243.

215. Vieceli, J.; Roeselova, M.; Potter, N.; Dang, L. X.; Garrett, B. C.; Tobias, D. J., Molecular dynamics simulations of atmospheric oxidants at the air-water interface: Solvation and accommodation of OH and O_3. *J. Phys. Chem. B* **2005,** *109* (33), 15876-15892.

216. Ammann, M.; Pöschl, U.; Rudich, Y., Effects of reversible adsorption and Langmuir–Hinshelwood surface reactions on gas uptake by atmospheric particles. *Physical Chemistry Chemical Physics* **2003,** *5* (2), 351-356.

217. Smith, G. D.; Woods, E.; DeForest, C. L.; Baer, T.; Miller, R. E., Reactive Uptake of Ozone by Oleic Acid Aerosol Particles: Application of Single-Particle Mass Spectrometry to Heterogeneous Reaction Kinetics. *The Journal of Physical Chemistry A* **2002,** *106* (35), 8085-8095.

218. King, M. D.; Rennie, A. R.; Thompson, K. C.; Fisher, F. N.; Dong, C. C.; Thomas, R. K.; Pfrang, C.; Hughes, A. V., Oxidation of oleic acid at the air-water interface and its potential effects on cloud critical supersaturations. *Physical Chemistry Chemical Physics* **2009,** *11* (35), 7699-7707.

219. Berkemeier, T.; Steimer, S. S.; Krieger, U. K.; Peter, T.; Poschl, U.; Ammann, M.; Shiraiwa, M., Ozone uptake on glassy, semi-solid and liquid organic matter and the role of reactive oxygen intermediates in atmospheric aerosol chemistry. *Physical Chemistry Chemical Physics* **2016,** *18* (18), 12662-12674.

220. Maranzana, A.; Serra, G.; Giordana, A.; Tonachini, G.; Barco, G.; Causà, M., Ozone Interaction with Polycyclic Aromatic Hydrocarbons and Soot in Atmospheric Processes: Theoretical Density Functional Study by Molecular and Periodic Methodologies. *The Journal of Physical Chemistry A* **2005,** *109* (48), 10929-10939.

221. Gonzalez-Labrada, E.; Schmidt, R.; DeWolf, C. E., Kinetic analysis of the ozone processing of an unsaturated organic monolayer as a model of an aerosol surface. *Physical Chemistry Chemical Physics* **2007,** *9* (43), 5814-5821.

222. Titov, V. N.; Konovalova, G. G.; Lisitsyn, D. M.; Razumovskii, S. D.; Nezhdanova, I. B.; Kukharchuk, V. V., Kinetics of fatty acid oxidation in low density lipoproteins evaluated by registration of the oxidizer consumption and reaction product yield. *Bull. Exp. Biol. Med.* **2005,** *140* (1), 38-40.

223. Rosen, E. P.; Garland, E. R.; Baer, T., Ozonolysis of Oleic Acid Adsorbed to Polar and Nonpolar Aerosol Particles. *The Journal of Physical Chemistry A* **2008,** *112* (41), 10315-10324.

224. Arangio, A. M.; Slade, J. H.; Berkemeier, T.; Pöschl, U.; Knopf, D. A.; Shiraiwa, M., Multiphase Chemical Kinetics of OH Radical Uptake by Molecular Organic Markers of Biomass Burning Aerosols: Humidity and Temperature Dependence, Surface Reaction and Bulk Diffusion. *J. Phys. Chem. A* **2015,** *119* (19), 4533–4544.

225. Berkemeier, T.; Ammann, M.; Krieger, U. K.; Peter, T.; Spichtinger, P.; Pöschl, U.; Shiraiwa, M.; Huisman, A. J., Technical note: Monte Carlo genetic algorithm (MCGA) for model analysis of multiphase chemical kinetics to determine transport and reaction rate coefficients using multiple experimental data sets. *Atmos. Chem. Phys.* **2017,** *17* (12), 8021-8029.

226. Berkemeier, T.; Huisman, A. J.; Ammann, M.; Shiraiwa, M.; Koop, T.; Pöschl, U., Kinetic regimes and limiting cases of gas uptake and heterogeneous reactions in atmospheric aerosols and clouds: a general classification scheme. *Atmos. Chem. Phys.* **2013,** *13* (14), 6663-6686.

227. Renbaum-Wolff, L.; Grayson, J. W.; Bateman, A. P.; Kuwata, K.; Sellier, M.; Murray, B. J.; Schilling, J. E.; Martin, S. T.; Bertram, A. K., Viscosity of α-pinene secondary organic material and implications for particle growth and reactivity. *Proc. Natl. Acad. Sci. U.S.A.* **2013,** *110* (20), 8014-8019.

228. Bjoerseth, A.; Ramdahl, T., *Handbook of polycyclic aromatic hydrocarbons, volume 2, emission sources and recent progress in analytical chemistry*. Marcel Dekker, Inc.,New York, NY: United States, 1985.

229. Vander Wall, A. C.; Lakey, P. S. J.; Rossich Molina, E.; Perraud, V.; Wingen, L. M.; Xu, J.; Soulsby, D.; Gerber, R. B.; Shiraiwa, M.; Finlayson-Pitts, B. J., Understanding interactions of organic nitrates with the surface and bulk of organic films: implications for particle growth in the atmosphere. *Environ. Sci. Processes Impacts* **2018,** *20* (11), 1593-1610.

230. Li, Y. J.; Liu, P.; Gong, Z.; Wang, Y.; Bateman, A. P.; Bergoend, C.; Bertram, A. K.; Martin, S. T., Chemical Reactivity and Liquid/Nonliquid States of Secondary Organic Material. *Environ. Sci. Technol.* **2015,** *49* (22), 13264-13274.

231. Vesna, O.; Sax, M.; Kalberer, M.; Gaschen, A.; Ammann, M., Product study of oleic acid ozonolysis as function of humidity. *Atmos. Environ.* **2009,** *43* (24), 3662-3669.

232. Zahardis, J.; Petrucci, G. A., The oleic acid-ozone heterogeneous reaction system: products, kinetics, secondary chemistry, and atmospheric implications of a model system - a review. *Atmos. Chem. Phys.* **2007,** *7*, 1237-1274.

233. Zahardis, J.; Geddes, S.; Petrucci, G. A., The ozonolysis of primary aliphatic amines in fine particles. *Atmos. Chem. Phys.* **2008,** *8* (5), 1181-1194.

234. Maertens, R. M.; Yang, X.; Zhu, J.; Gagne, R. W.; Douglas, G. R.; White, P. A., Mutagenic and Carcinogenic Hazards of Settled House Dust I: Polycyclic Aromatic Hydrocarbon Content and Excess Lifetime Cancer Risk from Preschool Exposure. *Environ. Sci. Technol.* **2008,** *42* (5), 1747-1753.

235. Weschler, C. J.; Carslaw, N., Indoor Chemistry. *Environ. Sci. Technol.* **2018,** *52* (5), 2419-2428.

236. Weschler, C. J.; Nazaroff, W. W., SVOC exposure indoors: fresh look at dermal pathways. *Indoor Air* **2012,** *22* (5), 356-377.

237. Weschler, C. J.; Nazaroff, W. W., Growth of organic films on indoor surfaces. *Indoor Air* **2017,** *27* (6), 1101-1112.

238. Liu, Q.-T.; Chen, R.; McCarry, B. E.; Diamond, M. L.; Bahavar, B., Characterization of Polar Organic Compounds in the Organic Film on Indoor and Outdoor Glass Windows. *Environ. Sci. Technol.* **2003,** *37* (11), 2340-2349.

239. Weschler, C. J., Ozone in indoor environments: Concentration and chemistry. *Indoor Air* **2000,** *10* (4), 269-288.

240. Bates, J. T.; Weber, R. J.; Abrams, J.; Verma, V.; Fang, T.; Klein, M.; Strickland, M. J.; Sarnat, S. E.; Chang, H. H.; Mulholland, J. A.; Tolbert, P. E.; Russell, A. G., Reactive Oxygen Species Generation Linked to Sources of Atmospheric Particulate Matter and Cardiorespiratory Effects. *Environmental Science & Technology* **2015,** *49* (22), 13605-13612.